UNIVERSITÀ DELLA CALABRIA

Dipartimento di Meccanica Energetica e Gestionale

Dottorato di Ricerca

Ingegneria Civile e Industriale

CICLO XXIX

THERMO-FLUID DYNAMICS STUDY OF OXY-MILD COMBUSTION OF PULVERIZED COAL IN FURNACES AND IN A NOVEL CONCEPT OF BOILER

Settore Scientifico Disciplinare ING-IND/08

Coordinatore: Ch.mo Prof. Franco Furgiuele

Firma _____

Supervisore: Ch.mo Prof. Mario Amelio

Firma Mario Amelio

Dottorando: Dott. Diego Perrone

Firma Diego Perrone

'What lies behind us and what lies ahead of us
are tiny matters to what lies within us
and our greatest glory is not in never falling,
but in rising every time we fall.'

UNIVERSITÀ DELLA CALABRIA

Sommario

Dipartimento di Ingegneria Meccanica Energetica e Gestionale
Dottorato in Ingegneria Civile e Industriale
Dottorato di ricerca

Studio Termo-Fluidodinamico dell' Ossi Combustione Diluita in Fornaci e in un Nuovo Concept of Boiler

di Diego Perrone

Gli impianti per la generazione di energia elettrica che utilizzano carbone come fonte di energia primaria presentano molteplici problemi legati all'emissioni di sostanze inquinanti e di gas effetto serra (CO_2) in atmosfera. A questa problematica si aggiunge il fatto che i convenzionali generatori di vapore contribuiscono notevolmente all'aumento di queste sostanze nocive. Scopo di questo lavoro è quello di proporre e analizzare la possibilità di combinare due nuove tecnologie di combustione: l'ossicombustione e la cosiddetta combustione diluita. La prima permette la cattura dell'anididride carbonica mentre la seconda presenta vantaggi, non solo in termini di riduzione degli ossidi di azoto, ma anche perchè è caratterizzata dall'avere flussi termici uniformi in camera di combustione. La sfida pertanto è combinare le due tecnologie con applicazioni in fornaci e a nuovi concept di generatori di vapore. Per questi ultimi le applicazioni previste riguardano gli impianti ultra super critici. A tale scopo, sono state effettuate simulazioni numeriche mediante tecnica CFD (Computational Fluid Dynamics) dal momento in cui è difficile prevedere sperimentazioni su scala industriale. Una prima fase del lavoro prevede l'applicazione delle due tecnologie in fornaci. Una prima sulla combustione diluita nella quale sono state analizzate differenti posizioni del getto del polverino di carbone, mentre una seconda ha riguardato l'applicazione della combinazione delle due al fine di vederne gli effetti in termini di distribuzioni delle temperatura e dei gas combusti. La fase successiva è stata incentrata su di un innovativo generatore di vapore. Sono state testate diverse soluzioni geometriche e diversi modelli di combustione del char, al fine di vederne gli effetti sulla temperatura, concentrazioni delle specie, burnout e soprattutto in termini di flusso termico a parete. Questi ultimi risultati sono stati confrontati con i tradizionali boilers e con risultati forniti dalla letteratura. Il valore aggiunto del lavoro è stato quello di analizzare i vantaggi della combinazione di due tecnologie in nuovi concept di generatori di vapore, in modo da ridurre le emissioni di sostanze inquinanti, di gas effetto serra e di ottenere prestazioni migliori rispetto allo stato dell'arte attuale.

UNIVERSITÀ DELLA CALABRIA

Abstract

Department of Mechanical, Energy and Management Engineering
Doctor of Philosophy in Civil and Industrial Engineering

Doctor of Philosophy

Thermo-Fluid Dynamics Study of Oxy-MILD Combustion of Pulverized Coal in Furnaces and in a Novel Concept of Boiler

di Diego Perrone

The thermal power plant for the generation of electricity, which uses coal as a primary energy source, presents multiple issues linked to the emission of pollutants and greenhouse gas (CO_2) into the atmosphere. Furthermore, the conventional boilers greatly contribute to the increase of these harmful substances. The aim of this work is to propose and analyze the possibility of combining two new combustion technologies: the so-called oxy and MILD combustion. The first one, allows to capture the carbon dioxide, while the second one provides several advantages, not only because it reduces the emission of nitrogen oxides, but also because it is characterized by uniform flows in the combustion chamber. Therefore, the challenge is to combine the two technologies with applications in furnaces and a new concept of boiler. For the latter, the planned applications include the ultra-super critical plants. For this reason, numerical simulations have been carried out by means of technical CFD (Computational Fluid Dynamics) because it is hard to provide large-scale tests. The initial phase of the work involves the application of the two technologies in furnaces. The first one focuses on the MILD combustion by analyzing different positions of the pulverized coal jet, while the second one focuses on the application of the combination of the two technologies in order to analyze their effects in terms of temperature and species concentration distributions. The next phase of the work, instead, has a focus on an innovative boiler. The testing of different geometrical solutions and models of char combustion has also allowed to study their effects in terms of temperature, combustion products concentrations, burnout and, above all, wall heat flux. These latter results have been compared with the ones of traditional boilers and the results reported in the literature. The final aim of this work is to analyze the advantages deriving from the combination of two technologies into a new concept of boiler, in order to reduce pollutant emissions, greenhouse gases and obtain a better performance than the one at the current state of the art.

Acknowledgements

I would like to thank my research advisor Prof. Mario Amelio, from University of Calabria, for his precious guidance and support.

I am also grateful to Dr. Adam Klimanek, from Institute of Thermal Technology for his valuable comments and suggestions.

A special thanks to Dr. Andrzej Szlek who gave me the opportunity to be part of his research group and work in such an active and friendly environment.

Thanks to all the colleagues, always available to offer a professional and human point of view.

Thanks to all the people I met during this great experience, with its up and down.

Contents

List of Figures

List of Tables

Acronyms

AFT	**A**diabatic **F**lame **T**emperature
ASTM	**A**merican **S**ociety **T**esting **M**aterials
C NMR	**C**arbon **N**uclear **M**agnetic **R**esonance
CCR	**C**arbon **C**apture **R**ecovery
CCS	**C**arbon **C**apture **S**torage
CPD	**C**hemical **P**ercolation **M**odel
CFD	**C**omputational **F**luid **D**ynamics
DPM	**D**iscrete **P**hase **M**odel
EDM	**E**ddy **D**issipaion **M**odel
EEC	**E**xcess **E**nthalpy **C**ombustion
EPA	**E**nvironmental **P**rotection **A**gency
FANS	**F**avre **A**veraged **N**avier **S**tokes
FGR	**F**lue **G**as **R**ecirculation
FLOX	**FL**ox **OX**idation
FRM	**F**inite **R**ate **M**odel
HSRG	**H**eat **S**team **R**ecovery **G**enerator
HTAC	**H**igh **T**emperature **A**ir **C**ombustion
IFRF	**I**nternational **F**lame **R**esearch **F**oundation
IEA	**I**nternational **E**nergy **A**gency
ISO	**I**nternational **S**tandardization **O**rganization
ITM	**I**onic **T**ransport **M**embrane
LNCFS	**L**ow NO_x **C**oncentric **F**iring **S**ystem
MILD	**M**oderate or **I**ntensive **L**ow oxygen **D**ilution
NFK	**N**ippon **F**urnace **K**yogo
OFA	**O**ver **F**ire **A**ir
PC	**P**ulverized **C**oal

PRESTO!	**PRE**ssure **ST**aggering **O**ption
RANS	**R**eynolds **A**veraged **N**avier **S**tokes
SIMPLE	**S**emi **I**mplicit **M**odel for **P**ressure **L**inked **E**quation
SOFA	**S**econd**O**ver **F**ire **A**ir
SR	**S**toichiometric **R**atio
USC	**U**ltra **S**uper **C**ritical

Nomenclature

A	Pre-Exponential Factor	$[\frac{kg}{m^2 s}]$
a	Absorption Coefficient	-
A, B	Constants of EDM	-
C	Linear-Anisotropic Phase Function Coefficient	
c_p	Specific Heat Capacity	$[\frac{J}{molK}]$
C_μ	Constant of $k-\epsilon$ model	-
D	Mass Diffusion Coefficient	$[\frac{m^2}{s}]$
Da	Damkhöler number	-
d	Diameter	[m]
E	Activation Energy	$[\frac{J}{kmol}]$
$\mathbf{f}$	External Forces Term Vector	$[N]$
G	Incident Radiation	$[\frac{W}{m^2}]$
g_x	Gravity Constant	$[\frac{m}{s^2}]$
k	Thermal Conductivity	$[\frac{W}{mK}]$
k	Turbulent Kinetic Energy	$[\frac{kgm^2}{s}]$
M_w	Molecular Weight	$[\frac{kg}{kmol}]$
J	Diffusion Flux	$[\frac{mol}{m^2 s}]$
h	Total Enthalpy	$[\frac{W}{m^2 K}]$
I	Unit Tensor	-
l	Characteristic Length	[m]
n	Refractive Index	-
p	Pressure	$[Pa]$
$\mathfrak{R}$	Reaction Rate	$[\frac{mol}{m^3 s}]$
R	Ideal Gas Constant	$[\frac{J}{molK}]$
S	Source Term	$[\frac{kg}{m^3 s}]$
T	Temperature	$[K]$

t	Time	$[s]$
u	x-velocity	$[\frac{m}{s}]$
v	y-velocity	$[\frac{m}{s}]$
$\mathbf{v}$	Velocity Vector	$[\frac{m}{s}]$
w	z-velocity	$[m/s]$
s, y, z	Cartesian Coordinates	$[m]$
Y	Mass Fraction	-

Greek symbols

δ	Kronecker Symbol	-
ϵ	Turbulent Dissipation Energy	$[\frac{m^2}{s^2}]$
η_r	Effectiveness Factor	-
Γ	Diffusivity	$[\frac{m^2}{s^2}]$
μ	Dynamic Viscosity	$[Pas]$
ρ	Density	$[\frac{kg}{m^3}]$
$\overline{\overline{\tau}}$	Viscous Stress Tensor	$[Pa]$
ϕ	General Transport Variable	-
ϕ	Thiele Modulus	-
ν	Stoichiometric Coefficient	-

subscript

0	Initial
h	Hentalpy
i	Specie
j	Particle Species
m	Mass
p	Particle
r	Reaction
s	Solid
t	Turbulent
ref	Reference

To my family

and

To you, who are with me forever

Chapter 1

Characteristics of Coal and Pulverized Coal-Firing boilers

The use of coal dominates the world–wide energy production and accounted for nearly half of the increase in global energy use over the past decade. The respective share of world energy consumptions reached 30% in 2010, the highest value recorded since 1970 [1] and can be compared with 23 % in 2000. Coal is the backbone of the global electricity generation and, in 2010, it accounted for over 40% of electricity. Even in the countries which are part of the OECD, coal fueled more than one–third of electricity generation of 2010. Furthermore, in non–OECD countries, where coal resources are often abundant and low cost, coal is the most important fuel. Indeed, it accounted for 35% of the total primary energy use, 36% of the total industry consumption and almost half of the total electricity generation in 2010 [2]. Recently, the safeguard of the environment has become the most important target for all and especially for coal–fired power plants in the world. However, because international agreements regulating the emission of greenhouse gases have not been signed yet, coal still constitutes the major energy source throughout the world. The US Energy Information Administration predicted an average annual increasing rate of approximately 1.5 % of its consumption from 40.7 sextillion kWh (139 quadrillion Btu) in 2008 to 61.2 sextillion kWh (209 quadrillion Btu) in 2035 [3]. This substantial increase in coal consumption can find an explanation in the rapid and solid economic growth of emerging countries as China and India. Power generation remains the main driver of global coal demand and will, therefore, play a significant role in meeting the global energy needs. Considering the present consumption rate and the current technology, coal reserves around the world will still provide exploitable resources for about 150 years, as the International Energy Outlook [2] pointed out. The estimation of undiscovered resources increases world energy supply from coal to about 3,000 years and due to the development of technology and the change in market conditions, even more coal will be proven over time. The International Energy Agency (IEA) along

with the US Environmental Protection Agency (EPA) expect that, in the new policies scenario, coal–fired plants will account for around 27 % of the total new additions to generating capacity worldwide between 2011 and 2020, and around 22 % between 2011 and 2035 [2,4].

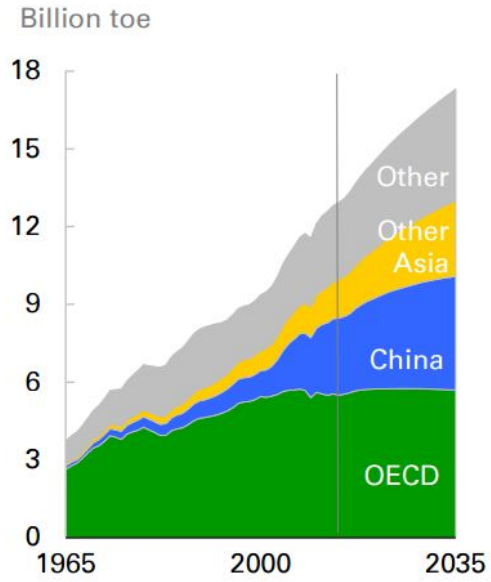

FIGURE 1.1: Perspective of the global coal demand by region [4]

1.1 Characteristics of Coal

Coals pertains to a category of complex substances whose geological origin can be found in the combination of time, pressure, and heat of the earth over several millennia, starting from ancient vegetation. They are material of extreme heterogeneous nature, indeed, their chemical compositions and properties might vary widely depending on how long the vegetable matter has been subjected to the conditions mentioned before. Because of this great diversity, coal can be classified according to a variety of methodologies. The most common one sorts coal by its carbon content from low (45 wt.– %, lignite) to high (95 wt.–%, anthracite), and it is referred to as 'coal rank' [5]. The standard method which allows to distinguish coal by its rank takes into account the coal's progressive alteration in the natural metamorphosis from low (lignite) to high (anthracite). In order to classify coal, the fixed carbon and gross calorific value are calculated through a mineral–matter–free basis [6]. More in depth, mineral matter consists in the parent material from which ash is generated during the combustion process. Mineral matter, furthermore, may vary and result in generally lower weight for ash than for its source minerals. Coal quality can be estimated according to the amount of mineral matter present in the coal. The grade of the coal can also be described by the sulfur content, ash behavior at

high temperatures, and quantity of trace elements. Formal classification systems do not always take into consideration the grade of coal, but the latter is very important for the power plant. The coal industry has great consideration of the rank of the coal, its quality, and burning behavior; for this reason, almost every coal–producing country has developed its own economic coal classification. These classification methods are based mainly on certain rank parameters which have been defined under the jurisdiction of several organizations for standardization, e.g. the American Society for Testing and Materials (ASTM) or the International Organization for Standardization (ISO). The volatile content,the carbon and the hydrogen contents are also often used to classify coals. Figure 1.2 gives an overview [7].

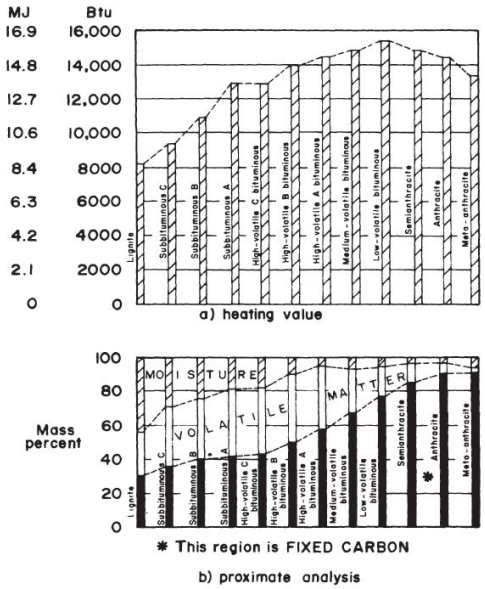

FIGURE 1.2: Classification and energy content of coals (ASTM) coal rank [5]

The proximate and ultimate analysis of coal is very useful for the provision of important information as specific energy, inert fraction (ash), moisture content, volatile matter content, and elementary components [7].
The proximate analysis of coal is a commonly applied characteristic test which yields: total moisture, inherent moisture, volatile matter, ash and fixed carbon. The ultimate analysis, instead, determines the elemental compositions of the organic fraction as the proportion of carbon, hydrogen, nitrogen, oxygen, sulfur and others by laboratory standard procedures. Table 2 provides a typical proximate and ultimate analysis for coals and char. Figure 1.3 provides a typical proximate and ultimate analysis for coals and char [7].

In particular, the proximate analysis is important to determine the moisture content of a specific coal because of its widely possibility of variation. The ultimate analysis, instead, is used along with the heating value of the coal to perform

Coal I.D. rank	Utah Church Mine, bituminous	Pittsburgh,[b] bituminous	Pittsburgh,[b] bituminous (high-volatile)	Sewell[b] bituminous (medium-volatile)	Anthracite[b] (low-volatile)	Illinois coal, bituminous	Illinois[c] coal char
Moisture %	2.5–2.7	2.0	1.0	1.9	1.3	10.1	0.9
Proximate %							
Volatiles	44.1–45.5	36.6	28.9	16.3	8.8	39.9	2.4
Fixed carbon	42.6–44.2	55.4	63.2	75.6	71.8	52.0	76.8
Ash	9.2–9.5	6.0	6.9	6.2	18.1	8.1	20.8
Ultimate %							
Carbon	69.8–71.5	77.5	80.6	84.2	73.2	68,3	74.0
Hydrogen	5.5–5.6	5.3	4.9	4.3	3.1	5.0	0.7
Nitrogen	1.4–1.5	1.5	1.5	1.2	0.9	1.3	1.0
Sulfur	0.4–0.7	1.2	0.7	0.7	0.9	3.5	3.3
Oxygen	11.2–13.2	8.5	5.4	3.4	3.8	13.8	0.2
Ash	9.2–9.5	6.0	6.9	6.2	18.1	8.1	20.8

FIGURE 1.3: Typical proximate and ultimate analysis for coals and char [7]

combustion calculations, including the determination of coal feed rates, combustion air requirements, and weight of products of combustion to determine fan sizes, boiler performance, and sulfur emissions [8].

The boiler performance can be greatly impacted by the coal quality with respect to efficiency, emissions, fly ash quality, slagging and fouling behavior, but the boiler's maintenance and availability are also influenced. Therefore, it is important to determine coal properties in order to assess if a specific coal or coal blend can be fired in a particular unit.

1.2 Combustion of Coal

A complex series of different reactions are involved in the combustion of coal. A fresh coal particle injected into the combustion chamber, indeed, may undergo the following processes: [9,10]:

1) Thermal shock fragmentation;
2) heating and drying;
3) ignition of volatiles;
4) devolatilization and volatile combustion;
5) char combustion;
6) secondary fragmentation.

Only for some types of coal the events 1), 5) and 6) occur. Figure 1.4 shows the stages of combustion for 10-mm Polish hard coal particle in the air at 850 °C [10].

The rate at which the particle heat and the maximum particle temperature influence the coal reaction process. The heating of the particle is very complicated because, while the particle heats the devolatilization process starts at 300 °C. The heating of particle is retarded by the release of volatile matter from the particle itself. The temperature that surrounds the particle changes as the combustion of volatiles takes place. Gradually, the temperature rises and the moisture present in the coal

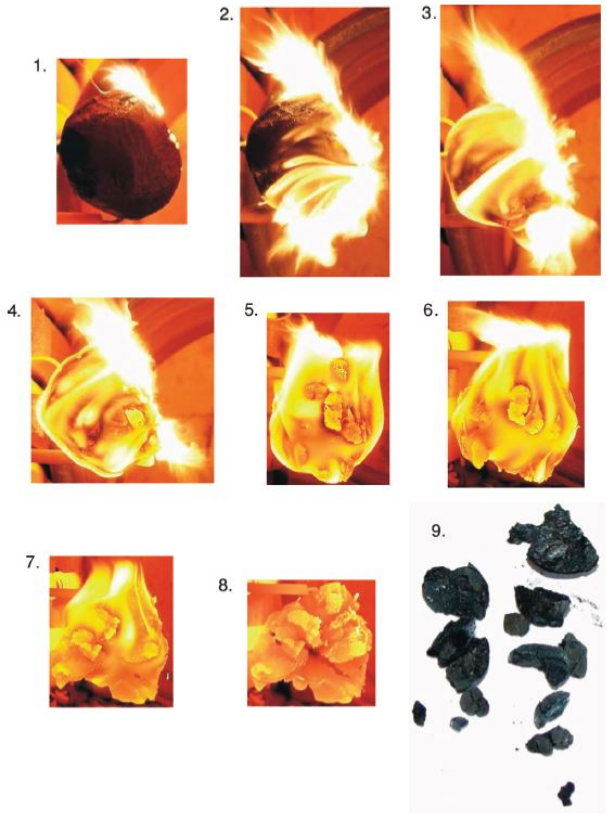

FIGURE 1.4: Stages of combustion for a Polish hard coal particle combusted at 850 °C

evolves. The moisture content in the coal deeply influences the beginning and the duration of the devolatilization process. Lower devolatilization rate and longer devolatilization time are shown in particles with higher moisture contents. [10].

The ignition of volatiles takes place only once certain temperatures are achieved or a visible flame is presented. Furthermore, factors such as coal type, volatiles content, particle size, gas composition, moisture content etc. influence the coal ignition temperature.

The ignition of coal particles affects the stability of flame, the pollutant emissions and flame extinction. Therefore, it is important to study this process in order to design the coal combustor and to control combustion process. The ignition phenomenon is characterized by heat, mass and momentum transfers. The balance between heat release and heat loss influences the ignition temperature.

After the ignition occurs, the events of devolatilization process and the combustion of volatiles take place (Figure 1.4). The pyrolysis or devolatilization is a decomposition of fuel in which a wide range of gaseous products are released. The volatiles are released in stages (Figure 1.4) and are made of several hydrocarbons. The first stage release occurs around 500-600 °C, while the second one occurs at around 800-1000 °C [11].

The volatile matters are constituted by light gases including CH_4, C_2H_4, C_2H_6, CO, CO_2, H_2, H_2O and heavy tars are released during pyrolysis. Once the

hydrocarbons are released, the char remains in the coal structure. The distribution of gases, tar and char are determined by the pyrolysis process and depends on coal type, temperature, pressure, heating rate and particle size [12]. Figure 1.5 shows the schematic process of coal combustion [13].

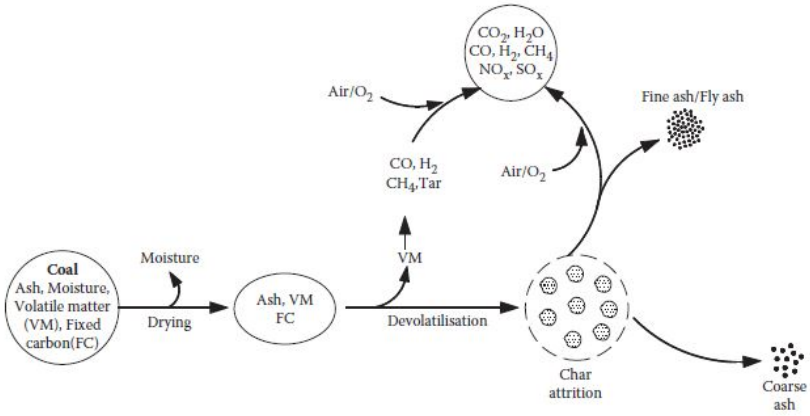

FIGURE 1.5: Schematic process of coal combustion [13]

The coal rank also influences the devolatilization behavior. A sub-bituminous coal (low rank) produces a high level of light gases and very little tar. On the contrary, a bituminous coal produces more tar than a sub-bituminous one and moderate amounts of light gases. A higher rank coal produces low levels of both gases and tar. In figure 1.6 the trend of the pyrolysis with the rank coal are shown [14,15]. The devolatilization of large coal particles has been described by several mathematical. It has been found that heat transfer and chemical kinetics dominate the overall reaction mechanism [9].

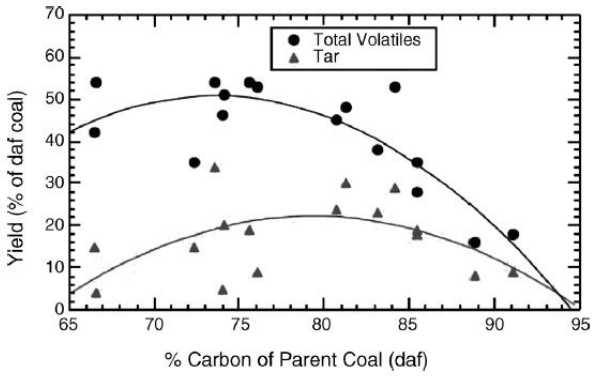

FIGURE 1.6: Total volatile yields and tar from devolatilization as a function of the carbon content of parent coal [14, 15]

The char combustion occurs over a much longer time than the devolatilization and volatile combustion. The char is mainly constituted by fixed carbon, ash, nitrogen and sulfur. The char oxides producing gases (CO, CO_2, SO_2, NO_x) when the temperature reaches 750 °C.

The simplest form of char combustion is the oxidation of carbon to carbon dioxide:

$$C + O_2 \rightarrow CO_2 + 394\ kJmol^{-1}\ (exothermic\ reaction) \tag{1.1}$$

In figure 1.7 is shown the three possible mechanism of combustion of non-porous carbon [13].

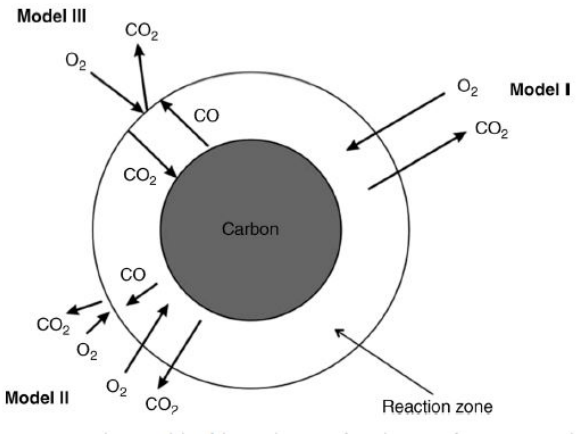

FIGURE 1.7: Three models of the mechanism of combustion of non-porous carbon [13]

In the **Model I** the oxygen diffuses to the carbon surface and oxidizes it to CO. The CO oxidizes further to CO_2 in a gas-phase reaction so close to the carbon surface. In this case the CO_2 may be considered the primary combustion product. Model I is predominant when the Reynolds number flow is low, for large char particles (d > 1mm) or at high temperatures (900–1300).

According to the **Model II** Oxygen diffuses to the carbon surface and produces both CO and CO_2 which diffuse away from the carbon surface. CO further meets in a gas-phase reaction with oxygen arriving from the bulk gas and forms CO_2. If the temperature is low or particle size is small CO may escape into the free stream unburnt. This Model may be described by these three reactions:

$$Surface\ reactions:\ C + \frac{1}{2}O_2 \rightarrow CO + 111\ kJmol^{-1} \tag{1.2}$$

$$C + O_2 \rightarrow CO_2 + 394\ kJmol^{-1} \tag{1.3}$$

$$Gas - phase\ reaction:\ CO + \frac{1}{2}O_2 \rightarrow CO_2 \tag{1.4}$$

Model III is another mechanism which is involved when oxygen cannot reach the carbon surface. Oxygen, indeed, reacts with the CO in a gas-phase reaction away from the carbon surface. A part of the formed CO_2 diffuses back to the carbon surface to be

reduced to CO.

The oxidation reaction of char can be represented for all three models as:

$$C + \frac{1}{\Phi}O_2 \rightarrow \left(2 - \frac{2}{\Phi}\right) CO + \left(\frac{2}{\Phi} - 1\right) CO_2 \tag{1.5}$$

1.3 Pulverized Coal-Firing System

In this section, PC (pulverized coal) combustion, sometimes called PF (pulverized fuel) combustion, is introduced as a more commonly used coal combustion technology. Literally, PC combustion means that the coal received is grounded into fine particles and then burnt in a combustion device, which is called PC fired boiler or PC boiler. In the furnace, PC particles are suspended and surrounded by hot gases and flames. Heat transfer between these fine particles and the surrounding high temperature flue gas is extensive, just as the mixing of them with the oxidant. In addition, the PC particles have a large specific surface area, 2–3 times larger than the one of the raw coal particles, and can therefore be robustly combusted in the furnace. Normally, in the furnace, PC particles can be nearly completely burnt out in about 2–3 s, with a high heating rate of $10^5 - 10^6 Ks^{-1}$. Therefore, PC combustion is regarded as an efficient and intensive combustion method for coals. Conventionally, like other boilers, PC boilers with steam output less than $10kgs^{-1}$ are called industrial boilers. Those supplying steam for turbine in thermal power plant are called utility boilers. PC boilers also can be classified accroding to the pressure (P) of the steam generated. When $P < 4MPa$, $4MP \leq P < 10MPa$, and $10MP \leq P < 14MPa$ a boiler is called medium, high and super high pressure boiler, respectively. When P = 17–18MPa, the boiler is called a subcritical boiler. When main steam parameters are higher than the critical point value (22.06 MPa and 374 °C), there is not a clear distinction between water and vapor, and the boiler is called a supercritical boiler. When the main steam is 25–30 MPa and $\geq 600C$, the boiler is called an ultra-supercritical (USC) boiler.

Power generation is dominated by PC firing. Figure 1.8 shows the schematic of a PC fired thermal power plant. The main constituents are the boiler, the steam turbine, and the electrical generator. The boiler produces steam at the high purity, pressure, and temperature required for the steam turbine that drives the electrical generator. After the steam passes through the turbine, it is condensed in a condenser. In thermodynamics, the working cycle of water/vapor is a Rankine cycle. The boiler consists of a combustion system, a steam generation system, and a few auxiliary systems. The combustion system mainly consists of the furnace and the burners (the fuel nozzles).

PC boilers with large capacity and high parameters are the most widely used in power generation because of their high efficiency, low unit kilowatt investment and operation

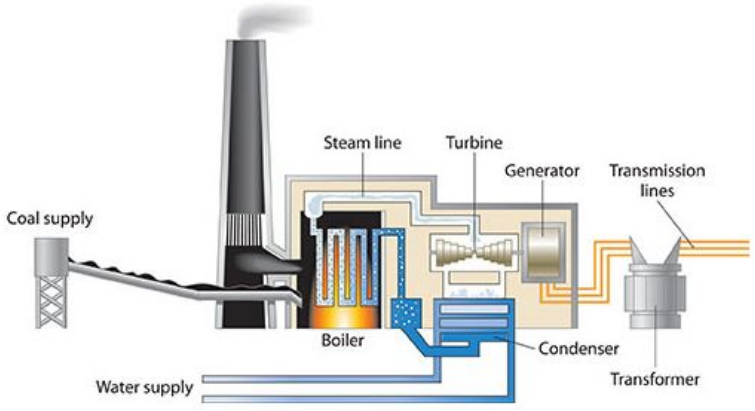

FIGURE 1.8: Schematic of Coal Fired Plant [16]

cost. Figure 1.9 shows the general layout of a 1000 MWe ultra-supercritical (USC) PC boiler recently built in the Zhouxian Power Plant, China [16]. For this USC boiler, one of the largest and most modern units in China, the designated steam output is $3033th^{-1}$, with pressure and temperature of 26.25 MPa and 605 °C respectively. The boiler makes use of once-through and forced circulation, without a water drum installed. The dimension of the boiler is very large. The cross-section of the furnace is $15.6X34.0m$. The furnace height is 64 m. The height of the top beam is 84.4 m. The entire boiler is hanged on the metal structural frame.

1.3.1 Furnace Layout and Firing Type

The boiler furnace is a device meant to organize the mixing of fuel and air for the entire combustion process, from ignition to burnt-out of the coal particles, right after they are airblown in through the burners. Coupling with the burners, the furnace maintains the designated hydrodynamic field inside to ensure the fullness of the flames, protecting the membrane waterwall from erosion and slugging, forming a uniform heat release rate on the wall, realizing efficient combustion and low NO_x formation. The furnace design is important for the hydrodynamic safety of the evaporation heating surface [17,18].

Figure 1.10 shows three typical furnace layouts with different firing styles, tangential firing (T-firing), wall firing, and arch firing. Obviously, the furnace layout strongly couples with the burners and burner arrangement. Specifically, in the tangential firing boiler, once-through burners are used. The furnace is usually square or nearly square shaped in cross section and the once-through burners are usually installed in the corners or on the walls. Wall firing boilers, instead, make use of swirling burners and the furnace presents a rectangular cross section. For large capacity units, the burners are installed on the two longer sides, forming opposed flames in the furnace. The arch firing boiler is specially designed to burn low volatile coals like lean coals and anthracite coals. In

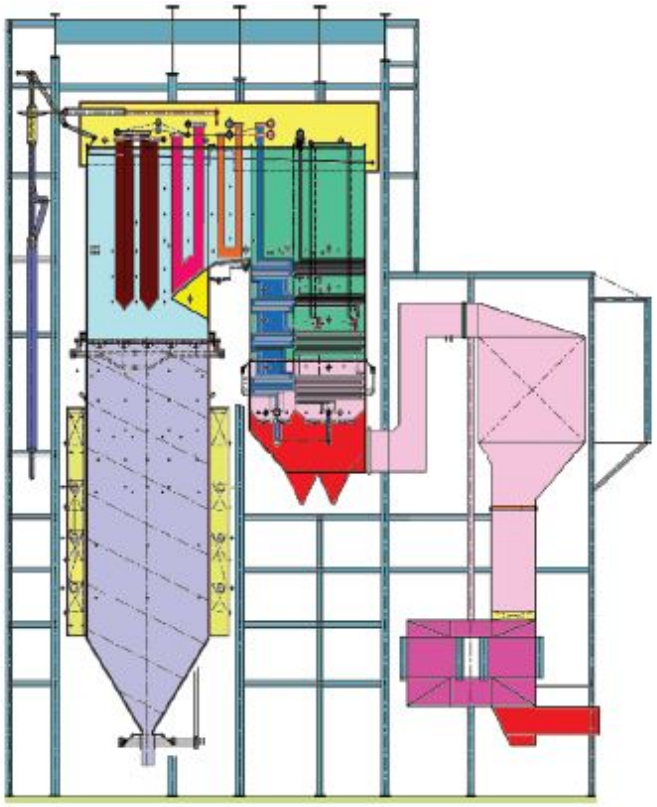

FIGURE 1.9: General layout of a 1000 MWe pulverized coal (PC) fired boiler in Zhouxian Power Plant, China.

such a boiler, the burners can be either once-through type or swirling type, and they are installed on the arch of the furnace wall. The jets shoot downwards from two sides, forming a W-shaped flame in the furnace. It has a rather large bottom furnace that is mostly covered with refractory material, partially to stabilize the ignition and combustion. Obviously, arch firing boiler is more complex and costly in construction.

Figure 1.11 shows the flame shape or temperature distribution for the three typical firing boilers [17,18]. A tangential firing boiler forms a rotating flame in its furnace. In fact, the flame of a corner is supported by the flame of the right upstream corner, and on the other side it supports the flame of the right downstream corner. Thanks to the rotation, the flame is stable and it fills most of furnace. In addition, PC particles can reside for a long time in the furnace, resulting in excellent burn out.

1.4 NO_x Formation Mechanism

Typical combustion gases during PC firing contain mainly two kinds of nitrogen oxides: NO and NO_2. Other kinds of nitrogen oxides, nitrous oxide N_2O, nitrogen trioxide N_2O_3 and nitric anhydride N_2O_5 are encountered only in rudimental amounts, so that do not play any essential role. Among all the nitrogen oxides, nitrogen dioxide

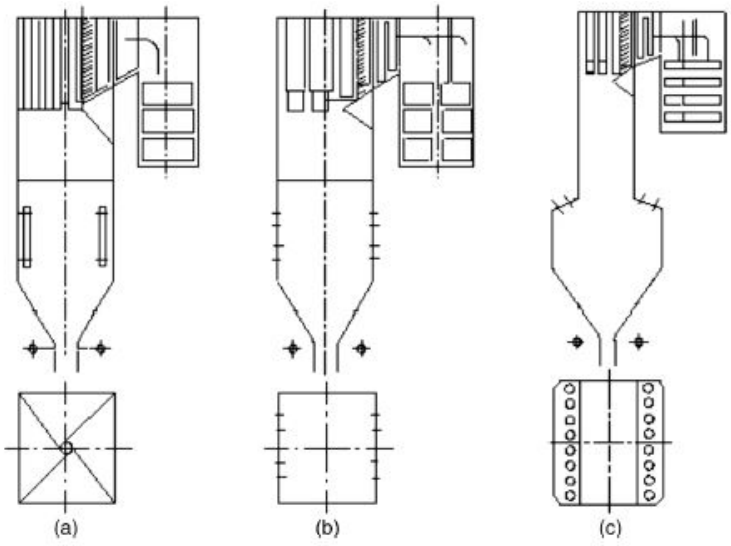

FIGURE 1.10: Typical layout of a pulverized coal fired (PC) furnace: (a) tangential firing, (b) wall firing, and (c) arch firing[17,18]

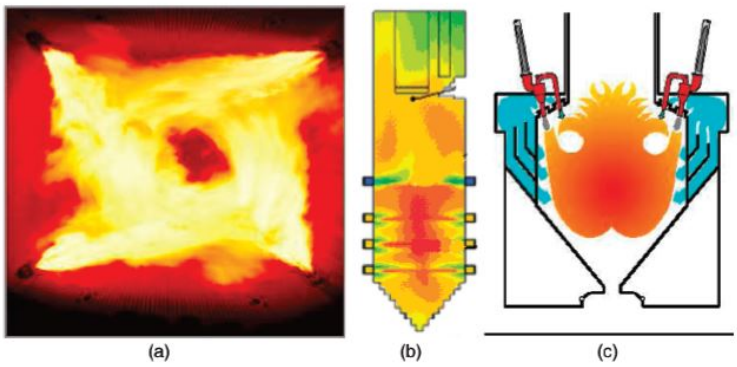

FIGURE 1.11: Typical flame shape in a pulverized coal fired (PC) furnace with different firing styles: (a) tangential firing, (b) wall firing, and (c) arch firing [17,18]

is most harmful.

Nitrogen oxide NO is not so harmful as NO_2. Moreover, NO is the main source of NO_2, because having been emitted into the atmosphere, nitrogen oxides, among others, due to the ultraviolet radiation of the Sun form into nitrogen dioxide. From all the nitrogen oxide N_2O also called laughing gas, is least harmful for the human organism. It is, however, detrimental, because it participates in the reduction of the ozone-layer around our globe and also contributes to the formation of the greenhouse effect, increasing the concentration and amount of triatomic gases emitted.

At the present state of knowledge, four different are known mechanisms causing the formation of NO, and one mechanism causing the formation of NO_2 [18]. In the case of NO these are the mechanisms:

- The thermal mechanism.

- The prompt mechanism.
- By means of N_2O.
- The fuel NO_x.

The formation mechanisms of thermal NO, fuel NO, are dominant [18,19,21]. Understanding the mechanism of the NO_x formation is very important for furnace and burner design and operation, as well as other NO destruction measures.

1.4.1 Thermal Nitrogen Oxide

The thermal mechanism of NO generation is rather well known and has been accepted as a whole. It consists in the reactions of oxidation of nitrogen taken from the air. The rate of these reactions is significant at temperature exceeding 1500 C. These reactions were described by Zeldovich and his co-workers [18,22]. For PC boilers, only small amounts of NO is formed because the furnace temperature is lower than 1500 °C. When the temperature increases exceeding 1500 °C, the reaction rate increases about 6-7 times. From a temperature increment of 100 °C at temperature around 1600 °C, the amount of thermal NO may account 25-30% in the total [21]. The Zeldoivich mechanism will occur shown in the Mathematical Model section.

To sum up this section concerning thermal NO, the following generalizations might be suggested:

1. Thermal nitrogen oxides come into being just behind the flame front in the zone of still high temperature ($T < 1500C$).
2. The value of the NO concentration is determined by the maximum temperature of the flame, the local concentration of nitrogen molecules and, the residence time in the high-temperature zone.
3. Thermal nitrogen oxides are generated mainly in the case of lean flames ($\lambda > 1$).
4. The concentration of thermal NO is much smaller than the equilibrium concentration of NO.
5. During the combustion of hydrocarbon fuels or very moist solid fuels the hydroxide group OH is of essential importance in formation of NO.

1.4.2 Fuel Nitrogen Oxide

Nitrogen is one of the most common elements in nature, furthermore, it is also a component of the vegetable substances from which solid fuels have generated, i.e. peat, lignite, hard coal and anthracite. The nitrogen content in hard coal ranges from 0.5 ÷

2.9%, but it may oscillate, depending on the given coal seam, within of ±20%. The content of Polish hard coal does not exceed 1.7%.

In PC fired boiler, fuel NO is about 70-90% of the total NO. The formation mechanism for the fuel NO is not fully known. It depends on the N-containing compositions left in the residues during the devolatilization process, the PC coal properties, as well as the temperature and the flue gas components during the combustion. The primary nitrogen components of coal rapidly change into stable compounds like hydrogen cyanide HCN, ammonia NH and small amounts of cyanogen CN during the heating process, around the pre-flame zone and at the front of the flame.

The total amount of released N element is called volatile-N. The N element remaining in the char is called char-N. The NO products of volatile-N and char-N are called volatile NO and char NO, respectively. The most important fuel-N species are HCN and NH_3. Their ratio depends on the coal type, volatile properties, combination of N with HC compound, combustion temperature, O_2 concentration, and so on. Normally, HCN, for bituminous coal, dominates over NH_3 in fuel-N, while for low rank coal more NH_3 is formed than HCN in fuel-N. Both HCN and NH_3 are produced in small amounts in anthracite coal. When fuel-N is in aromatic form, it is converted mostly into HCN during the devolatilization process. When fuel-N is in amine form, it is converted mostly into NH_3. The production of HCN and NH_3 increases with temperature. When the temperature is over 1100 °C, NH_3 becomes saturated and more fuel-N is converted into HCN.

Part of fuel-N can react with other species to give N_2, and part of the product NO is reduced to N_2 as well. The maximum conversion percentage for volatile-N into NO is about 50%. For this reason not all of the fuel-N is converted into NO. Consequently, it is of great significance to convert fuel-N into volatile-N.
There are three main paths for NO destruction:

1. Reduced by CH_i radicals or carbon, into N_2.
2. Reduced by NH_i and N radicals into N_2.
3. Reduced by CH_i radicals or carbon, but into N_2O.

1.5 Techniques for the reduction of NO_x emissions during the combustion

The reduction of NO_x emissions in the course of combustion belongs to the so-called primary methods of the decrease of the NO_x emission. These methods consist

in an interference into the combustion process inside the combustion chamber. The emission of NO_x can be reduced in the course of combustion by:

- Staged combustion.
- Reducing the temperature in the flame.
- Supply of ammonia or urea into the combustion chamber.

In the following part the first two methods of low-emission combustion will be presented and analyzed.

1.5.1 Staged Combustion

Staged combustion is based on the assumption that, at some given stage, combustion takes place with a depletion of oxidizers ($\lambda < 1$). Two technologies of staged combustion are currently used, the one by air staging and the one by air and fuel staging [24]. Figure 1.12 shows schematically the principle of the functioning of both these methods.

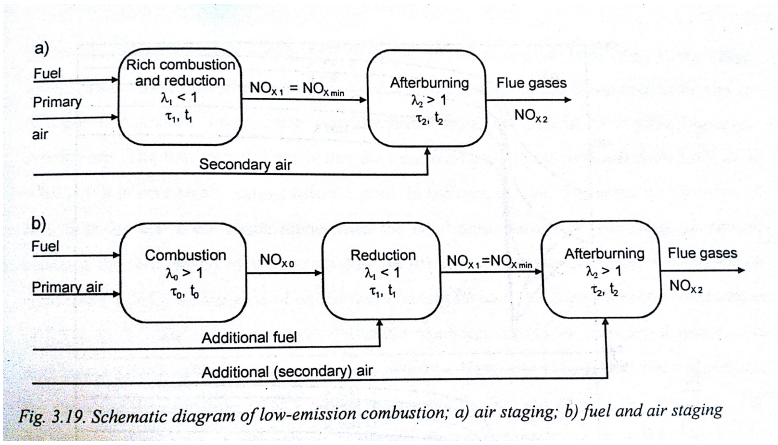

FIGURE 1.12: Schematic diagram of low-emission combustion; a) air staging; b) fuel and air staging [24]

In case of combustion with air staging (Figure 1.12a), the primary excess air ratio during the first stage of combustion should be $\lambda_1 = 0.6 \div 0.8$. Under such conditions a relatively large amount of reductive radicals (HCN CH_i or NH_i) is produced, which consequently reduces the existing NO_x and prevents larger emissions of NO_x.

In order to prevent the formation of relatively large amounts of the products of incomplete combustion (CO, soot and carbon in flay-ash or slag), a second stage of combustion must be realized by reburning of CO, soot and carbon by means of secondary air supplied to the after-burning zone. The excess air ratio λ_2, otherwise, would exceed the value of 1. In a combustion with air and fuel staging (Figure 1.12b) a normal combustion with an excess of air $\lambda_0 = 1.05 \div 1.2$ occurs in the first stage, in which the normal amount of NO_x is generated. In the next stage, a reducing zone with

an excess ratio of $\lambda_1 = 0.7 \div 0.9\%$ is created by additional fuel supply. Under these conditions, reductive radicals CHi are formed, which transform NO in N_2. During the third stage the secondary air is supplied so that the total excess air ratio becomes $\lambda_2 > 1$. Thanks to CO, soot and carbon material contained in the ash and slag can be completely combusted.

The air staging constitutes the theoretical basis for the technology of low emission combustion, e.g. the OFA, SOFA (Over Fire Air), LNCFS (Low NOx Concentric Firng System) and their combination, as well as low-emission burners with an external staged air EASB (Externally Air Staged Burner), aerodynamically stage air AASB (Aerodynamically Air Staged Burner) and burners with externally staged air combined with a pre-combustor chamber, ASPB (Air Staged Precombustor Burner). Such burners were firstly developed by the IFRF (International Flame Research Foundation) in Ijmuiden, Netherlands [24].

A disadvantage of the air staging technology is due to the following factors:

1) A high effectiveness of the reduction of NO_x emissions by 50% and more requires a long retention time in the reducing atmosphere, amounting up to 4 sec. The designs of many older working power boilers prevent such a long retention of the reagents in the reduction zone of the combustion chamber.

2) A rather high CO emission and considerable content of carbon in the ash and slag exceeding 5%

3) Difficulties concerning the stabilization of the flame and the slagging of the combustion chamber.

4) The effectiveness of the reduction of the NO_x emission is limited in the case of coal with small content of volatile particles and furnaces with wall swirled burners.

The air and fuel staging method is also called "reburning" or "fuel staging". The efficiency of reburning is determined by the following parameters:

1) In the first stage zone of combustion: by the value of the excess ratio λ_0, the kind of applied basic fuel and the level of $NO_{x,0}$ emission from this zone.

2) In the reduction zone: by the kind of reducing (reburning) fuel and share of nitrogen in this fuel, the rate of mixing the reburning fuel with the combustion gases, the excess air ratio λ_1, the residence time τ_1 and the temperature level in the reduction zone t_1.

3) In the after-burning zone: the total excess air ratio λ_2, the temperature level in this zone and the rate of mixing with reburning air.

1.5.2 High Temperature Air Combustion Burner

A new low-emission technique of combustion of gas, solid and liquid fuels is based on a very effective initial preheating of the combustion air up to $800 \div 1300C$, which

allows a simultaneous recirculation of the hot flue gases. This technique is called Highly Preheated Air Combustion (HTAC) or Excess Enthalpy Combustion (EEC) or Flameless Oxidation (FLOX) or Courless Oxidation or MILD combustion (in Italy). The patented HTAC (High Temperature Air Combustion) burner, whose work principles are shown in figure 1.13, can be used in both wall fired and tangential fired PC boilers.

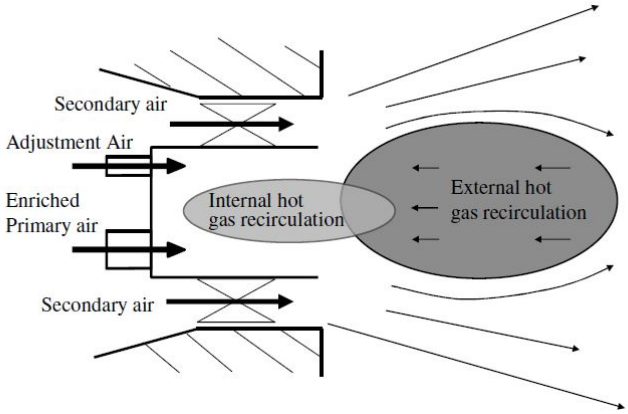

FIGURE 1.13: Schematic diagram of HTAC (High Temperature Air Combustion) burner

The HTAC burner is featured with a preheating chamber with one end connecting to the primary air and the other end opening to the furnace. Inside the specially structured chamber, hot flue gas recirculation is effectively established. The primary air flow is constituted of concentrated PC particles. A combustible mixture, rather than a combustion air, is highly and rapidly preheated. An air stream is induced from the back of the chamber to adjust the vacancy corresponding to the changes in fuel properties, boiler loads, and other conditions. The burner does not only hold the performance of traditional HTAC technology, valid only for gaseous fuels, but it also excels in terms of slagging prevention, automatic control, and simple operation. The performance of HTAC ensures the NO_x reduction. The HTAC technology is the main topic of this work. The next chapter is focused on the state of the art of MILD and Oxy combustion.

1.6 Carbon Dioxide Emissions, Storage and Capture

Coal combustion is one of the largest sources anthropogenic CO_2 emissions. Every year, about three million tonnes of CO_2 are emitted in the atmosphere from a typical 500 MW_el coal-fired power plant, the equivalent of the total CO_2 emissions from 374000 passenger cars.

The carbon (CO_2) capture and storage (CCS) is one of the many options to stabilize CO_2 levels in atmosphere. This technology allows to remove the CO_2 from emission gases by storing the transported CO_2 in a location where it is isolated form the atmosphere

(sequestration).

Currently, the technologies for the CO_2 capture that have reached level of industrial-scale demonstration are the following:

- Post-combustion capture: the nitrogen may be direct removed by the flue gases through the action of absorbers and cryogenic coolers action to produce high CO_2 flue gas.
- Pre-combustion capture: the coal is gasified with pure oxygen in order to obtain a gaseous fuel constituted of carbon monoxide (CO) and hydrogen (H_2. The CO and water is converted to H_2 and CO_2 by means of the water-gas shift. A physical sorbent is then used to capture CO_2.
- Oxy-fuel combustion: the nitrogen and the oxygen are separated in advance, and only the oxygen is fed into the combustion chamber. The coal is then burnt in pure oxygen (oxygen-rich environment), either with oxygen-enriched air or in the mixture of oxygen and CO_2-rich recycled flue gas, instead of in normal air. Thereby the CO_2-enriched flue gas is ready for sequestration once water is condensed from the flue gas and other impurities are removed.

The oxy-fuel combustion is one of the most elegant approaches for CO_2 capture. Figure 1.14 shows a plant scheme of this technology in which the pulverized coal is fired in an oxygen-rich environment.

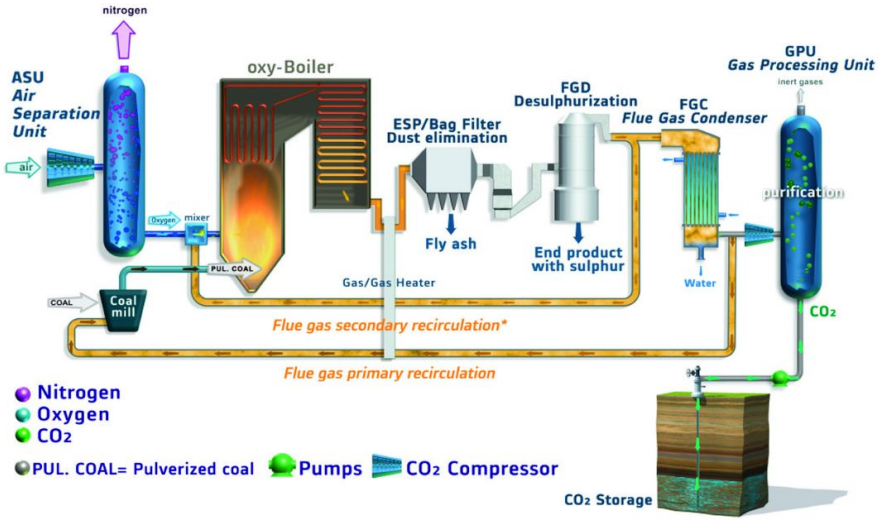

FIGURE 1.14: Schematic oxy-fuel plant layout

There are some variations of the possible systems in which the pulverized coal may burn in an oxygen-enriched environment. Because this technology is one of the two subjects of this work, further detailed studies, such as the state of art, the concepts and components, the combustion in oxy-fuel etc. will be conducted in the next chapter.

Chapter 2

State of the Art of the MILD and Oxy-Fuel Combustion

The definition of the terms "high temperature air combustion (HiTAC)" and "moderate or intense low oxygen dilution (MILD)" combustion has been given only in the past few years. The definition of these terms was, indeed, first published in the Combustion Institute Proceedings in 1998 [25] and then in the Mediterranean Combustion Symposium Proceedings in 2000 [26], only after series of publications which have stressed on features of interest pertaining to energy conversion and pollutant formation reduction. Moreover, proceedings papers concerning HiTAC [27,28] have added information on possible variants of the process. The review paper of Cavaliere and de Joannon [29] and the monographic papers of de Joannon et al. [26, 30] and Peters [31] have discussed the possibility of extending the application of MILD combustion by studying the process in a simple well-stirred reactor. Although there are no difficulties in classifying a process as HiTAC or MILD combustion when the process is evaluated based on its beneficial effects, it is not always clear to which elementary process these effects should be attributed.

2.1 MILD Combustion

2.1.1 Basic Principles of MILD Technology

The basic principles of this technology are as follows [33,24]:

1) The temperature of combustion air has to be higher than the autoignition point of the combustible mixture. The combustion air is preheated to a temperature higher than 800 ℃ (for natural gas as fuel). In such conditions, the phenomenon of combustion is in its character similar to a volume and flameless combustion. Thanks to this, the temperature level inside the combustion chamber is relatively uniform, and temperature peaks ($T \geq 1400C$) at which thermal nitrogen oxides are formed, are avoided.

2) The fuel nozzles are positioned away from the air nozzles supplying the gas fuel into hot flame gases. Both fuel jets and air entrain large quantities of combustion products and substrates before their mixing takes place. Conventional stable flames are possible over the whole range of chamber temperature, but at ambient temperature of air it is possible only for exhausted gas recirculation ratio up to 0.3. The stable HTAC is possible only when the temperature is greater than 800 °C and when the value of recirculation ratio is higher than 3. For this reason, it is not possible to operate a burner of HTAC in a cold combustion chamber. Figure 2.1 shows a schematic diagram of the stability limits from different combustion modes [34].

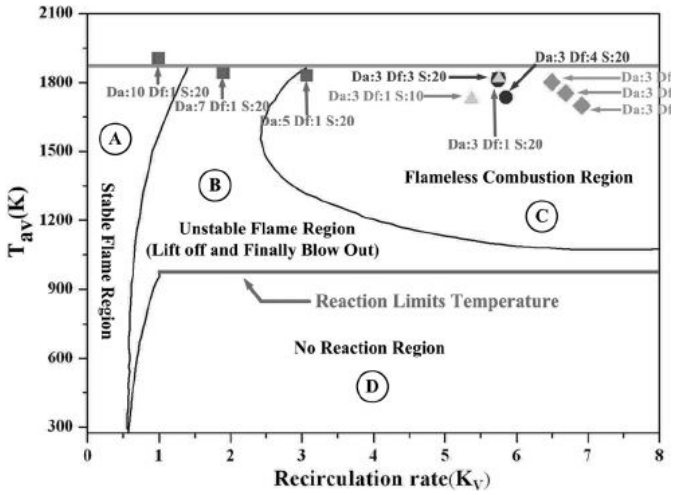

FIGURE 2.1: Different combustion modes, 1, conventional, 2, unstable HTAC, 3, stable HTAC. [34]

MILD Combustion is defined by Cavaliere and de Joannon [29] as follows:

> A combustion process is termed mild when the inlet temperature of a reactant mixture is higher than the self-ignition temperature of the mixture, whereas the maximum allowable temperature increase with respect to the inlet temperature during combustion is lower than self ignition temperature

Figure 2.2 shows the concept of the HTAC, compared with that of a conventional furnace combustion [35]. The direct combustion between fuel and high temperature fresh air provides extremely high temperature flames. Because of the modifications of the furnace geometry, the shear motion of high velocity inlet air not only produces the extinction of base flames, but also makes the dilution of air with burned gas (BH) occur prior to the combustion, by separating fuel and air inlets. Keep in mind that those are the conditions in which ordinary combustion cannot be sustained with ambient temperature air. The fuel injected separately into the furnace also entrains burned gas in the furnace, and some changes in the fuel, such as pyrolysis. The combustion follows

in the mixing zone of fuel and diluted air with a large amount of burned gas (B*F*BH). Consequently, the combustion reactions may occur between fuel and entrained product (B*F). The flame may change, due to a low concentration of oxygen caused by the high rate of recycling of burned gas. Direct combustion between fuel and fresh air (F*A) occurs in the near-field of the burner, when the combustion occurs without preheated air. The greatest emission of nitric oxides from the furnace are formed close to the burner, in which the Combustion (F*A) shows the maximum temperature in the furnace. However, combustion in this region is essential to sustain the combustion in the furnace, and the whole flame cannot exist if extinction occurs in this portion.

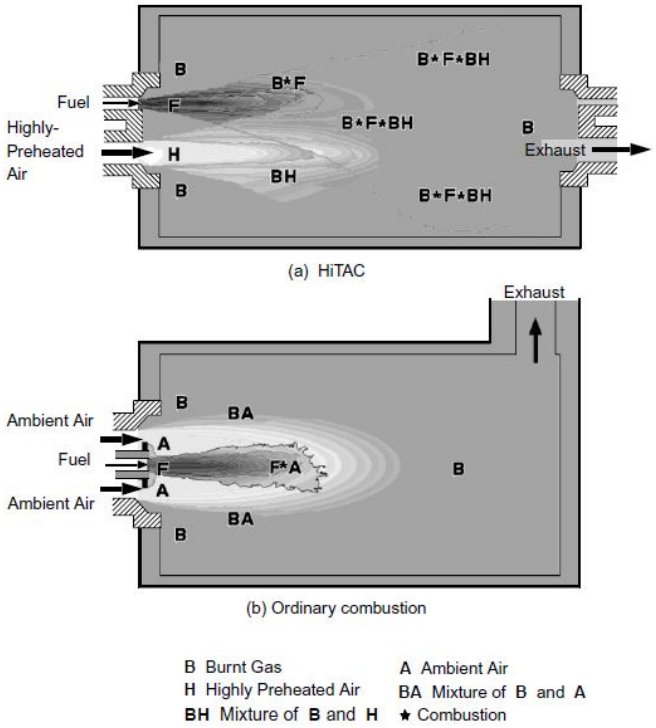

FIGURE 2.2: Mixing and combustion in furnace.

2.2 Literature Review

The first CFD modeling of HTAC technology effort originated from Japanese industry where Ishii et al. [108,109,110] simulations of an experimental continuous slab reheating furnace with particular attention on NOx formation were carried out. The study showed how the numerical code could describe the main characteristics in terms of the flow and temperature fields and how to detect the best low-emissions furnace configuration. Other simulations made by Guo et al. [111] put in evidence that the combustion in preheated air and flue gas recirculation improved the combustion efficiency and decreased NOx emissions but unlikely was not a correct evaluation

about the temperature uniformity and the contributions of thermal NO and prompt NO emission.

A study made by Wunning [112] proved that, the temperature and the flow conditions in the combustion chamber were suchlike for experiment and measurements excluding the areas close to the burner. In 1997 the IFRF [113,114] performed new measurements of temperature field, velocity, the pollution emissions and heat flux and this set of data was the starting point for Orsino et al.[115] who built models to predict the flow , chemistry and temperature field. Another study made by Mancini and Weber [116] put more attention on the predict of NO_x emissions, in particular on the rule that temperature has on them.

Going ahead with his study, Mancini [117] focused on the IFRF experiments making a comparison between some turbulence models and results showed as the entrainment in the weak fuel is not related to any chemistry model.

Plessing et al. [118] focused their attentions on Laser Optical investigation of HTAC system with strong exhaust gas recirculation putting in evidence how it is possible to make a prediction of flow field and heat transfer fired in FLOX mode. Contemporary studies by Weihong and Blasiak [119,120,121] focused on of the calculation of numerical parameters in a single propane gas combustion through different model such as k-ϵ model, EDC concept with multistep chemical reaction and Discrete Ordinates for the radiation model. The advantages of HTAC technology were assessed in terms of large flame volume, low temperature and greater heat transfer. Dong and Blasiak [122] performed numerical simulation basing on the model of IFRF experiments on gas combustion with preheated air and the results were good but the model itself could be improved. The simulation made on a single fuel jet flow in high temperature showed a small difference in the turbulent models for example Large Eddy simulations or Reynols Stress Model. The simulation made by Pasenti et al. [123] on a 200 KW FLOX burner under cycling showed the increase of NO_x emissions increasing the furnace exit temperature. The simulation made by Tobacco et al.[124] regarding a combustion chamber equipped with a FLOX burner showed how in the calculations the k-ϵ RNG model was used as turbulence model and 2 other models(PDF and EBU models) to compare which one was the best way to make a prediction of the ignition temperature. Cavaliere and de Joannon [125] concentrated their study on Mild combustion of Methane analyzing the measurements on the chemical side, in particular on a well stirred reactor at low oxygen concentrations. The results showed how in a determinate range of temperature the gas reached super adiabatic values. Going on the analysis of this reactor with numerical methods, was possible to predict the region of flame oscillations and shape but not the amplitude and the frequency at high temperature.

The first does not succeed in the purpose, the second one made a correct prediction about the area close to the burner but not at the end of furnace. The superiority of EBU model in order to predict NO furnace emission was confirmed by Porcheron et al. [126] simulating a test furnace fired using NFK burners.

Another kind of test in a semi industrial environment were performed by Corus RDT [127]. For the calculations FLUENT standard sub models were used and three models were analyzed: PDF equilibrium model, PDF flamelet model and Eddy Break Up model and using the Discrete Ordinates as radiation model.

All the models predicted in a good way from a qualitative point of view the air and fuel jet behavior with the corresponding chemical reactions and diffusion processes but there are margins of improvement from a numerical point of view.

For the experiment built by Lupant et al.[128] were used as well the sub models present in the CFD FLUENT code. In particular were used the k-ϵ model for turbulence and a PDF and a Finite Rate/Eddy-Dissipation Models for chemical turbulent combustion. At the ends the values measured of NO were the same as the computed ones, but the temperature field used for NO computation was substantially different from the measured values.

The works mentioned till now were about the combustion of gaseous fuel but the CFD modelling of HTAC was also implemented for oil and coal combustion.

Misztal [129] used the CFD FLUENT code to simulate a combustion chamber fired with oil operated under HTAC conditions. The prediction made using as model for turbulence the k-ϵ and Discrete Ordinates (DO) model for radiation described in a correct way the oil combustion.

Heil et al. [130] started experiment on MILD coal combustion under high pressure that was modelled by Erfurth et al. [128] using the CFD FLUENT code. This simple mathematical model was able to predict well the flow field and the recirculation inside the combustion chamber. The temperatures were over- predicted compared with the experimental data while the species concentrations differed substantially from the measured values.

2.3 Characteristics of Combustion Chamber

The previous section places MILD combustion in an atypical range of temperatures with respect to all other oxidation processes associated with combustion. Combustors working under MILD combustion conditions have been developed and studied both in industry and academia [36,37]. One of the most striking characteristics of such combustors is that they develop oxidation processes with negligible visible emission. For this reason, they are called flameless or colorless flames and generally involve several hydrocarbon fuels when air, diluted with flue gases, is used. An

example of such a unique phenomenology is shown in the pictures given in figure 2.3. Figure 2.3a shows a traditional flame combustion in which the fuel is fed by a central nozzle. In this case a diffusion-controlled flame with both shape and visible emission of traditional characteristics was stabilized. A compact yellow region develops around the burner axis and extends throughout the combustion chamber. Figure 2.3b, instead, shows a flameless combustion. This condition can be obtained by changing the fluid-dynamic configuration. In this case, natural gas was injected by lateral nozzles into the exhaust gas flow of the internal recirculation drawn into the inlet air flow. The "inertisation" and preheating of reactants are carried out to a large degree, upstream of the burner because combustion air is vitiated (with inert gases) and preheated. Quite evidently, reaction steps follow chemistry paths which are different from the conventional burner-stabilised flame and there is no wonder that pollutant formation and heat flux distribution are quite different. This may be exploited in practice for clean firing technologies and for improved process performance.

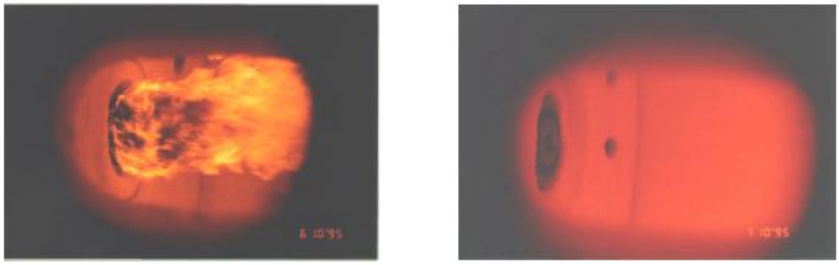

(A) Flame mode, normal air at 250 °C

(B) Flameless, vitiated air O_2 10% at 500 C

FIGURE 2.3: Flame and flameless firing of heavy fuel oil

Temperature and species concentration profiles measured in burners working in diluted high-temperature conditions present a fairly uniform distribution. The graph in figure 2.4 shows the wall radiative heat flux on left-hand axis and the wall temperature on the right-hand axis as a function of axial coordinate. Both wall radiative heat flux and wall temperature are quite constant along the whole furnace [38]. This testifies that a main reaction zone, with strong gradients, is not presented in a localized region of the combustion chamber, as it would be generally expected for a standard furnace. In this case, the reaction zone extends almost in each point of the available volume [29,38].

This graph highlights another characteristic: a relatively high radiative heat flux. This is due to high concentrations of species strongly emitting in the infrared region, such as CO_2 and H_2O.

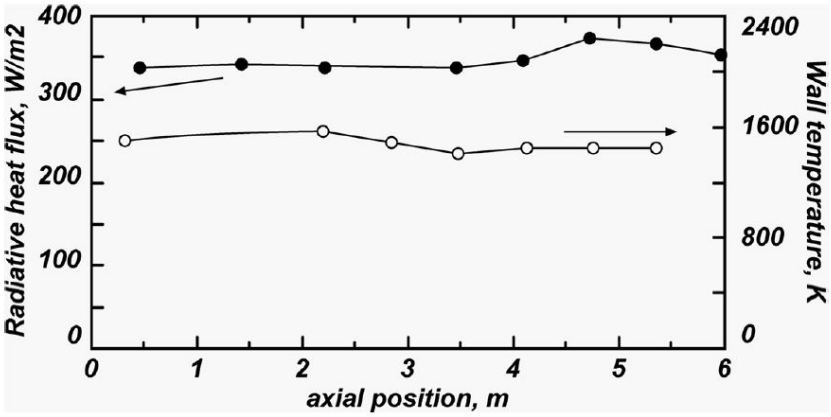

FIGURE 2.4: MILD Combustion regime: Radiative heat flux (left-hand axis) and wall temperature profile (right-hand axis) [38]

2.3.1 Burners of MILD Technology

Commercial applications of HTAC technology are present in both ceramic and steal works industry, especially in the Far East [33]. In the case of high temperature melting furnaces a regeneration inside Regemat burners is applied. In this case, flue gases with a high temperature transfer their high enthalpy to the flux of combustion air via a set of regenerating heat exchanger of the "'honeycomb"' type which are integrated with the burners. The German version of this technology is called FLOX (FLameless OXidation) and their thermal input is typically not larger than $200 \div 300kW$ [24,34]. The FLOX burner is composed by a central jet of fuel and six or twelve air jets. Figure 2.5 shows the FLOX burner.

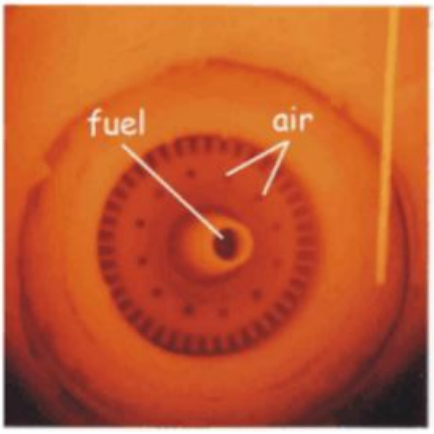

FIGURE 2.5: FLOX burner

Another kind of burner is the Nippon Furnace Kyogo (NFK) design, in which the fuel (natural gas) is injected through several injectors located on the circumference, while the oxidizer is injected through a central jet. Figure 2.6 shows a schematic NFK/IFRF [39,40] burner design.

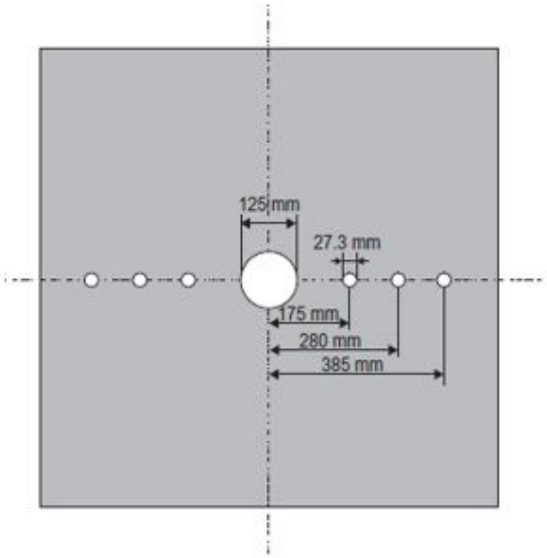

FIGURE 2.6: NFK burner

Both of the burners share the same goal: allowing the fuel to burn in a diluted environment with the combustion products. This is made possible by injecting the preheated air jets into the combustion chamber with very high speed. For this reason, the fuel does not mix with the air (traditional combustion). Instead, it first entrains a large amount of inert gases like N_2, CO_2, H_2O, and then it burns with some oxygen, typically not more than 5%. The high momentum of the oxidizer jet produces a strong internal recirculation of combustion products. This is the key point of MILD combustion: creating a strong internal recirculation. This condition leads to uniform temperature and species concentration distributions in the whole volume of the combustion chamber. Because the fuel does not rapidly mix with the air jet and therefore does not burn with the oxygen, the ignition takes place in a diluted environment. A lower peak of temperature is consequently generated. Nevertheless the temperature is lower than a traditional combustion, but at the same time, the MILD technology provides high and uniform values of total heat fluxes in the combustion chamber. This is due to the radiative properties of combustion products, which recirculate in the chamber.

2.4 Application of MILD combustion in Furnaces

HTAC technology has mainly used in industrial applications together with heat recovery systems in order to save fuel. The number of of industrial furnaces which applied this kind of technology are in the order of some hundreds where combustion air is highly preheated which leads to reduced specific fuel consumption. So far, there is an increase of efficiency of 30% than using conventional furnaces and there were a decrease of the emission of harmful substances including NO_x emissions [131]. The common

furnaces has a max working temperature about 500 degrees that is really low compared to the HTAC concepts ones that present temperature above the self ignition point (850 degrees) that allows savings in terms of fuel consumption and reduction of CO_2,NO_x and other pollutants emissions to the environment. At the same time the size of the furnace can be decreased up to about 20% [132]. Metal and steel industry, ceramic industry and chemical industry are the ones that could benefit to a grater extend of the advantages of these burners [133, 134, 135, 136].

2.5 Application of MILD Combustion in Gas Turbines and Boilers

2.5.1 Application in Coal-Fired Boilers

Although the main goal of this work is to study and analyze the application of two technologies (MILD and Oxy-Fuel combustion) which have been used separately until this point, it is interesting to analyze the application of MILD combustion in gas turbines and in power station boilers fired pulverized coals. Furthermore, because the most applications are mainly in the field of industrial furnaces, research should aim at the possibility to apply this technology to power plants. It is expected that the application to the power plants provides the same advantages of the MILD application to the industrial furnace. This is confirmed also by the Natalia's work [41,42].

An issue of MILD or HTAC combustion is how to utilize the enthalpy of the boiler exhaust gas to heat up the air at very high temperature. A conventional boiler is made up of two sections: the radiative heat transfer section and the convective heat transfer one. Because the adiabatic flame temperature in HTAC boiler is higher than that of a conventional boiler and the heat transfer inside the boiler is dominated by radiative phenomena, it may be advantageous to design a boiler without the convective section by maintaining the same thermal output. This will lead to a significant reduction of the boiler's size and cost.

2.5.2 Application in Gas Turbines

2.5.2.1 External Control of MILD Combustion

It is well known that gas turbines present some constraints which are difficult to overcome. For instance, the material robustness of the blades along with mechanical tolerance and lubrication problems, limit the turbine inlet temperature and the compressor/turbine efficiency. A practical high performance limit for the temperature is around 1573 K, whereas a more ambitious feasible limit can be around 1673 K. The

compressor outlet pressure, which is also the pressure in the isobaric combustion chamber, can vary between 3 and 30 bar, while the inlet combustion chamber temperatures, consistent with these values, can range between 200°C and 600°C. Therefore, inlet and outlet temperatures of the gas turbine combustion chamber are suitable for MILD combustion applications as long as it is recognized that autoignition of mixtures is favored at high pressures. There is anyway the need to discuss Specific temperature and pressure limits for each application in reference to a variety of possible configurations that would ensure their feasibility. These configurations fall into two categories: MILD combustion with external control (independent source, external recirculation, and sequential combustion), and MILD combustion with internal recirculation. The dilution of the oxidant with inert gases can be achieved in open and closed gas turbine cycles through species that are not related to the gas turbine itself. For economic reasons the type of gas, for open cycles, is flue gas from a combustion source. This makes the gas turbine outlet flow a possible candidate, as in sequential combustion and in systems with external recirculation.

In gas turbines, the flue gas and air can be mixed, compressed, and distributed to the combustion chamber inlet with the oxygen concentration consistent with ignition and maximum allowable temperatures for MILD combustion. Therefore, the goal is to create at the combustion chamber inlet very high compression ratios with high temperature in order to favor the autoignition. These elevated ratios are convenient not only for very high compressor/turbine efficiencies, but also for high turbine inlet temperatures. This is shown in figure 2.7 in which the efficiencies of a Brayton cycle, which is based upon thermodynamic conditions sketched in the inset of the figure, are reported for two different final combustion temperatures and two values of the compressor/turbine efficiency.

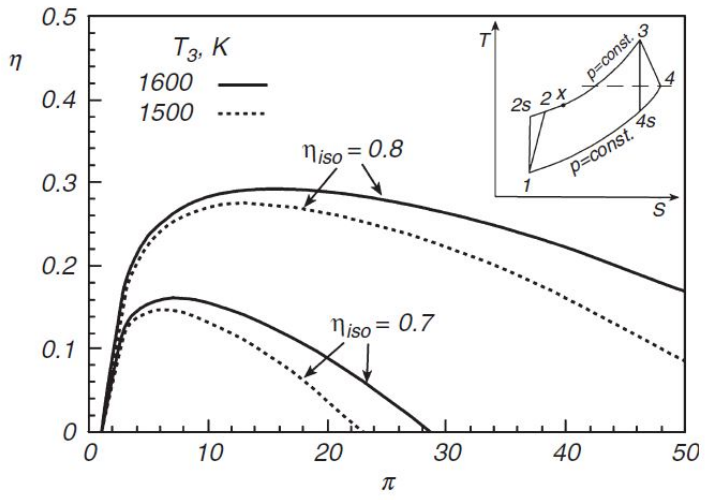

FIGURE 2.7: Efficiency of Brayton cycle as a function of compression ratio for two final combustion temperatures (T_3) and two compressor/turbine efficiencies

Figure 2.8, instead, shows the importance of high compression ratios in order to achieve high values of T_3 and η_{iso} for suitable use in MILD combustion. Both the inlet temperature and the oxygen concentration depend on the compression ratio. This graph shows the inlet temperature (short dashed line), the oxygen concentration (continuous line) referred to the left axis and the autoignition delay time (dotted line) referred to the right axis.

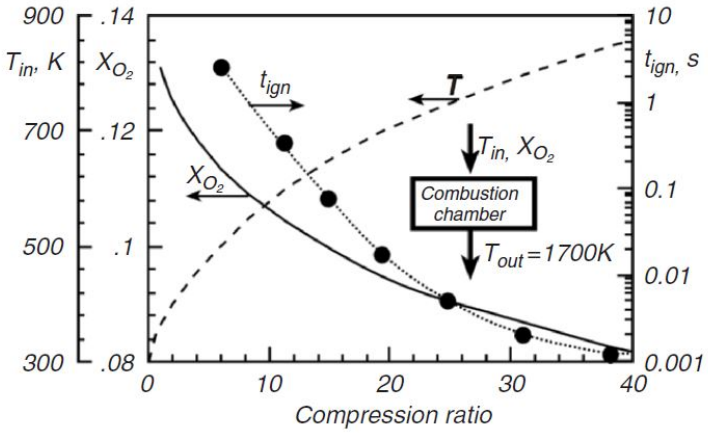

FIGURE 2.8: Temperature and oxygen concentrations at combustion chamber inlet Vs. compression ratio for a fixed inlet turbine temperature on the left axes and the related ignition delay time on the right axis.

In diluted case the autoignition delays decrease with the increasing of pressure and temperature. But this benefit is partially counter-balanced by the dilution itself. This is made possible by the oxygen concentration decreases and according to Joannon et al. [29] this parameter affects the autoignition delay following a power law with an exponent of 0.3 for temperatures lower than 700 K, of around unity for temperatures higher than 1000 K, and of around 2 in a narrow temperature range centered around 900 K.

Another application can be in a closed cycle turbine. In this case an internal heating system based on MILD combustion can substitute the heater. To allow the autoignition to occur in a time consistent with the allowable residence time in the engine, both temperature and pressure would have to be sufficiently high for autoignition and thus separate the combustion products from the working fluid.

Another potential application is a semi-closed combined cycle gas turbine proposed by Camporeale et al. [43]. Figure 2.9 shows the schematic of a plant layout.

The compressor C1 compresses the air at low pressure, while the recuperator R2 heats it. When the air mixes with recirculated flue gases, the whole is compressed with the high-pressure compressor C2 and heated in the recuperator R1. In order to provide an oxygen concentration of 10% and a temperature and pressure of 1000 K and 20 bar, respectively, the mass flow, the compressor, and the heaters are adjusted. The cooled blade turbine T1 allows the combustion products to expand at 1700 K. The

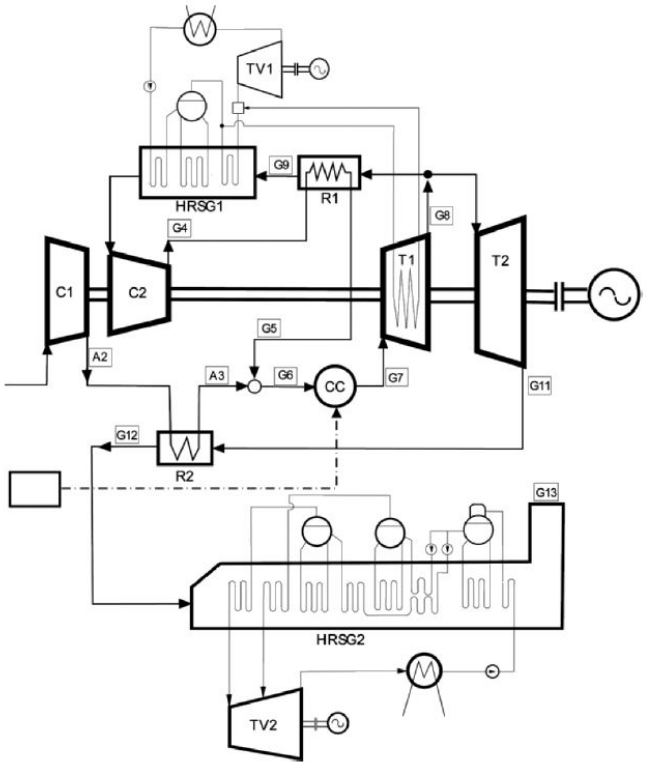

FIGURE 2.9: Plant layout of a semi-closed combined cycle gas turbine plant where the MILD combustion concept is used. [43]

turbine T1 first feeds the heat recovery steam generator HRSG1, then the low-pressure turbine T2 and the heat recovery steam generator HRSG2. The thermodynamic cycle efficiency of this plant has been assessed to be around 0.6 for a power corresponding to 100 kg/s under realistic efficiency assumptions of the components. There are other applications of MILD combustion of gas fuel in cycle proposed by some authors [44,45] According to the author, it is interesting to highlight a last example of external control of MILD combustion conditions is the sequential combustion used in some recently designed advanced turbines. (www.power.alstom.com), represented in figure 2.10

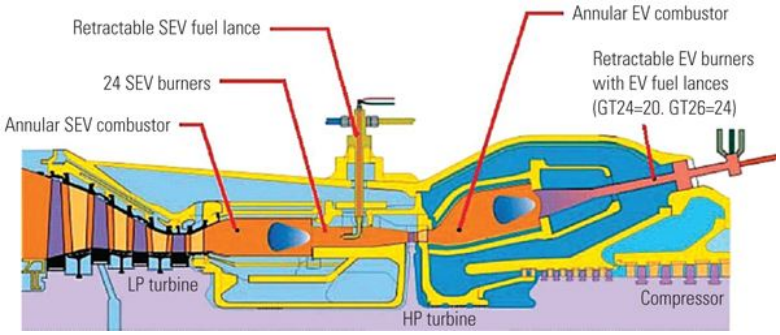

FIGURE 2.10: Layout of sequential combustion gas turbine (www.power.alstom.com).

The concept leverages the unique advantages of the sequential combustion engine designed to allow the combined-cycle plant to achieve best-in-class turndown while

maintaining low emissions and very high efficiency, if compared to single combustor engine architectures. The first combustion chamber, on the left of the figure, is close to the air-diluted system designed for low NO_x emission. In the central part of the system, the turbine extracts part of the enthalpy content so that the stream outlet is formed, starting from partially exhausted gas with a lower content of oxygen if compares to standard turbine at temperatures. The exhausted gas reburns in the second combustion chamber, as portrait-ed on the right side of figure 2.9

2.5.2.2 Internal Control of MILD Combustion

The design of the system described in the previous subsection refers to the gas turbine configurations, which work under well-defined conditions that can be controlled during plant operation. Alternative combustion configurations meant to produce local MILD combustion conditions, such as high initial temperatures and high levels of dilution, need a fluid dynamic constraints. The goal of the internal control, indeed, is to create such intense internal recirculation using fluid motion in order to let the mass flow rate of recirculated flow be comparable to, or even higher, than the one of the inlet fresh mixture. The gas turbines present the constraint of the final outlet temperature, which cannot be higher than the one that cooled metal can resist, which settles around 1673 K (1400 °C) under present technological limitations. For this reason, it is necessary to include an external dilution with an inert species, as analyzed in the previous subsection, or with a lean mixture (since employing rich mixtures is not compatible with constraints linked to pollution and power maximization). Thus, to allow an internal recirculation, the lean condition is the only plausible choice.

2.6 Oxy-Fuel Combustion

2.6.1 Technologies of Carbon Capture and Storage

The oxy-firing or oxy-fuel combustion is one of the most important and elegant technologies to capture carbon dioxide. Figure 2.11 shows schematically the layout of a power plant of this technology, in which the wet and dry recycle of flue gas is represented [46].

The flue gas is composed primarily of carbon dioxide and water with nitrogen, oxygen and some traces such as sulfur and nitric oxides. When the CO_2 content reaches values of 96% to 99% [47], it is compressed and condensed to be sequestered for storage (CCS) or for use in subsequent processes (CCR). Currently, there are two technologies in order to provide the oxygen necessary for an oxyfuel process:

- Oxygen supply by a cryogenic technique (Figure 2.11)

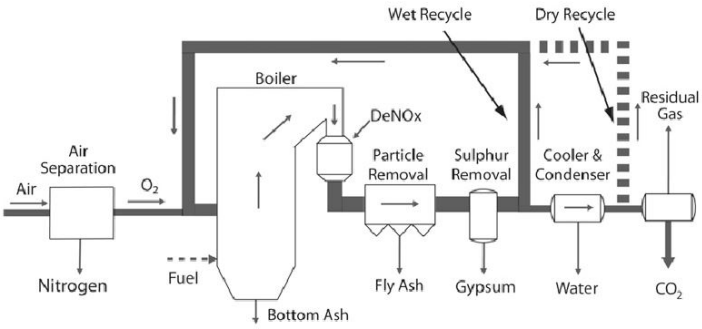

FIGURE 2.11: Oxy-fuel combustion layout with wet and dry recycle of flue gas

- Oxygen supply through the use of a high-temperature ceramic ion-transport membrane (ITM) (figure 2.12).

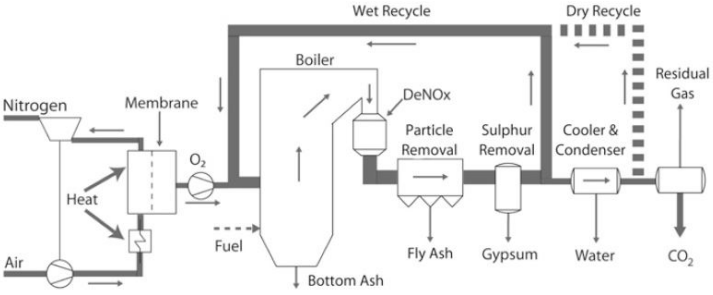

FIGURE 2.12: Oxy-fuel combustion layout with ITM for oxygen supply

The first technology is already well established in the industry, thus can be easily implemented. An issue of this technology is the energy demand for oxygen production. It is, in fact, about 240 kWh per ton of O_2 and, by addition of the CO_2 compression, the net efficiency drop at power plant is about 8-10% points [48,49]. Though the optimization of the cryogenic air separation, this energy penalty can be reduced to values around to 160 kWh per ton O_2. The second method, which is based on a high-temperature oxygen ion-transport membrane (ITM), seems to be more a cost- and energy-effective alternative to the cryogenic process [50,51]. This is due to the reduction of auxiliary power required for oxygen production.

Other modifications of the ITM technology are possible [46]. For further detailed study about this technology can be found in several works [52]. It is important highlights some issues that the R&D should face before applying the oxy-coal technology. These issues are:

- Recirculation of flue gas: determination of the place of extraction of the flue gas.
- Corrosion: material choice, excess oxygen ratio, controlled flame temperature.

- Combustion stability: shape and temperature flame, PF and oxygen concentrations, flame stability, the volume of the RFG etc.
- Start up and shutdown: burner settings and design.
- Thermal efficiency: heat transfer inside the combustion chamber.
- ASU and CO_2 compression: oxygen quality, FG composition, emissions etc.
- Slagging and fouling: composition of combustion products and ash quality.
- Burner design: gas velocities, swirl ratio, flame characteristics etc.
- Boiler design: retrofit or new design.

The oxy-coal may be a zero-CO_2-emission emerging technology with strong commercial interest. In order to advance the oxy-firing technology, the combustion science and modeling are needed. There are already several demonstration projects planned for the PF oxyfuel technology, a 30 MW_{th} pilot plant and a 250 MW demonstration plant in Schwarze Pumpe, Germany; a 30 MW_{th} retrofitted boiler in Biloela, Australia, and a 30 MW_{th} pilot plant and a 323 MW full-scale demonstration plant in El Bierzo, Spain [46].

The realization of these projects is very important to bring information that is necessary to understand the effect of a CO_2-rich atmosphere on the oxy-combustion of PF in real scales and important know-how for the potential scale-up and construction of a CO_2 emission-free coal-fired power plant [46].

2.6.2 Characteristic of Combustion in CO_2 Atmosphere

In the previous chapter, the combustion of coal from a global point of view has been introduced. It consists of a complex process governed by several physical and chemical phenomena. When the coal burns in a CO_2 atmosphere, the particle will meets a recycled flue gas containing mainly CO_2. This condition will change the gas properties in the combustion chamber. Thus, the effect of the changed gas properties will have consequences on the homogenous and heterogeneous reactions, as well as on the heat transfer that takes place during PF oxy-combustion.

2.6.2.1 Combustion in Air and in CO_2 Atmosphere

In conventional coal-fired boilers the air is used for the combustion in which the nitrogen is approximately 79% vol. While in the oxy-fuel combustion pure oxygen (grater than 95% purity) with recycled flue gas is used. The concentration of CO_2 in the flue gas is between 70% and 90% depending on the cycle mode (wet and dry). Recirculating the flue gas is very important in order to control the flame temperature. Several works [52],

in which the oxy-fuel combustion has been applied in bench, pilot and demonstrate-scale experiments, have shown different characteristics of combustion process if compared to the air combustion. These characteristics are:

- Reduction of flame temperature.
- Delay of flame ignition.
- NO_x emissions reduction.
- SO_x emissions reduction.
- Change of heat transfer.

These effects are owing to the different gas properties of CO_2 and N_2 in term of thermo-physical and optical properties. These properties can influence both combustion reaction rates and heat transfer. Table 2.1 shows some gas properties of N_2 and CO_2.

TABLE 2.1: Gas Properties for N_2 and CO_2 at 900 °C [52]

Properties	N_2	CO_2	ratio CO_2/N_2
Thermal conductivity, 10^{-3}, W/mK	74.67	81.69	1.09
Molar heat capacity $c_p, kJ/kmolK$	33.6	56.1	1.67
Density $\rho, kg/m^3$	0.29	0.45	1.55
O_2 diffusion coeff. D_o,10^{-4}, m^2/s	3.074	2.373	0.77
Thermal Diffusivity, 10^{-7}, m^2/s	2168	1420	0.65
Molecular weight M, kg/kmol	28	44	1.57
Energy per volume, ρc_p, $M^{-1}J/m^3K$	0.34	0.57	1.67

CO_2 is a bigger heat sink than the nitrogen because the molar heat capacity of carbon dioxide is higher than the one of nitrogen. Thus, the adiabatic flame temperature (AFT) in oxy firing, with the same level of oxygen, is lower than the one of the combustion in air. Because the molecular weight of CO_2 is bigger than the N_2, the density of the flue gas is higher in oxy-fuel combustion. Consequently, the velocities of flue gas are lower and the residence times of particles are higher in the combustion chamber. The ratio between the oxygen diffusion in CO_2 and in N_2 is around 0.8. This affects the oxygen availability at the char surface. The flame propagation in oxy-fuel case is slower than the air case because of a lower value of thermal diffusivity of CO_2. The temperature of combustion gases is lower than the air-firing (if O_2 content is kept at the same level as for air) because CO_2 has a higher energy for volume than the N_2. The properties of gas have influence on the homogenous and heterogeneous reactions, which take place during PF oxy-fuel combustion.

2.6.2.2 The influence of CO_2 on coal pyrolysis and on particle ignition

CO_2 concentrations in the bulk gas could influence the coal devolatilization process in two main ways [82].

- The carbon dioxide could affect the composition of volatiles because itself is a product of coal pyrolysis.
- The carbon dioxide is this case is also a reactant in the char combustion, which may make differences in the formation of SO_x/NO_x precursors.

The presence of CO_2 retards single coal particle ignition [52]. This may be due to the high value of the heat capacity of a gas mixture when a higher CO_2 concentrations are presented [53].According to Suda et al. [54], who investigated a PF flame in a small spherical chamber, the flame propagation velocity of a PF cloud in a CO_2/O_2 atmosphere is lower than (around 1/5 to 1/3) that in a N_2/O_2 atmosphere at the same O_2 concentration level. This is linked to the larger heat capacity of CO_2. As the oxygen concentration increases the ignition of particle accelerates both in N_2/O_2 and in CO_2/O_2 atmospheres. According to Shaddix and Molina [55] the particle devolatilization proceeds more rapidly with higher O_2 concentrations and decreases with the use of CO_2 diluent. This because these two species influences the mass diffusion rates of O_2 and fuel volatiles. Therefore, if the oxygen concentration increases for PF oxy-firing, can produce ignition times and volatile flames similar to those obtained under PF–air combustion conditions [52]. Molina et al. [56] studied the ignition of groups of particles of high-volatile bituminous coal with oxygen concentrations ranging from 12% to 48%, with N_2 or CO_2 as diluent gas, at two gas temperatures (1130 K and 1650 K) in an optical entrained flow reactor (at Sandia National Laboratories). To measure the ignition delay and the variation in time of the flame location, the standoff distance from the coal flame to the burner was used as a metric. The variation in time of the flame location is used as an indication of the flame stability. It was reported that at 1130 K, the ignition decreases when the oxygen concentration increases. This difference is more evident with N_2 as balance gas than with CO_2. The CO_2 provides a delay ignition at 1130 K with the same oxygen concentration. However, when the gas temperature reaches 1650 K an opposite trend has been observed. In this case, a higher oxygen concentration had a damaging effect on flame stability. This can occur because at high particle temperature the char-CO_2 gasification reaction can compete with the char-O_2 reaction. Since the gasification reaction is endothermic, this can cause combustion instability.

2.6.2.3 Char Reactions in CO_2/O_2 Environment

The heterogeneous char gasification and combustion on particle surface were reviewed by Laurendeau [79], Hurt [80], and Essenhigh [81]. The reactions occur by means of both diffusion and chemical steps as follows:

- The reactant gases (O_2, CO_2, H_2O, H_2) diffuse from the bulk gas phase to the solid surface of the particle and into capillary or pore structure of the particle through the boundary layer.
- The reactants can be adsorbed by the solid.
- Surface chemical reaction.
- Desorption of surface reaction products.
- Diffusion of the gas products into the bulk gas phase.

Shaddix and Molina [57] defined different ways in which the presence of CO_2 in the bulk gas phase may influence the pulverized char combustion:

- The presence of CO_2 could reduce the burning rate because it can hinder the diffusion of O_2 to the char surface.
- The heat released in the char particle boundary layer during the oxidation of CO could transfer back to the particle, and thus, the higher heat capacity of CO_2 may reduce the peak gas temperature. The heat transfer back to the particle can reduce the burning rate.
- The burning rate decreases also because the dissociative adsorption of CO_2 on the char surface could provoke a surface coverage and therefore a competition for available reaction sites for oxygen.
- The burning rate increases because of the direct gasification of char carbon by CO_2. However, the Boudouard reaction, because of the endothermicity, would bring to lower the char temperature and thereby lower the overall burning rate.

Shaddix and Molina [57], in their work on char combustion in N_2/O_2 and in CO_2/O_2 environment, observed a reduction of char temperature in the CO_2 environments, implying a lower overall burning rate. This is due to the slower diffusion of O_2 through the film layer surrounding the reacting char particle (oxygen diffusion is approximately 20% slower in CO_2 than in N_2; see Table 2.1). The effect of CO_2 on oxygen diffusivity is the reduction of char particle temperatures by approximately 50 K at enriched oxygen levels and decreases the burning rate by approximately 10%. This

can be valid, however, for the very high temperature regimes (Model III; see Figure 1.6), where the bulk diffusion is the rate-limiting factor. It has been demonstrated that the char combustion is not influenced by the higher molar-specific heat of CO_2.

Wall et al. [52] investigated the char reactivity in a drop tube furnace both in air and oxy-fuel conditions as function of oxygen concentrations. According to their results the char burnout increases as the O_2 concentration increases.

Shaddix et al. [57] investigated the effects of coal rank and gas temperature on char-burning rates in oxy-fuel combustion. The results showed that the char reactivity decreases with the increasing of coal rank. The CO_2 diluent provides similar mean particle temperatures as for N_2 diluent at 1130 K. In a furnace environment, where the temperature are high and the oxy-coal combustion is used, for low and mid-rank coals the char particles burn at lower temperature.

Schiebahn [58] performed numerical simulation in order to get the conversion rates of char particle in oxy-fuel environment using kinetic data from different authors. During the numerical study they considered the variation of O_2 content in the O_2/CO_2 mixture, the particle temperature and the char type. According to their results the char-CO_2 gasification reaction does not have an important role in low and moderate particle temperatures.

Oxy-fuel combustion have been studied both numerically and experimentally by Geier et al. [59]. They studied the influence of oxy-fuel combustion on char combustion rates for different sizes of pulverized coal. The boundary layer became important for particle sizes greater than 60 μm and reach the a maximum for particles around 75 μm in size. For bigger particles (larger than 100 μm) the particles burn close to the diffusion limit.

2.6.2.4 Combustion of Volatiles in Oxy-Fuel Condition

According to Zhu et al. [60] the combustion in CO_2 environment leads to a reduction of the propagation flame velocity. The distribution of temperature and species are different in the combustion chamber, and the reduction of flame speed provokes a poor combustion performance. The reduction of burning velocity for oxy-fuel combustion can be influenced by the following features:

- Lower thermal diffusivity of CO_2.
- Higher molar heat capacity of CO_2.
- Chemical effects of CO_2.
- Modified radiative heat transfer.

The effects of the molar heat capacity influences the flame temperature. To increase the adiabatic flame temperature in oxy-fuel combustion the concentration of oxygen should increase in the CO_2/O_2 gas mixture in order to reach similar flame temperature levels as in air combustion [77,78].

According to Shaddix and Molina [57] the heating rate is proportional to the product of the temperature difference between gas and particle and to the thermal conductivity. At elevated temperature the thermal conductivity of N_2 is practically equal to the thermal conductivity of CO_2. For this reason there are not significant difference in particle heating rates for the two diluents.

Toporov et al.[60] in their experimental study on oil flame (50 kW) found that the reaction rates decrease as the CO_2 concentration increases in the combusting mixture. Furthermore, the increasing of CO_2 led to shortening the flame and a reduction of the luminescence of the flame. These results have been found by keeping the O_2 content at the same level (21 vol %) in the CO_2/O_2 mixture. By increasing the O_2 concentration in the combusting mixture, the stabilization of the flame has been obtained. This demonstrates that under oxy-firing conditions, the gaseous flame velocity is reduced mostly because of the increased specific heat. The growth of the specific heat in the gas reduces the flame temperature and in turn the overall reaction rate.

These results have been confirmed by Andersson and Johnsson [61], who experimentally studied a propane flame (80 kW) in air and in CO_2/O_2 mixture. The flame temperatures with 21 vol % O_2 (oxy-fuel-21) are lower than in air owing to cooling caused by recirculation of CO_2. The temperature levels increase when the oxygen concentration increases to 27 vol % O_2 (oxy-fuel-27), and this condition allows to improve the mixing between fuel and O_2, thus improves the fuel burnout.

Through numerical calculations Liu et al. [62] investigated the chemical effects of carbon dioxide in term of burning velocity. It is important to note that the reduction of burning velocity is not only owing to the physical properties of CO_2, but the carbon dioxide influences the combustion reactions especially via the following reaction:

$$CO + OH \rightarrow CO_2 + H \tag{2.1}$$

The carbon dioxide, as the previous reaction shows, reduces the concentration of radicals H, OH and O in the combustion chamber, which are responsible of the burning velocity. Thus the burning velocity decreases. Thus, an important chemical effect of CO_2 is the reduction of burning velocity of a fuel.

2.6.3 NO_x Emissions of Pulverized Coal Combustion in CO_2/O_2 Environment

During coal combustion the oxidation of fuel-N by oxygen and other oxidizing agents affect the formation of NO_x. An opposing factor can reduce the already NO_x produced through reducing agents. These reducing agents are hydrocarbons, which originate from devolatilization in homogeneous reactions and resident char in heterogeneous reactions.

The flue gas recirculation (FGR) is a method to reduce the NO_x. The flue gas recycled from the stack is injected into the combustion with the air supply of the burners. This condition provides lower peak temperatures and lower oxygen concentrations in the flame zone. Actually, the major effect of FGR is on thermal-NO_x formation and it has not a great impact on fuel-NO_x production. Because more than half of the total NO_x produced in a pulverized coal boiler are fuel-NO_x, the FGR method has not been considered as possible option for the reduction of NO_x in large coal-fired boilers [76].

The oxy-fuel technology allows to reduce the NO_x emissions without resort to staged combustion. The NO_x emissions generated per unit of energy, during oxy-fuel combustion, are around 70% lower than air-fired units. The percentage reduction depends on the burner design, coal type and operating conditions [63,64,65]. This NO_x reduction is due to the following mechanism [67,67]:

- Since the atmospheric N_2 is absent the thermal NO are reduced.
- The CH fragments from the pyrolysis of volatile matter reduces the recycled NO; the reduction can also occur on the char surface, which can be enhanced by an increased CO concentration due to high CO_2 concentrations in the furnace and by interaction between recycled-NO and released fuel-N, mainly HCN, in order to form N_2.

Park et al. [73] investigated the conversion of fuel-N during the char reactions of coal with O_2, CO_2 and H_2O under several conditions. They found that the char-N is converted to N_2 when the char reacts with CO_2, to NO and N_2 when it reacts with O_2, and to HCN, NH_3, and N_2 when it reacts with H_2O.

According to Liu and Okazaki [74] the heat recirculation could reduce NO emission further in three ways:

1. less exhausted flue gas (high recycling ratio);
2. a low oxygen-fuel stoichiometric ratio (SR);
3. an increase in flame temperature.

The NO_x emissions are affected by the flue gas recycling ratio, because when it decreases the concentrations of O_2 in the inlet gas and reducing agents increase simultaneously.

According to the works of Hu et al. [67] and Liu et al. [68]the conversion of nitrogen content in the fuel to nitric oxides increases with the oxygen concentration in the mixture. If the recycling ratio increases, the oxygen content decreases and thus the NO_x reduction efficiency improves [67,69]. This opposite effect of oxygen content on the NO_x emission from fuel-N and the reduction of recycled-NO_x has been studied on a real oxy-coal combustion [67,68].

In the experimental work of Shaddix and Molina [70] in a down-fired entrained flow measurements were performed on NO_x formation at three different oxygen concentrations (12%, 24% and 36%) in both N_2 and CO_2. The NO_x formation decreases in a combustion in CO_2/O_2 environment. This is owing to the lack of thermal-NO_x production, lower volatile and char combustion flame temperatures.

The NO_x originate from volatiles are a larger fraction of the total coal-NO_x generated at enhanced oxygen levels. The cause could be effect of oxygen on the volatile flame temperature compared to char combustion temperature.

2.6.4 Heat Transfer in CO_2/O_2 Environment

When the gas products are recycled from the outlet to the furnace inlet, the convective and radiative heat transfers inside the furnace will be modified. The convective heat exchange will be modified due to the changing of the gas heat capacity and gas temperature, while the radiative heat flux will be different because of the different values of emissivity and absorptivity of the mixture. In conventional air combustion of pulverized coal the major contributor of heat transfer is the radiative component from hot particles and from combustion products such as water vapour, carbon dioxide, sulphur dioxide, and carbon monoxide [71,72]. Figure 2.13 shows the interaction between the radiative heat transfer and several different phenomena in the combustion process [52].

2.6.4.1 Radiative Properties of CO_2

Contrary to particles, which emit in whole spectrum, the gases emit and absorb the radiant energy only in a narrow frequency bands. Thus, the combustion gases participate in a certain spectrum. It is well known that the absorption band size depends on temperature, partial pressure of absorbing gases, and path length. Figure 2.14 shows this concept for the carbon dioxide [75].The spectra absorptivity α_{CO_2} increases as the pressure and path length increase.

Blokh [71] summarized the total emissivities for both CO_2 and H_2O obtained by

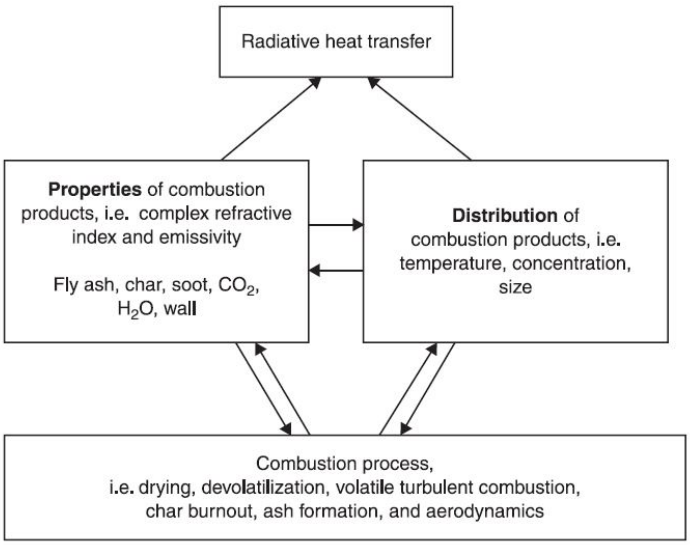

FIGURE 2.13: Interaction between radiative heat transfer and combustion process

several authors. The H_2O emissivity , for a given pL (partial pressure and optical length), is higher than CO_2 one. Thus, during oxy-firing it has to be considered.

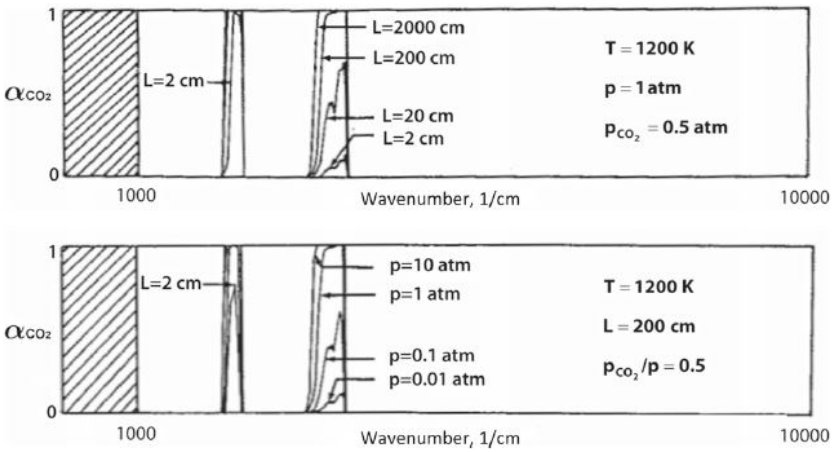

FIGURE 2.14: CO_2 spectra: (top) influence of path length on absorptivity (bottom) influence of pressure on absorptivity

Chapter 3

Mathematical Model

The performance of a PC fired boiler or furnace depends on parameters linked to furnace volume, burner type, distribution of coal/air, excess air, burner settings. Other parameters, instead are linked to the quality of coal such as, char content and particle size distribution [83,54,85]. The main goal of combustion researchers is to develop advanced and novel burners, furnaces and boilers in order to increase the efficiency and reduce the pollutant emissions. For this reason, new concepts and novelties for different combustion processes must be continuously developed, and at the same time, computer simulation using CFD technology, are also extremely important for the design and development of new advanced furnaces.

The CFD (*Computational Fluid Dynamics*) is the study of *fluid dynamics* through numerical methods on high-speed digital computers (*Computational*). The partial differential equations describe the physical behavior of the fluid in motion. These mathematical equations are converted into discrete forms using high-level computer programming languages into in-house computer programs or commercial CFD software packages. These algebraic equations are solved through dedicated techniques. In this Chapter, the governing equations of fluid flow (mass, momentum and energy conservation equations) will be presented. Because, the combustion process include chemical species, the species conservation equation will be added. Furthermore, the coal combustion requires the use of sub-routines in order to describe the phenomena such as devolatilization and char combustion. This sub-models interact with the governing equations.

3.1 Governing Equations

The governing equations of fluid flow represent mathematical statements of the conservation laws of physics:

- The mass of a fluid is conserved.

- The rate of change of momentum equals the sum of the forces on a fluid particle (Newton's second law).
- The rate of energy is equal to the sum of the rate of heat addition to and the rate of work done on a fluid particle (first law of thermodynamics).

Through these physical fundamentals the conservation equations can be obtained, which correspond to the CFD modeling base.

3.1.1 Conservation Equation of Mass (Continuity Equation)

The equation of continuity can be developed by writing a mass balance over a volume element. The overall mass of the gaseous phase is conserved. The equation can be written as:

$$\frac{\partial \rho}{\partial t} + (\nabla \cdot \rho \mathbf{v}) = S_m \tag{3.1}$$

In equation eq. 3.1 the fluid density is represented by ρ, t is the time, and $\mathbf{v}$ is the velocity vector. The term $\nabla \cdot \rho \mathbf{v}$ is the divergence of the mass flux $\rho \mathbf{v}$, which represents the net rate of mass flux per unit volume. The source term S_m takes in account the mass transfer from solids phase to the gas phase. For instance, in a multiphase flow could appear from vaporization from a dispersed phase.

3.1.2 Momentum Equation (Navier-Stokes Equation)

The equation of motion can be derived by means of a momentum balance over a volume element [86]. The momentum equation is well known as the Navier-Stokes equation. It is presented in the following way:

$$\frac{\partial}{\partial t}(\rho \mathbf{v}) + \nabla \cdot (\rho \mathbf{v}\mathbf{v}) = -\nabla p + \nabla \bar{\bar{\tau}} + \rho \mathbf{f} \tag{3.2}$$

Momentum acceleration = convection + molecular transport (pressure term + viscous term + external forces term)

where the left side is the rate of increase of momentum per unit volume, the second term is the rate of momentum addition by convection per unit volume. The first two terms on the right side of the equation represent the rate of momentum addition by molecular transport owing to pressure and viscous forces respectively, while the last term is the gravitational and external forces term. The viscous stress tensor is defined as:

$$\bar{\bar{\tau}} = \mu \left[\nabla \mathbf{v} + \nabla \mathbf{v}^T - \frac{2}{3} \nabla \cdot \mathbf{v} \bar{I} \right] \tag{3.3}$$

Where μ is the molecular viscosity, I is the unit tensor, and the second term on the right hand side is the effect of volume dilation.

3.1.3 Energy Equation

The energy conservation equation is based on the first law of thermodynamics. The general form of the energy equation can be written as:

$$\frac{\partial}{\partial t} (\rho E) + \nabla \left(\mathbf{v} \left(\rho E + p \right) \right) = \nabla \cdot \left(k_{eff} \nabla T - \sum_i h_i \mathbf{J_i} + (\bar{\bar{\tau}} \cdot \mathbf{v}) \right) + S_h \tag{3.4}$$

Transient term + Convection = Conduction + Species Diffusion + Viscous Dissipation + External Heat source

The first and the second terms on the left side of equal sign are the increase in energy per unit volume and the energy increase owing to convective transport and compression. The effective conductivity k_{eff} is the sum of the thermal conductivity k and the turbulent thermal conductivity k_t. $\mathbf{J_j}$ diffusion flux of species j, while h_j is the species enthalpy. On the right side of equation eq. 3.4 are presented the energy transfer due to conduction, species diffusion, and viscous dissipation, respectively. The source term S_h represents an external heat source, which may be the heat released from chemical reactions and the radiation term when enabling radiation model.

The energy equation, for a non-premixed combustion, can be written in term of the total specific enthalpy h for a multicomponent medium, defined as:

$$h = \sum_i Y_i h_i \tag{3.5}$$

where Y_i is the mass fraction of each species i in the mixture. The total enthalpy of each species i is defined by:

$$h_i = h^0_{T_{ref,i}} + \int_{T_{ref}}^{T} c_{p_i} (T) \, dT \tag{3.6}$$

where $h^0_{T_{ref,i}}$ is the enthalpy of formation, T_{ref} is the reference temperature and $c_{p_i} (T)$ is the specific heat at a constant pressure.

3.1.4 Species Transport Equation

In reactive flows analysis the conservation of chemical species need to be take in account. Thus, the conservation equation of chemical species (species transport equation) is a convective-diffusion equation, written as follows:

$$\frac{\partial}{\partial t}\left(\rho Y_i\right) + \nabla \cdot \left(\rho \mathbf{v} Y_i\right) = -\nabla \cdot \mathbf{J_i} + R_i + S_i \tag{3.7}$$

Transient term + Convection = Species Diffusion + Chemical Reaction + External Production

In eq. 3.7 R_i represents the rate of production/consumption of species owing to chemical reaction and S_i is a source term. The eq. 3.7 is solved for $n-1$ species where n is the number of chemical species in the system. The diffusion flux $\mathbf{J_i}$ is given by:

$$\mathbf{J_i} = -\left(\rho D_{i,m} + \frac{\mu_t}{Sc_t}\right)\nabla Y_i \tag{3.8}$$

where $D_{m,i}$ is the mass diffusion coefficient, μ_t is the turbulent viscosity and Sc_t is the turbulent Schmidt number, defined as follow:

$$Sc_t = \frac{\mu_t}{\rho D_t} \tag{3.9}$$

D_t is the effective mass diffusion coefficient owing to turbulence. The eq. 3.8 is better known as Fick law (the thermal or Soret diffusion coefficient has been left out of equation).

3.1.5 General Transport Equation

All conservation equations are particular equations of a more general equation written for a variable ϕ. Thus, a general transport equation can be written as follows:

$$\underbrace{\frac{\partial}{\partial t}\left(\rho\phi\right)}_{Unsteady\ Term} + \underbrace{\nabla \cdot \left(\rho\phi\mathbf{v}\right)}_{Convective\ Term} = \underbrace{\nabla \cdot \left(\Gamma_\phi \nabla\phi\right)}_{Diffusion\ Term} + \underbrace{S_\phi}_{Source\ Term} \tag{3.10}$$

By substituting ϕ with 1,u,v,w, the total energy E and the mass fraction Y_i of specie i it can be obtained the mass, momentum, energy conservation and species transport equation, respectively. The table 3.1 highlights the variable that ϕ could represent.

TABLE 3.1: General form of governing equations for compressible flow

Equation	ϕ	Γ_ϕ	S_ϕ
Continuity	1	0	0
Momentum	u,v,w	μ	-
Energy	h	$\frac{k}{c_p}$	S_h
Species	Y_i	$\rho D_{m,i} + \frac{\mu_t}{Sc_t}$	$R_i + S_i$

3.2 Mathematical Sub-Models

The mathematical analysis of a combustion process requires the description and the use of appropriate sub-models. In Table 3.2 the sub-models used in this thesis are summarized:

TABLE 3.2: Sub-Models to describe the combustion process

Physical Process	**Sub-Models**
Turbulence	k-ϵ Model
Chemistry-Turbulence Interaction	Eddy Dissipation Model (EDM) Finite Rate Model (FRM)
Lagrangian Particle Tracking	DPM (Discrete Phase Model)
Devolatilization	Two Competing Rates (Kobayashi) Model Chemical Percolation Devolatilization (CPD) Model
Char Combustion	Intrinsic Model Multiple Surface Reactions Model
Radiative Heat Transfer	P1 Model

3.2.1 Turbulence Model

Turbulent flows is the motion of a fluid becoming intrinsically unstable and unsteady so that the final state of the fluid can be described in a random and chaotic manner. In order to describe this random fluctuations in the fluid, the best exemplified way is to introduce a temporal variation of a transport property ϕ. According to the Reynolds

decomposition, the instantaneous property ϕ can be decomposed into the mean motion $\overline{\phi}$ and a fluctuating motion $\phi^{'}$:

$$\phi = \overline{\phi} + \phi^{'} \tag{3.11}$$

where $\overline{\phi}$ is defined as follows:

$$\overline{\phi} = \frac{1}{t_0}\int_0^{t_0} \phi dt \tag{3.12}$$

It is important to note that the time averaged of the fluctuating component $\phi^{'}$ is, by definition, zero:

$$\overline{\phi'} = \frac{1}{t_0}\int_0^{t_0} \phi^{'} dt \equiv 0 \tag{3.13}$$

The time interval t_0 is large enough in order to exceed the time scales of the slowest variations (due to largest eddies) as shown in Figure 3.1 [86].

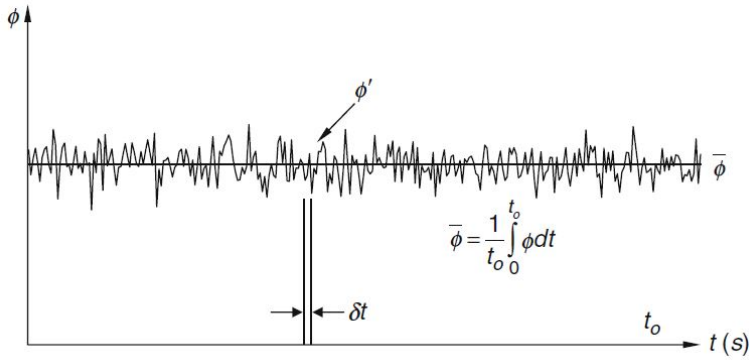

FIGURE 3.1: Transport property ϕ fluctuating with time at some point in a turbulent flow [86]

Instantaneous density, velocities, enthalpy, scalar property can be expressed in terms of their mean and fluctuating quantities through eq. 3.11. The system of equations well known as the Reynolds-Averaged Navier- Stokes (RANS) equations can be derived by substituting the average variables into the governing equations. They can be expressed in compact form in Table 3.3.

In Table 3.3 the term δ_{ij} is the Kronecker symbol and it is given by $\delta_{ij} = 1$ if $i = j$ and $\delta_{ij} = 0$ if $i \neq j$.

Because in turbulent flames, the thermal heat release provokes the density fluctuations. The Reynolds-averaging does not consider the effect of density or mass variability. Thus, is not applicable in turbulent flames. Another type of averaging procedure is the Favre-averaging [87,88]. It is possible introduce a mass-weighted mean property ϕ

TABLE 3.3: Reynolds-Averaged Navier-Stokes equations in Cartesian coordinates

Time-Average Mass

$$\frac{\partial \overline{\rho}}{\partial t} + \frac{\partial}{\partial x_j}\left(\overline{\rho u_j} + \overline{\rho' u_j'}\right) = S_m \quad j=1,2,3$$

Time-Average Momentum

$$\frac{\partial}{\partial t}\left(\overline{\rho u_i} + \overline{\rho' u_i'}\right) + \frac{\partial}{\partial x_j}\left(\overline{\rho u_i u_j} + \overline{\rho} \overline{u_i' u_j'} + \overline{u_i}\overline{\rho' u_j'} + \overline{u_j}\overline{\rho' u_j'} + \overline{\rho' u_i' u_j'}\right) = \frac{\partial \overline{\sigma}_{ij}}{\partial x_j} + \overline{S}_{u_i}$$

where

$$\overline{\sigma}_{ij} = \overline{p}\delta_{ij} - \mu\left(\frac{\partial \overline{u}_i}{\partial x_j} + \frac{\partial \overline{u}_j}{\partial x_i}\right) + \frac{2}{3}\mu\frac{\partial \overline{u}_i}{\partial x_j}\delta_{ij} \quad i,j=1,2,3$$

Time-Average Enthalpy

$$\frac{\partial}{\partial t}\left(\overline{\rho}\overline{h} + \overline{\rho' h'}\right) + \frac{\partial}{\partial x_j}\left(\overline{\rho u_j}\overline{h} + \overline{\rho} \overline{u_j' h'} + \overline{u_j}\overline{\rho' h'} + \overline{u_j}\overline{\rho' h} + \overline{\rho' u_j' h'}\right) = \frac{\partial}{\partial x_j}\left(\frac{k}{C_p}\frac{\partial \overline{h}}{\partial x_j}\right) + \overline{S}_h \quad j=1,2,3$$

$$\widetilde{\phi} = \frac{\overline{\rho\phi}}{\overline{\rho}} \tag{3.14}$$

and the Favre operator:

$$\widetilde{\phi} = \frac{1}{\rho}\overline{\frac{1}{\Delta t}\int_{t+\Delta t}^{t} \rho\phi' dt} \tag{3.15}$$

The generic transport variable ϕ can be written as:

$$\phi = \widetilde{\phi} + \phi'' \tag{3.16}$$

where ϕ'' is the superimposed velocity fluctuation.

It is worthwhile noting that the Favre averaging is only a mathematical definition in order to get a suitable formulation equations. By manipulating the definition of mass-weighted mean property ϕ and the instantaneous value of ϕ, and substituting the instantaneous density, velocities, enthalpy, in terms of their mass-weighted mean and fluctuating quantities, it is possible obtain the Favre-Averaged Navier-Stokes. In Table 3.4 the system of governing equation with the Favre averaging.

It is important to highlight that the Favre averaged conservation partial differential equations eliminates the fluctuation of density from the time-averaged equations. Furthermore, the terms in common are only the Reynolds and scalar stress terms: $\overline{\rho u_i'' u_j''}$ and $\overline{\rho u_i'' h''}$.

TABLE 3.4: Favre-Averaged Navier-Stokes equations in Cartesian coordinates.

Favre-Averaged Mass

$\frac{\partial \overline{\rho}}{\partial t} + \frac{\partial}{\partial x_j}\left(\overline{\rho}\widetilde{u_j}\right) = S_m \quad j=1,2,3$

Favre-Averaged Momentum

$\frac{\partial}{\partial t}\left(\overline{\rho}\widetilde{u_i}\right) + \frac{\partial}{\partial x_j}\left(\overline{\rho}\widetilde{u_i}\widetilde{u_j} + \overline{\rho' u_j'' u_j''}\right) = -\frac{\partial \overline{\sigma}_{ij}}{\partial x_j} + \overline{S}_{u_i}$ where

$\overline{\sigma}_{ij} = \overline{p}\delta_{ij} - \mu\left(\frac{\partial \widetilde{u_i}}{\partial x_j} + \frac{\partial \widetilde{u_j}}{\partial x_i}\right) + \frac{2}{3}\mu\frac{\partial \widetilde{u_i}}{\partial x_j}\delta_{ij} \quad i,j=1,2,3$

Favre-Averaged Enthalpy

$\frac{\partial}{\partial t}\left(\overline{\rho}\widetilde{h}\right) + \frac{\partial}{\partial x_j}\left(\overline{\rho u_j}\widetilde{h} + \overline{\rho u_j'' h''}\right) = \frac{\partial}{\partial x_j}\left(\frac{k}{C_p}\frac{\partial \widetilde{h}}{\partial x_j}\right) + \overline{S}_h \quad j=1,2,3$

The Favre averaged conservation equations are used in the FLUENT code. These equations are closed by means of appropriate sub-models.

3.2.1.1 Standard $k-\epsilon$ Turbulent Model

The continuity and momentum equations allow to describe the turbulent flow. The computations of stationary turbulent flows requires the knowledge of the components $\overline{\rho u_i'' u_j''}$ of Reynolds stress tensor. To determine these terms the standard $k-\epsilon$ model by Launder and Spalding [89] has been used in order to close the problem (turbulence closure problem). In the Favre-averaged form of the momentum equation, according to the Boussinesq [90] hypothesis, the turbulent stresses can be be written as follow:

$$-\overline{\rho u_i'' u_j''} = -\overline{\rho}\widetilde{u_i'' u_j''} = \mu_T\left(\frac{\partial \widetilde{u_i}}{\partial x_j} + \frac{\partial \widetilde{u_j}}{\partial x_i}\right) - \frac{2}{3}\left(\mu_T\frac{\partial \widetilde{u_i}}{\partial x_j} + \overline{\rho}k\right)\delta_{ij} \tag{3.17}$$

where μ_T is the turbulent viscosity.

Similarly, the scalar stress for the enthalpy is proportional to the gradient of the mean value of the transported quantity:

$$-\overline{\rho u_i'' h''} = -\overline{\rho}\widetilde{u_i'' h''} = \Gamma_h^T\frac{\partial \widetilde{h}}{\partial x_i} \tag{3.18}$$

where Γ_h^T is the turbulent diffusivity for enthalpy.

The local turbulent viscosity μ_T can be obtained from dimensional analogy to the laminar viscosity as $\mu_T \propto \overline{\rho} v_t l$. The turbulent viscosity μ_T could be given as:

$$\mu_T = \overline{\rho} C_\mu \frac{k^2}{\epsilon} \tag{3.19}$$

where C_μ is an empirical constant. The turbulent kinetic energy k and the rate of dissipation of turbulent energy ϵ are respectively defined as

$$k = \frac{1}{2}\widetilde{u_i'' u_i''} \tag{3.20}$$

$$\epsilon = \frac{\mu_T}{\overline{\rho}}\widetilde{\left(\frac{\partial u_i''}{\partial x_j}\right)\left(\frac{\partial u_i''}{\partial x_j}\right)} \tag{3.21}$$

The values of k and ϵ must be known in order to evaluate the turbulent viscosity in eq. 3.21. To obtain the values of k and ϵ their respective equation have been solved.

$$\frac{\partial}{\partial t}\left(\overline{\rho}k\right) + \frac{\partial}{\partial x_j}\left(\overline{\rho u_j}k\right) = \frac{\partial}{\partial x_j}\left[\frac{\mu_T}{\sigma_k}\frac{\partial k}{\partial x_j}\right] + \underbrace{\mu_T \frac{\partial \widetilde{u_i}}{\partial x_j}\left(\frac{\partial \widetilde{u_i}}{\partial x_j} + \frac{\partial \widetilde{u_j}}{\partial x_i} - \frac{2}{3}\frac{\partial \widetilde{u_i}}{\partial x_j}\left(\mu_T \frac{\partial \widetilde{u_i}}{\partial x_j} + \overline{\rho}k\right)\delta_{ij}}_{Production} - \underbrace{\overline{\rho}\epsilon}_{Destruction} \tag{3.22}$$

$$\frac{\partial}{\partial t}\left(\overline{\rho}k\right) + \frac{\partial}{\partial x_j}\left(\overline{\rho u_j}\epsilon\right) = \frac{\partial}{\partial x_j}\left[\frac{\mu_T}{\sigma_\epsilon}\frac{\partial \epsilon}{\partial x_j}\right] + \underbrace{C_{\epsilon 1}\frac{\epsilon}{k}\left[\mu_T \frac{\partial \widetilde{u_i}}{\partial x_j}\left(\frac{\partial \widetilde{u_i}}{\partial x_j} + \frac{\partial \widetilde{u_j}}{\partial x_i} - \frac{2}{3}\frac{\partial \widetilde{u_i}}{\partial x_j}\left(\mu_T \frac{\partial \widetilde{u_i}}{\partial x_j} + \overline{\rho}k\right)\delta_{ij}\right.}_{Production} - \underbrace{C_{2}\overline{\rho}\frac{\epsilon^2}{k}\epsilon}_{Destruction} \tag{3.23}$$

The constants for the standard $k-\epsilon$ are the following values [89]:

C_μ=0.09;
σ_k=1.0;
σ_ϵ=1.3;
$C_{\epsilon 1}$=1.44;
$C_{\epsilon 2}$=1.92;

Finally, the transport equations bear many similarities with the generic transport equation:

The eddy viscosity hypothesis provides closure for the system of Favre-Averaged Navier-Stokes equations derived in table 3.4.

3.2.2 Chemistry-Turbulence Interaction Model

In all combustion processes the turbulence influences highly the chemical reactions. This is due to the change of mixing and heat transfer process. In order to close the problem related to the specie transport equations the chemistry-turbulence interaction

models are presented. These models used in this work are: the Eddy Dissipation Model (EDM) and the Finite Rate Model (FRM).

3.2.2.1 Eddy Dissipation Model

The EDM is based on the work of Masnussen and Hjertager [91].This model provides the production/consumption rate of species i due to reaction r, $R_{i,r}$, which corresponds to R_i, defined in previous section. According to this model, the $R_{i,r}$ is given by the smaller of the two expressions below:

$$R_{i,r} = v_{i,r}^{'} M_{w,i} A \rho \frac{\epsilon}{k} min_H \left(\frac{Y_H}{v_{H,r}^{'} M_{w,H}} \right) \tag{3.24}$$

$$R_{i,r} = v_{i,r}^{'} M_{w,i} AB \rho \frac{\epsilon}{k} \frac{\sum_p Y_p}{\sum_J^N v_{j,r}^{''} M_{w,j}} \tag{3.25}$$

where $v^{'}$ is the stoichiometric coefficient for reactants, $v^{''}$ is the stoichiometric coefficient for products and M is the molecular weight. Y_p is the mass fraction of any product species, P, and Y_H is the mass fraction of a particular reactant, H. A and B are empirical constants equal to 4.0 and 0.5 respectively. This model relates the rate of reaction to the rate of dissipation of the reactant and product containing eddies. According to the EDM, turbulent mixing controls the rate of the reaction. For this reason it is assumed that the Damkhöoler number is infinite. It is defined as the ratio between the characteristic mixing scale and the characteristic chemical time. Thus, the combustion is mixing-limited, and the chemical kinetic rates can be safely neglected.

It is important to note that the main idea of the EDM is to replace the chemical time scale of an assumed reaction by the turbulent time scale k/ϵ. Thereby the model eliminates the influence of chemical kinetics, representing the fast chemistry limit only.

3.2.2.2 Finite Rate Model

The finite-rate model computes the chemical source terms using Arrhenius expressions, and ignores the effects of turbulent fluctuations. Further details can be found in [92]. Furthermore, the code allows to choose the finite-rate/eddy-dissipation model, in which both the Arrhenius and eddy-dissipation (eq. 3.24 and eq. 3.25) reaction rates are calculated. The net reaction rate is the minimum of these two rates. Once the flame is ignited, the eddy-dissipation rate is smaller than the Arrhenius rate, thus the reactions are mixing-limited. In practice, the Arrhenius rate acts as a kinetic "switch".

3.2.3 Particle Combustion

In addition to solving transport equations for the continuous phase, it is possible simulate of a discrete second phase in a Lagrangian frame of reference. This second phase consists of spherical particles (which may also be taken to represent droplets or bubbles) dispersed in the continuous phase. The code computes the trajectories of these discrete phase entities, as well as the heat and mass transfer to/from them. The coupling between phases and the resulting impact on both the discrete phase trajectories and the continuous phase gas flow can be included. The discrete phase formulation contains the assumption that the second phase is sufficiently dilute that particle particle interactions and the effects of the particle volume fraction on the gas phase are negligible. In practice these issues imply that the discrete phase must be present at a fairly low volume fraction, perhaps less than 1012% [92], a value which is justified for the modelling work presented in this thesis. As mentioned in previous chapters, the combustion of coal is modeled according to the following steps: heating, devolatilization process, volatile combustion and char burnout. In this section the devolatilization and char combustion models will be presented. The author will present some general information about them.

3.2.3.1 Particle Tracking

The trajectory of the coal particle are calculated by integrating the force balance on the particle:

$$\frac{du_p}{dt} = \frac{18\mu}{\rho_p d_p^2}\frac{C_D Re}{24} \times (u - u_p) + \frac{g_x\left(\rho_p - \rho\right)}{\rho_p} \tag{3.26}$$

where u is the fluid phase velocity, u_p is the particle velocity, μ is the molecular viscosity of the fluid, ρ is the fluid density, ρ_p is the density of the particle, and d_p is the particle diameter, Re is the relative Reynolds number, g_x is the gravity constant.

3.2.3.2 Devolatilization Model

The devolatilization models allow to describe the devolatilization process of a solid combustion or gasification.

Kobayashi Model

According to the Kobayashi model (Two competing rates) the kinetic devolatilization rates are given by the following expressions:

$$R_1 = A_1 \exp^{-(E_1/RT_p)} \tag{3.27}$$

$$R_2 = A_2 \exp^{-(E_2/RT_p)} \tag{3.28}$$

where R_1 and R_2 are competing rates that may control the devolatilization over different temperature ranges. The devolatilization expression is the following:

$$\frac{m_v(t)}{(1 - f_{w,0})\, m_{p,0} - m_a} = \int_0^t (\alpha_1 R_1 + \alpha_2 R_2) \exp\left(- \int_0^t (R_1 + R_2)\, dt \right) dt \tag{3.29}$$

where $m_v(t)$ is the volatile yield upto time t, $m_{p,0}$ the initial particle mass at injection, α_1, α_2 the yield factors and m_a the ash content in the particle. According to Kobayashi [93] the yield of competing reaction, α_1, should be set to the fraction of volatiles given by the proximate analysis, because this rates represents devolatilization at low temperature. The second yield parameter, α_2, should be set close to unity, which is the yield of volatiles at very high temperature.

Chemical Percolation Devolatilization Model

CPD model in contrast to the empirical devolatilization models (i.e. single rate model and Kobayashi model) the Chemical Percolation Devolatilization (CPD) model [94,95,96] characterizes the devolatilization behavior of rapidly heated coal particle, based on the description of physical and chemical transformation of the coal structure. During coal pyrolysis, the labile bonds between the aromatic clusters in the coal structure lattice are cleaved, resulting in two general classes of fragments. One set of fragments has a low molecular weight (and correspondingly high vapor pressure) and escapes from the coal particle as a light gas. The other set of fragments consists of tar gas precursors that have a relatively high molecular weight (and correspondingly low vapor pressure) and tend to remain in the coal for a long period of time during typical devolatilization conditions. During this time, reattachment with the coal lattice (which is referred to as crosslinking) can occur. The high molecular weight compounds plus the residual lattice are referred to as metaplast. The softening behavior of a coal particle is determined by the quantity and nature of the metaplast generated during devolatilization. The portion of the lattice structure that remains after devolatilization is comprised of char and mineral-compound-based ash. An detailed description of this model can be found in [92].

3.2.3.3 Char Heterogeneous Combustion Model

In this work two kind of char model has been considered: the Intrinsic char Model and the Surface Combustion Model.

Diffusion-Limited Surface Reaction

According to the diffusion-limited surface reaction rate model the rate of surface reaction is determined by the diffusion of gaseous oxidant to the particle surface.

$$\frac{dm_p}{dt} = -4\pi d_p D_{i,m} \frac{Y_{ox} T_\infty \rho}{S_b(T_p + T_\infty)} \tag{3.30}$$

This Model is based on the Baum and Street [97]work. They assume that the char particles become more porous when the mass and density of the particles is decreasing.

Intrinsic Model

The Intrinsic char burnout model can be classified into two main categories: global models and intrinsic models [98]. Global models consider char particles impervious to pore diffusion effects or else lump intra-particle diffusion effects into the chemical reaction rate constants. These models are highly empirical, basing the reaction rate on the particle external surface area and on the oxidizer concentration at the external surface. In contrast, intrinsic models relate char oxidation rate to the active surface area involved in the reaction and consider the non-uniform oxidizer profile within the particle. Intrinsic models rely on pore structure models to describe gaseous diffusion through complex pore structures and to model the local oxidizer concentration at the active surface area. Thus the intrinsic model approach has high potential of providing coal-general kinetic rate constants instead of the coal-specific and condition-specific constants used in the global models. Intrinsic models vary in levels of sophistication and can be classified into two subcategories: macroscopic and microscopic. Macroscopic models use average properties of the particle to estimate the effective diffusivity in the porous structures in the char particle, and usually do not model the evolution of pore structure with burnout. Microscopic models involve the development of a reaction model for a single pore and then the prediction of the overall particle reactivity by an appropriate statistical description of the pore size distribution. If the pore structure is not allowed to change with conversion, and properties of the particle are assumed to be uniform, then the microscopic approach becomes equivalent to the macroscopic approach. Char particles produced from rapid pyrolysis are micro-porous solids whose properties can be described by their size, true and apparent density, porosity, pore volume distribution and surface area distribution. The rate of char oxidation is controlled by sequential or parallel processes of oxygen boundary layer diffusion, chemical reaction and pore diffusion. The intrinsic model for char burnout used in this work is based on the Smith's [98] macroscopic pore model which assumed that the char oxidation reaction:

$$C(s) + O_2(g) \rightarrow CO_2(g) \tag{3.31}$$

The chemical rate is expressed in terms of the intrinsic chemical and pore diffusion rates:

$$R_{IM} = \eta \frac{d_p}{6} \rho_p A_p k_i \tag{3.32}$$

In the previous relation, d_p is the particle diameter, ρ_p is the apparent density of char, A_g the specific internal surface of the char particle and k_i is the intrinsic reactivity. The factor η is known as effectiveness factor and is expressed in the following manner:

$$\eta = \frac{3}{\phi^2}(\phi \coth \phi - 1) \tag{3.33}$$

Where ϕ is the Thiele modulus:

$$\phi = \frac{d_p}{2} \left[\frac{S_b \rho_p A_g k_i p_{ox}}{D_e \rho_{ox}} \right]^{1/2} \tag{3.34}$$

S_b is the stoichiometric coefficient of the eq. 3.40. ρ_{ox} and p_x and p_{ox} are the density and the partial pressure of the oxidant in the bulk phase, respectively. The effective diffusion coefficient in the particle pores De is given by:

$$D_e = \frac{\theta}{\tau^2} \left[\frac{1}{D_{kn}} + \frac{1}{D_0} \right]^{-1} \tag{3.35}$$

This relation is based on the hypothesis that the pore size distribution is uni-modal and the bulk and Knudsen diffusion proceed in parallel. D_0 is the bulk molecular diffusion coefficient:

$$D_0 = C_1 \frac{[(T_p + T_\infty)/2]^{0.75}}{d_p} \tag{3.36}$$

θ is the porosity of the char, and it is given by:

$$\theta = 1 - \frac{\rho_p}{\rho_t} \tag{3.37}$$

D_{kn} is the Knudsen diffusion coefficient:

$$D_{kn} = 97.0 \overline{r_p} \sqrt{\frac{T_p}{M_{w,ox}}} \tag{3.38}$$

Where T_p is the particle temperature and r_p is the mean pore radius of the char particle, $M_{w,ox}$ is the molecular weight of oxygen. The parameter k_i, the intrinsic reactivity, in eq. 3.32, is of Arrhenius form

$$k_i = A_i e^{-(E_i/RT_p)} \tag{3.39}$$

A_i is the pre-exponential factor, while E_i is the activation energy.

Multiple Surface Reaction Model

In Oxy-Mild combustion the exhaust gas are full of CO_2. Therefore, another reaction has been added (gasification reaction) and it has been assumed that the product CO is transported away instead of CO_2. In order to take into account both heterogeneous reactions, the multiple particle surface model has been applied. In this model the particle surface species constitutes the reactive char mass of the particle, hence, if a particle surface species is depleted, the reactive char content of the particle is consumed, and turn, when a surface species is produced, it is added to the particle char mass.

$$C(s) + 0.5O_2(g) \rightarrow CO(g) \tag{3.40}$$

$$C(s) + CO_2(g) \rightarrow 2CO(g) \tag{3.41}$$

In agreement with the reaction r: particle species j + gaseous species n $\rightarrow$ products, the particle reaction rate can be expressed as:

$$\overline{R_{j,r}} = A_p \eta_r Y_j R_{j,r} \tag{3.42}$$

$$R_{j,r} = k_{kin,r} \left(p_n - \frac{R_{j,r}}{D_{0,r}} \right)^N \tag{3.43}$$

where $\overline{R_{j,r}}$ is the rate of the particle surface species depletion (kg/s), A_p is the external surface particle, Y_j is the mass fraction of surface species j in the particle, η_r is the effectiveness factor, $R_{j,r}$ is the rate of particle surface species reaction per unit area (kg/m^2/s),k$_{kin,r}$ is the kinetic constant of reaction r (kg/m^2/s),p$_n$ is the bulk partial pressure of the gas phase species (Pa), D_0, r is the bulk diffusion coefficient for reaction r (m/s), N_r is the apparent order of reaction r. Table shows the kinetic parameters of char heterogeneous reactions [99].

Thus, two type of model has been considered in this work: Intrinsic Char Model (only char oxidation) and Multiple Surface Reactions model in which are considered the char oxidation and gasification reaction. An detailed description of these models can be found in [92].

TABLE 3.5: Kinetic parameters of char heterogeneous reactions

Kinetic mechanism [kg/m^2/s]	A [$kg/m^2/s/Pa^\alpha$]	β	α	E [kJ/kmol]
$C(s) + 0.5O_2(g) \rightarrow CO(g)$	0.005	0	1	74000
$C(s) + CO_2(g) \rightarrow 2CO(g)$	0.00635	0	1	162000

3.2.4 Radiation Model

In combustion processes, the radiative exchange is the most important mechanism for heat transfer. In a oxy-mild coal pulverized combustion chamber there are many radiative contribution due to the coal and char particles, soot, walls and gaseous species as CO_2 and H_2O.

3.2.4.1 P-1 Radiation Model

In the P-1 radiation model [92] the transport equation for the incident radiation G is:

$$\nabla \cdot (\Gamma \nabla G) - aG + 4an^2\sigma T^4 = 0 \tag{3.44}$$

$$\Gamma = \frac{1}{3\,(a + \sigma_s) - C\sigma_s} \tag{3.45}$$

where a is the absorption coefficient, σ_s is the scattering coefficient, G is the incident radiation, σ is the Stefan-Boltzmann constant, n is the refractive index of the medium and C is the linear-anisotropic phase function coefficient.

When a gray, absorbing, emitting, and scattering medium contains an absorbing, emitting, and scattering particles, the transport equation for the incident radiation can be written as

$$\nabla \cdot (\Gamma \nabla G) + 4\pi \left(an^2 \frac{\sigma T^4}{\pi} + E_p \right) - (a - a_p)\, G = 0 \tag{3.46}$$

where E_p is the equivalent emission of the particles, a_p is the equivalent absorption coefficient.

Moreover, on the basis of the incident radiation G, it is possible to evaluate the radiation temperature in the particle energy balance as

$$\Theta_R = \left(\frac{G}{4\sigma} \right)^{1/4} \tag{3.47}$$

3.2.5 NO_x Model

NO calculations have been performed in post-processing. In order to calculate the NO concentrations, the transport equations for nitric oxide (NO) and for intermediate

species (HCN) have been solved. In this work the thermal, fuel, prompt and N_2O paths as well as NO reburning (both gaseous phase and char particle) have been considered for the application in furnace. The N_2O and N-radical concentrations are evaluated by means of the partial equilibrium assumption. The sources for HCN and NO have been calculated averaging the instantaneous source term (S_i = f(T)) over the temperature fluctuations:

$$\langle S \rangle = \int_{T_0}^{T_{max}} P(T) S_i(T) dT \tag{3.48}$$

using a PDF-β function. T_0 is the reference temperature of the system, T_{max} is the adiabatic flame temperature.

3.2.5.1 Thermal NO_x

Thermal NO_x is based on the reactions the oxide the nitrogen taken from the air. The rate is significant at temeprature above 1400 °C. The mechanism is described by Zeldovich et al. [23]

$$O + N_2 \overset{k_{thermal,1}}{\rightarrow} NO + N \tag{3.49}$$

$$O_2 + N \overset{k_{thermal,2}}{\rightarrow} NO + O \tag{3.50}$$

$$N + OH \overset{k_{thermal,3}}{\rightarrow} NO + H \tag{3.51}$$

where $k_{thermal,1}$, $k_{thermal,2}$, $k_{thermal,3}$ are coefficients of the reactions rates eq. 3.49, eq. 3.50, and eq. 3.51. NO formation rate is given by (partial equilibrium for N-radical assumption)

$$r_{thermal} = k_{thermal,1}[O][N_2] \frac{1 - \frac{k_{thermal,1} k_{thermal,2} [NO_2]^2}{k_{thermal,1}[N_2] k_{thermal,2}[O_2]}}{1 + \frac{k_{thermal,1}[NO]}{k_{thermal,2}[O_2] + k_{thermal,3}[OH]}} \tag{3.52}$$

According to the partial equilibrium approach the O and OH radical concentrations are calculated as:

$$O_2 + H \rightarrow OH + O \tag{3.53}$$

$$O_2 + M \rightarrow M + O + O \tag{3.54}$$

The thermal source term is:

$$S_{NO,thermal} = r_{thermal} M_{NO} 10^{-3} \tag{3.55}$$

3.2.5.2 Fuel NO_x

By assuming that all fuel nitrogen is converted into HCN, the following mechanism is considered:

$$coal - N \rightarrow HCN \tag{3.56}$$

$$HCN + O_2 \rightarrow NO + ... \tag{3.57}$$

$$HCN + NO \rightarrow N_2 + ... \tag{3.58}$$

The HCN release by char and volatile is given by:

$$S_{HCN,char} = \frac{\dot{m}_{char} w_{N,char} M_{HCN}}{M_N V} \tag{3.59}$$

$$S_{HCN,vol} = \frac{\dot{m}_{vol} w_{N,vol} M_{HCN}}{M_N V} \tag{3.60}$$

where $\dot{m}_{char}$ and $\dot{m}_{vol}$ are the combustion rates of char and volatile matter (in kg/s) respectively; $\dot{m}_{char}$ is delivered by the the intrinsic model and $\dot{m}_{vol}$ is calculated by means of the CPD; V is the cell volume. The rate of HCN for the reactions eq. 3.57 and eq. 3.58 are given by De Soete [100]:

$$r_{HCN_1} = k_{HCN_1} X_{HCN} X_{O_2} exp\left(-\frac{E_{HCN_1}}{RT}\right) \frac{p}{RT} \tag{3.61}$$

$$r_{HCN_2} = k_{HCN_2} X_{HCN} X_{N_2} exp\left(-\frac{E_{HCN_2}}{RT}\right) \frac{p}{RT} \tag{3.62}$$

where: k_{HCN_1}=3.5 10^{10} 1/s; k_{HCN_2}=3.0 1/s; E_{HCN_1}=280.5 $\frac{kJ}{mol}$; E_{HCN_2}=251.2 $\frac{kJ}{mol}$. The instantaneous source term S_{HCN} is:

$$S_{HCN} = S_{HCN,vol} + S_{HCN,char} - (r_{HCN_1} + r_{HCN_2}) M_{HCN} 10^{-3} \tag{3.63}$$

The NO source term from fuel nitrogen is given by the following expression:

$$S_{NO,fuel} = (r_{HCN_1} - r_{HCN_2}) M_{NO} 10^{-3} \tag{3.64}$$

3.2.5.3 Prompt NO_x

The chemical reaction rate for prompt NO formation are proposed by De Soete [174]:

$$r_{prompt} = fA[O_2]^b[N_2][FUEL]exp(-\frac{E_{prompt}}{RT})V \tag{3.65}$$

where b is an exponent, which may vary between 0 and 1, and depends on the local mole fraction of oxygen [92].

The constant A is $6.4 \cdot 10^6(\frac{RT}{p})^{b+1}$ and $E_{prompt} = 303.5\frac{kJ}{mol}$ The factor f accounts depends on the fuel and is given by:

$$f = 4.75 + 0.0819c - 23.2\frac{1}{\lambda} + 32\frac{1}{\lambda^2} - 12.2\frac{1}{\lambda^3} \tag{3.66}$$

where c is the number of carbon atoms in the fuel and is assumed to be $c = 1.2$ for the volatile matter of the Guasare coal and λ is the air excess ratio.

The NO prompt source is then:

$$S_{NO,prompt} = r_{prompt}M_{NO}10^{-3} \tag{3.67}$$

In this work the reburning in gaseous phase and the reburning on char particles are considered following the work of Chen and Levy [101] respectively. The N_2O is taken in account as well.

Chapter 4

Results and Discussion

4.1 Application of MILD combustion in Furnace

In order to analyze the MILD combustion, it is important to study some geometric features of this type of combustion. In this chapter, the temperature field and the specie concentrations of MILD coal combustion in a pilot furnace will be presented. The attention will be focused especially on the effect of the position of coal guns and their distance from the central air jet, in order to investigate both temperature and specie concentration distributions. Keep in mind that in mild combustion several geometrical parameters are very important to obtain the "mildness" condition. One of them is the internal recirculation, which does not depend only on the high momentum of the jet, but also on the position of the jet. Consequently, the distance between the coal gun and air jet plays a crucial role. The author has performed several simulations in three dimensional steady-state conditions of a quarter of the IFRF furnace using a high bituminous A coal. The Eddy Dissipation Model has been used to describe and model the interaction between turbulence and chemistry, while the P1 model has been used for the radiation. In order to describe the solid phase and the combustion process, the Lagrangian description has been used and sub-models have been implemented for devolatilization and char burnout. The Chemical Percolation Model (CPD) has been used for the devolatilization and the intrinsic model for the oxidation of char. The turbulence phenomenon has been modeled resorting to the standard k-ϵ model, by considering the standard wall functions for the wall treatment. These models have already been presented in the previous chapter but the final aim of this section is to understand which configuration is better.

4.1.1 Geometry Description of Furnace

The sizes of furnace are the following: a square cross-section of 2X2 m and an internal length of 6.25 m. In figure 4.1 is shown the classical NFK burner, which have

already been shown in Chapter 2. Two coal guns are located at three different distances from the centerline. During the trial, two different coal guns were tested: low and high velocity coal gun. In this study, the low-velocity coal gun 2 has been considered , which corresponds to a value of coal diameter of 27.3 mm. During several tests performed by [102] detailed in-flame and input/output measurements were carried out. Because of the fluid dynamic and geometry symmetry, a quarter of furnace has been modeled. The computational domain has been discretized by 590,000 structured cells as shown in figure 4.2. The grid is finer in the region near the coal and air jet. The number of cells is enough to consider the problem mesh-independent [41]

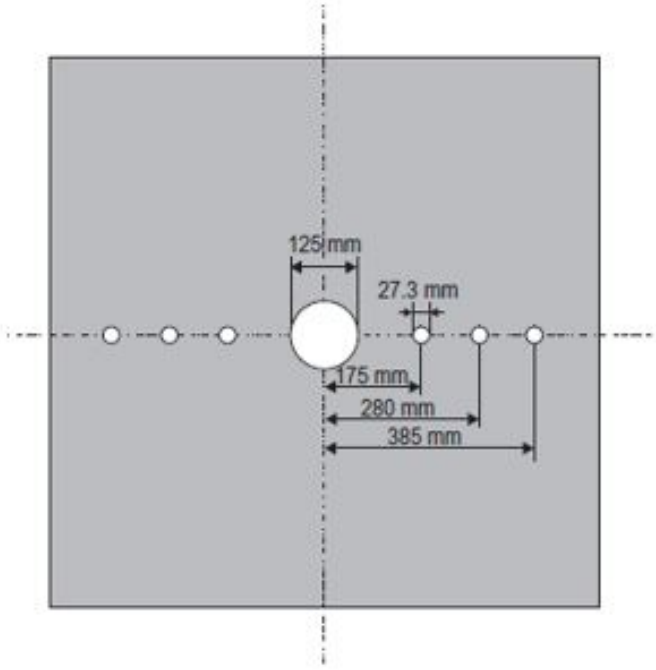

FIGURE 4.1: NFK burner

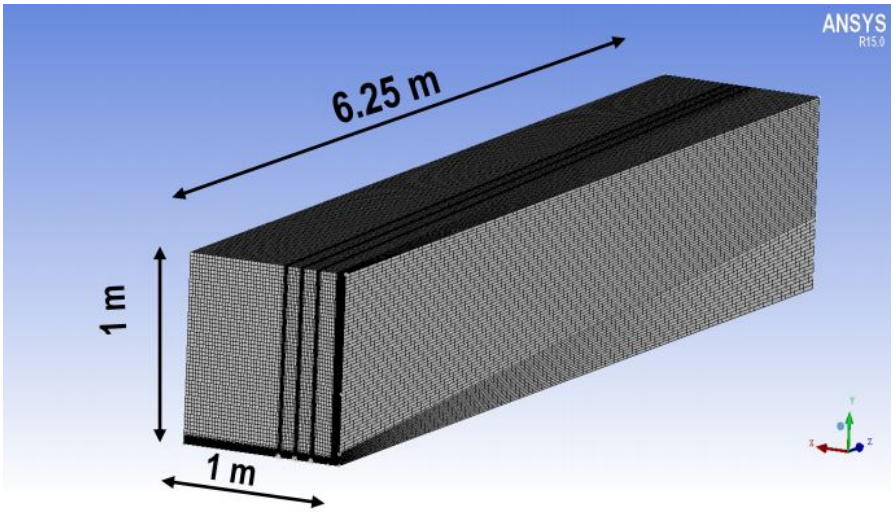

FIGURE 4.2: Geometry and computational grid of a quarter furnace

For further description of the IFRF Furnace the author suggests to consult the work of Schaffel [41]

4.1.2 Coal Properties

The high bituminous A coal has been used to perform the numerical simulations. The proximate and ultimate analysis of coal are given in table 4.1 and table 4.2, respectively. [41]

Table 4.1: Guasare Coal Proximate Analysis [41]

Composition	wt%
Moisture	2.9
Volatile Matter	37.1
Fixed Carbon	56.7
Ash	3.3
LHV	31.74 (MJ/kg)

Table 4.2: Guasare Coal Ultimate Analysis (dry-ash-free basis) [41]

Composition (wt% daf)	Coal	Char	Volatiles
C	81.6	92.6	72.51
H	5.5	1.3	9.10
N	1.5	1.7	1.3
O	10.7	4.0	16.3
S	0.6	0.4	0.8

Detailed information about the size particle distribution, other properties of this kind of coal, and the boundary conditions can be found in the Schaffel's work [41]

4.1.3 Parameters for the CPD model

As described in the Mathematical Model section, the CPD is a model that requires five input parameters in order to characterize the devolatilization process of coal. These five parameters could be determined from the C NMR spectroscopy [103]but it is a very complex procedure. Schaffel et al. [41] utilized the IFRF experimental data in order to characterize both devolatilization and char combustion of Guasare coal, and thus determine the five parameters of the CPD model. Since these procedures are expensive and time consuming, in this work the Genetti correlations have been used [103].They consist in a series of non-linear correlations capable to estimate the five parameters.

These parameters are: the average molecular weight per aromatic cluster (M_{cl}), the average molecular weight per side chain (M_{del}), the average number of attachments per cluster, referred to as the coordination number ($\sigma + 1$), the fraction of attachments that are bridges (p_0) and initial fraction of char bridges (c_0). Genetti suggests a quadratic correlation to obtain values for M_{del}, M_{cl}, and $\sigma + 1$.

$$y = c_1 + c_2 X_C + c_3 X_c^2 + c_4 X_h + c_5 X_H^2 + c_6 X_O + c_7 X_O^2 + c_8 X_{VM} + c_9 X_{VM}^2 \quad (4.1)$$

The values of p_0 and c_0 has been obtained from the work of Schaffel et al. [41]. The values of parameter of CPD model, obtained by Genetti correlation and by Schaffel work, are listed in Table table 4.3.

TABLE 4.3: Parameters for the CPD model [41]

Parameter	Symbol	Value	Unit
Cluster molecular weight	M_{cl}	33.6	kg/kmol
Side chain molecular weight	M_{del}	359	kg/kmol
Lattice coordination number	$\sigma + 1$	4.95	-
Initial fraction of bridges in coal lattice	p_0	0.51	-
Initial fraction of char bridges	c_0	0	-

4.1.4 Volatiles and Char Combustion

The combustion of volatiles has been represented by two step-chemical mechanism. It involves the oxidation of the pseudo specie volatile to CO in the first reaction, while in the second one of CO to CO_2 :

$$C_{1.33}H_{4.13}O_{0.50}N_{0.12} + 1.44O_2 \rightarrow 1.33CO + 2.06H_2O + 0.0595N_2 \quad (4.2)$$

$$CO + 0.5O_2 \rightarrow CO_2 \quad (4.3)$$

The rate of these two homogenous reactions is provided by EDM (Eddy Dissipation Model). According to the EDM, turbulent mixing controls the rate of the reaction. For this reason it is assumed that the Damkhöoler (Da) number is infinite. The Da number is the ratio between the characteristic mixing scale and the characteristic chemical time. Thus, the kinetic rates can be ignored, and the combustion is based on the mixing. It is important to notice that, for an assumed reaction, the main idea of the EDM is to consider the turbulent time scale k/ϵ, instead the chemical time scale. Thereby the model does not consider the effect of chemical kinetics. This model would seem appropriate for this kind of phenomenon as showed by several works [41,104].

It has been clearly stated and proved that char oxidation can occur in the internal pores of char particles. For this reason the rate of char oxidation (eq. 4.4) is provided by the the intrinsic model, based on the Smith's [98]. This Model has been presented in previous chapter.

$$C(s) + O_2(g) \rightarrow CO_2(g) \quad (4.4)$$

The input parameters for the intrinsic char model of Guasare coal are given by the Schaffel work [41], and they are shown in table 4.4.

Table 4.4: Parameters for the Intrinsic Char Combustion Model [41]

Parameter	Symbol	Value	Unit
Mass diffusion-limited rate constant	C_1	$5{\cdot}10^{-12}$	$m^3/K^{0.75}s$
Pre-exponential factor	A_i	$1{\cdot}10^{-3}$	kg/m^2s
Activation energy	E_i	$5 \cdot 10^7$	J/kmol
Char porosity	θ	0.74	-
Mean pore radius	r_p	$1 \cdot 10^{-7}$	m
Specific internal surface area	A_g	$2.5 \cdot 10^4$	m^2/kg
Tortuosity	τ	$\sqrt{2}$	-

table 4.5 summarizes the sub-models used for the application of MILD combustion in furnace.

Table 4.5: Mathematical Model for MILD combustion in furnace

Physical Process	Sub-Models
Turbulence	k-ϵ Model
Chemistry-Turbulence Interaction	Eddy Dissipation Model
Lagrangian Particle Tracking	Discrete Phase Model
Devolatilization	Chemical Percolation Devolatilization Model
Char Combustion	Intrinsic Model
Radiation Model	P1 Model

4.1.5 Temperature Field

The author finds it necessary to show the comparison between the different coal gun positions in order to analyze the temperature field, the species concentrations, and especially the NO_x emissions at the outlet. In this section, the temperature field will be presented. The configuration analyzed are shown in table 4.6

Table 4.6: Distance between air jet and coal guns for all configurations

Configuration	Distance between air jet and coal guns
1	175 mm
2	280 mm
3	385 mm

In figure 4.3, figure 4.4 and figure 4.5 are shown the temperature field for the configurations 1-2 and 3, respectively.

In the configuration 1, the coal and air mix with each other rapidly. For this reason, the flame is attached because the combustion takes place in environment with O_2 *vol*% dry higher than 3%. This configuration is closer to a traditional burner than the configuration 3, in which the coal entrains the combustion products. Because the

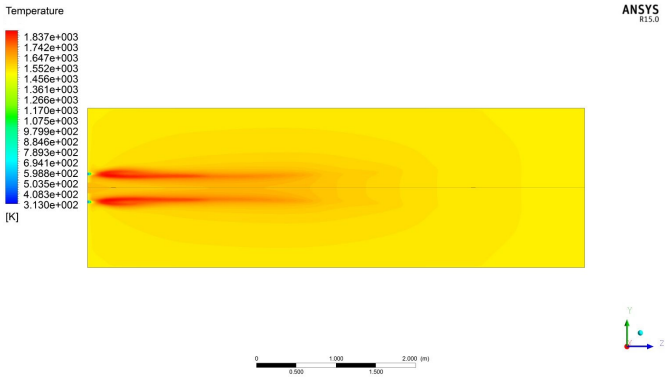

FIGURE 4.3: Temperature field for the configuration 1

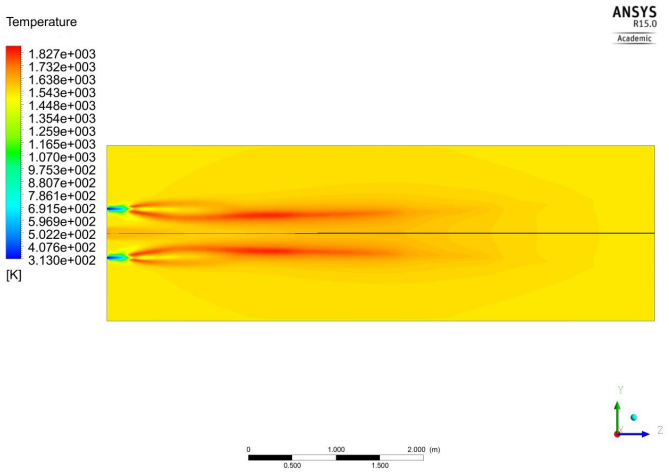

FIGURE 4.4: Temperature field for the configuration 2

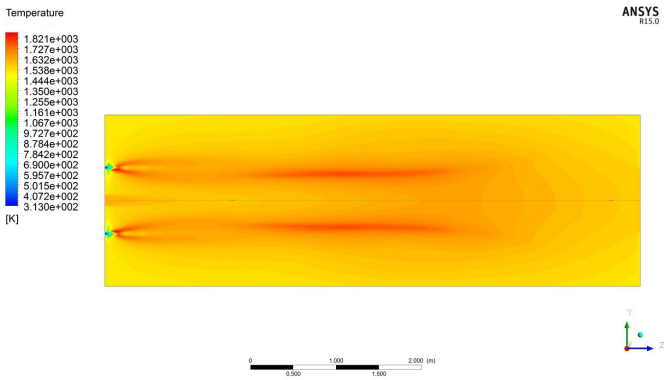

FIGURE 4.5: Temperature field for the configuration 3

combustion process occurs in a lower $O_2\%$ environment the zone becomes fuel-rich.

This process, called "intertisation", allows to obtain values of temperature very similar to the combustion products ones. This is owing to combustion takes place gradually and simultaneously entrains the combustion products at the process temperature. This phenomenon is mainly highlighted in the configuration 3. The figure 4.6 and figure 4.7 show real and simulated pictures of the flame in configurations 1 and 3.

The figure 4.8 shows the comparison for the temperature along seven radial traverses, which are taken in the plane crossing both the coal and the comburent jets at the following distance from the inlets: traverse 1: 0.15 m; traverse 2: 0.44 m; traverse 3: 1.32 m; traverse 4: 2.05 m; traverse 6: 3.22 m; traverse 7: 4.97 m.

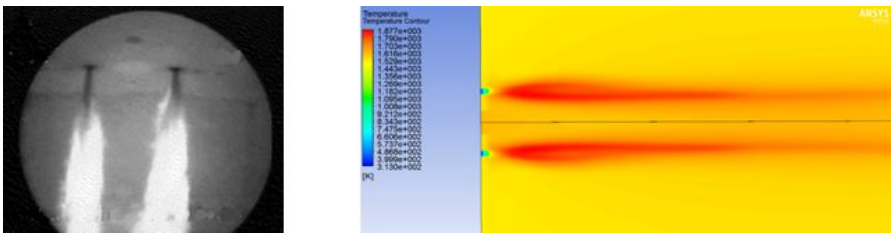

FIGURE 4.6: Real and simulated flame for configuration 1

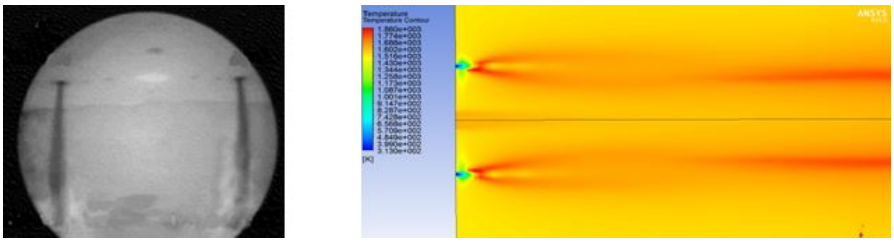

FIGURE 4.7: Real and simulated flame for configuration 3

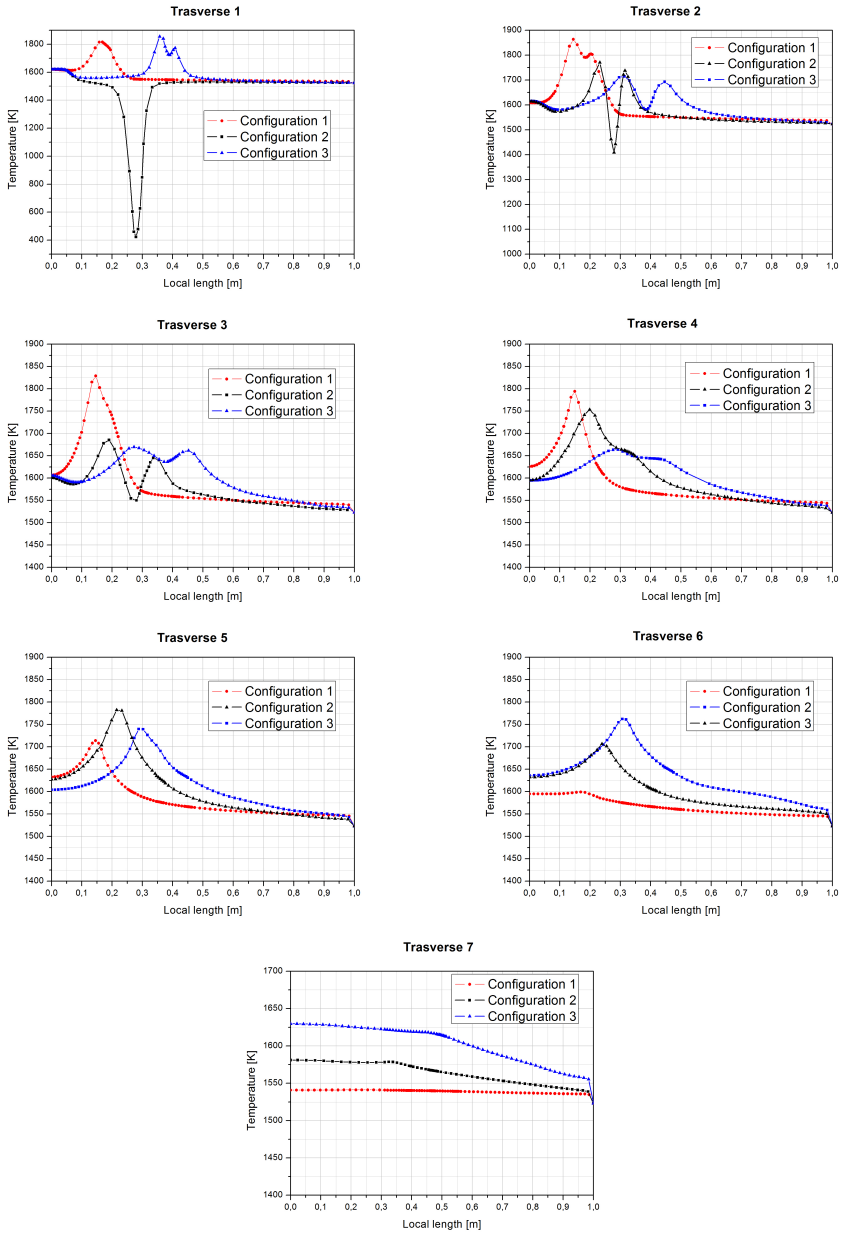

FIGURE 4.8: Temperature profiles for different traverses

4.1.6 Oxygen Concentration Field

In figure 4.9, figure 4.10 and figure 4.11 , the oxygen concentration fields for the respective configurations are shown. It is important to note that the concentration of oxygen assumes a uniform distribution downstream of the half furnace. Consequently, the radial profile is flat and assumes a value of about 3%. The combustion products fills the furnace with the 3% of O_2. In the configuration 3, the ignition stand – off at a distance, from the burner, farther than the configuration 1.

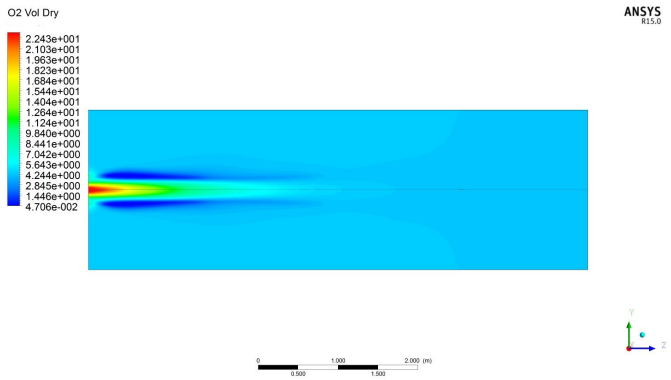

FIGURE 4.9: Oxygen concentration field for the configuration 1

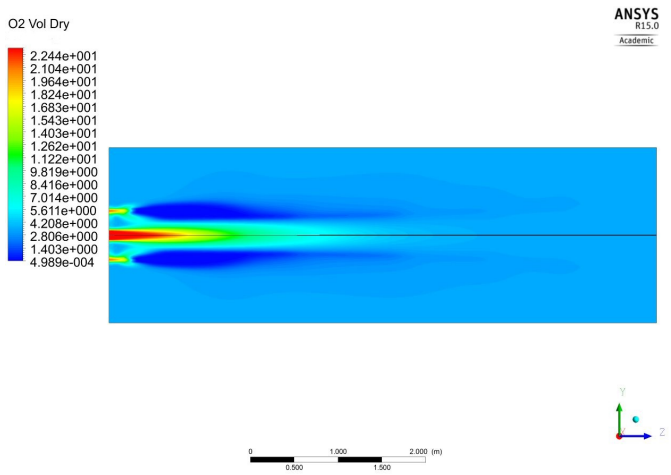

FIGURE 4.10: Oxygen concentration field for the configuration 2

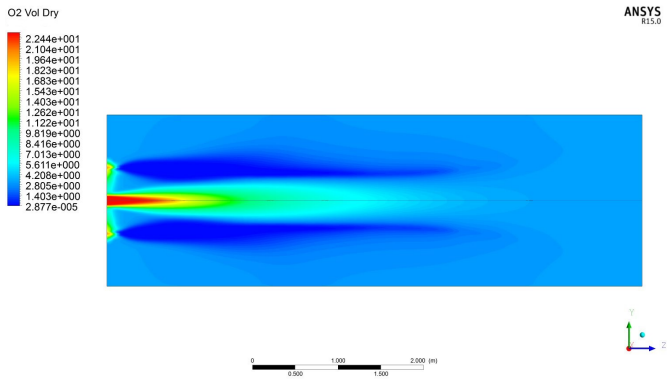

FIGURE 4.11: Oxygen concentration field for the configuration 3

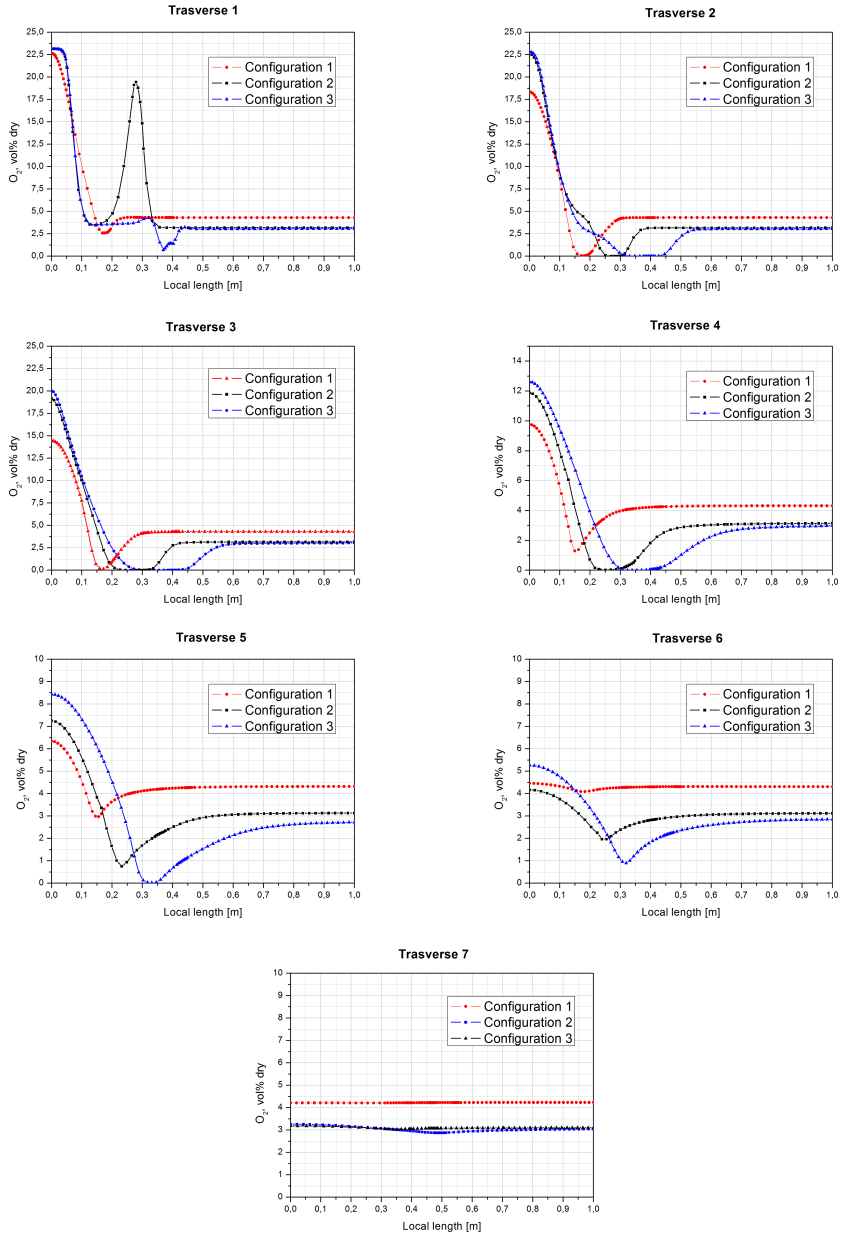

FIGURE 4.12: Oxygen concentration profiles for different traverses

4.1.7 Carbon Dioxide Concentration Field

Carbon dioxide concentration is shown in the figure 4.13, figure 4.14 and figure 4.15.

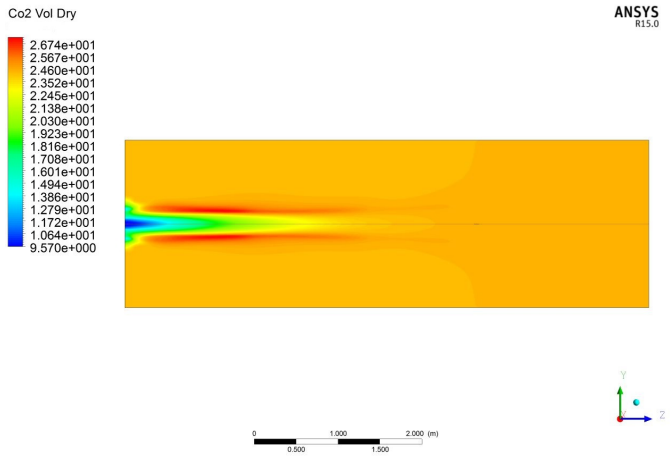

FIGURE 4.13: Carbon dioxide concentration field for the configuration 1

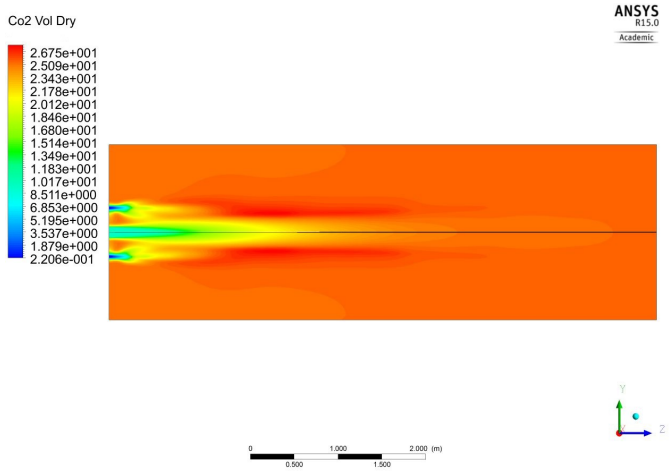

FIGURE 4.14: Carbon dioxide concentration field for the configuration 2

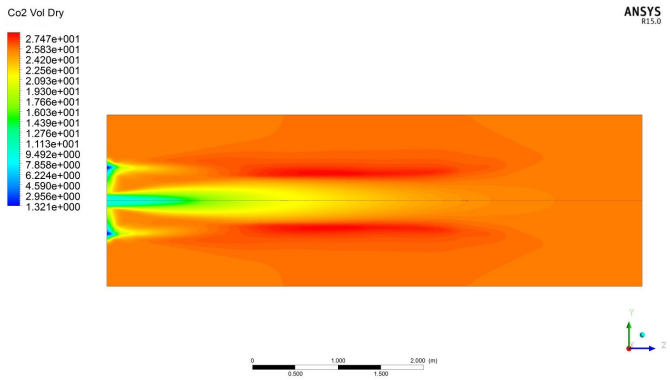

FIGURE 4.15: Carbon dioxide concentration field for the configuration 3

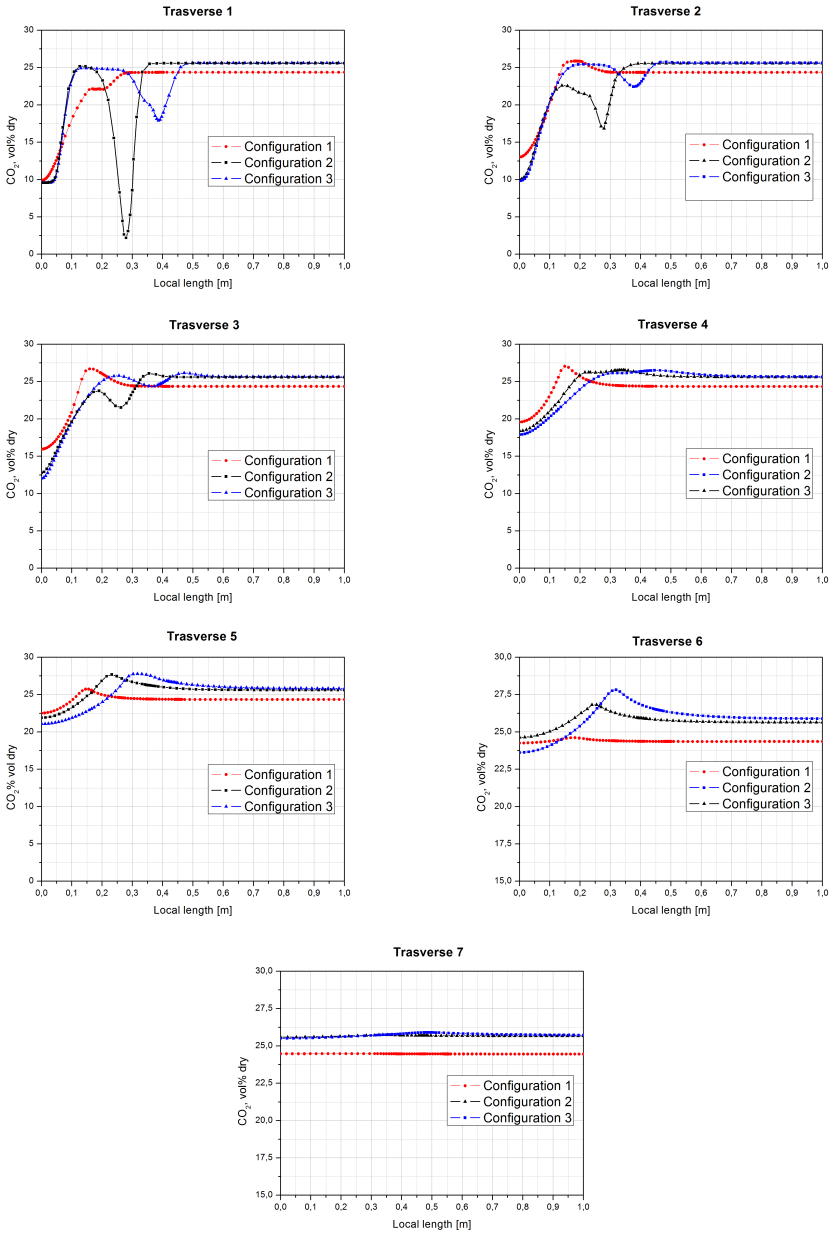

FIGURE 4.16: Carbon dioxide profiles for different traverses

The table 4.7 summarizes the temperature, oxygen and carbon dioxide concentrations at the outlet of furnace for the configurations 1,2 and 3.

TABLE 4.7: Numerical values at the furnace outlet

Configurations	O_2%	CO_2%	Temperature [K]
1 (175 mm)	4.22	24.47	1531.5
2 (280 mm)	3.31	25.38	1534.9
3 (385 mm)	3.15	25.61	1567.5

The work of Schaffel [41] provides the experimental results for the configuration 2. The numerical values calculated in this work agree with the measurements.

4.1.8 Nitric Oxides Emissions results

Another important objective of this work is to understand and show in what ways some geometric parameters are crucial to get low NO_x emissions. In other words, the distance between the coal and the air jet is essential for the formation of nitric oxides. First of all, the mild combustion allows to reduce the NO_x emissions without resort to the so-called primary methods. NO_x emissions decrease from configuration 1 to configuration 3 as shown in figure 4.17. In configuration 1, within the primary zone of the flame, the oxygen concentration is higher than the one in configuration 3. This is due to the distance between the coal gun and air jet. The third configuration allows to get a fuel-rich zone in which the NO_x is reduced due to the production of reductive radicals (HCN) which reduce the existing NO_x. In figure 4.17, the NO_x emissions at the outlet furnace for the three coal gun positions are shown.

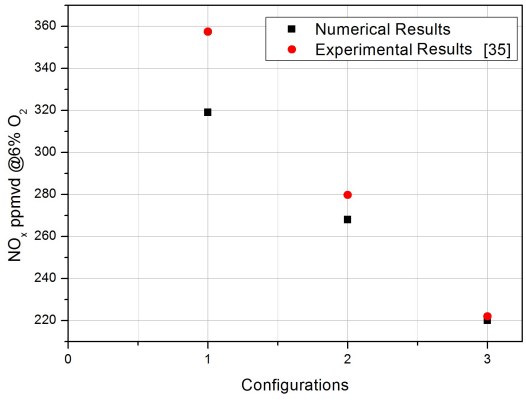

FIGURE 4.17: Numerical and experimental values of nitric oxides at the outlet for all configurations

The numerical results are in good agreement with the experimental results [35].For configuration 1 the NO_x at the outlet is overestimated. For the third one, on the contrary, it is practically the same value. Clearly, as mentioned before, in configuration

1 the flame is attached. This means that the coal is not able to entrain a large amount of combustion products, but the ignition occurs in an environment with higher O_2 concentration than the one of configuration 3. This is due to the fuel NO_x, which increases with the growing concentration of oxygen. The three configurations analyzed show different temperatures and species fields. This characteristics clearly show how the aerodynamic of combustion chamber is very important to get strong recirculation to achieve the "mildness" condition.

4.2 Application of Oxy-MILD Combustion in Furnace

The aim of this section is to demonstrate the advantages of a combination of these two combustion technologies in a pilot furnace to analyze the temperature and species concentrations field, but also the CO_2 and NO_x emissions by means of CFD. The final goal is to understand if it is possible to combine the MILD combustion and OXY one to reduce NO_x emissions and capture CO_2. The reference furnace is the IFRF which has already been described in previous sections.

4.2.1 Boundary Conditions

For the Oxy-Mild combustion in furnace, the properties of coal, the mathematical model for both gas and solid phase and the spatial discretization are the same of the previous simulations. The boundary conditions, instead, are listed in table 4.8 and table 4.9 for the two inlets.

Table 4.8: Boundary conditions for the secondary inlet

	Mass Flow Rate [kg/h]	T [K]	Composition (vol%)	Oxygen Mass Flow [kg/h]
Case 1	675	1623.15	CO_2 8.1%; O_2 19.7%; N_2 57.2%; H_2O15.1%;NO_x 70 ppm (dry)	138.5
Case 2	675	1623.15	O_2 19.7%; CO_2 81%	138.5

Table 4.9: Boundary conditions for the primary inlet

	Mass Flow Rate [kg/h]	T [K]	Composition (vol%)
Case 1	130	313.15	O_2 21%; N_2 79%
Case 2	130	313.15	O_2 21%; N_2 79%

In the both cases the burner works with a stoichiometric ratio of $\lambda = 1.2$. To achieve this condition, it has been essential to keep the same oxygen mass flow in both cases. In other words, all simulations have been performed maintaining the same oxygen excess in the air jet. Case 1 corresponds to the mild combustion in configuration 2, described and analyzed in the previous sections.

4.2.1.1 Results and Discussion

In this section, the results of the cases analyzed in term of temperature, species concentrations and NO_x pollutant emissions will be shown.

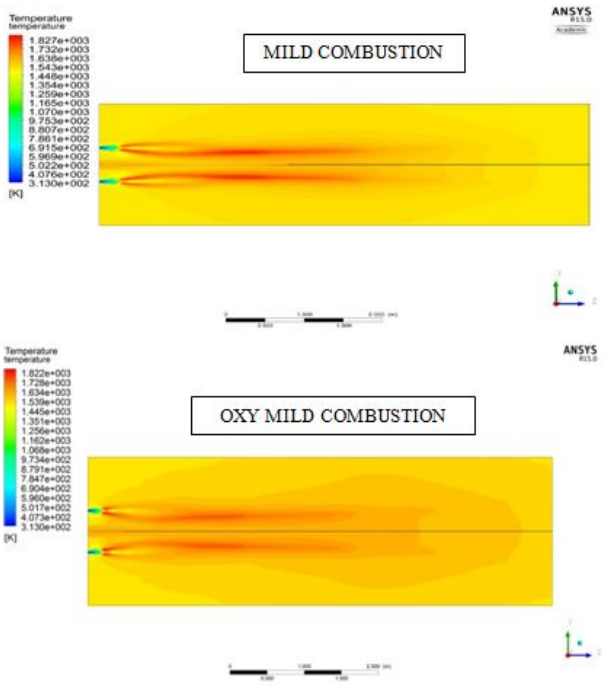

FIGURE 4.18: Contour plot of temperature for MILD and Oxy combustion

Figure 4.18 shows the contour plot on the symmetry section of temperature for the two cases, while figure 4.19 shows the comparison for the temperature along the seven radial traverses.

The temperature level and the peak of temperature are very similar in both cases. It is worth noticing that the oxy mild combustion provides a temperature level lower than the only mild combustion. This is due to the specific heat of CO_2 is higher than the N_2 when the temperature is around the typical flame temperature. This condition affects the production of Thermal NO_x. Nevertheless, It is well known that in coal combustion Thermal NO_x represents a little percentage of the total NO_x, but either way it is important to take in account in order to obtain very low NO_x emissions. Anyway, because the Fuel NO_x are affected by the oxygen distribution, it is noteworthy to analyze the oxygen profiles.

Figure 4.20 shows the contour plot of oxygen concentrations for both cases. Figure 4.21, instead, shows the oxygen concentrations profiles along the seven traverses. The trend is very similar for both cases, the oxy-mild provides a lower oxygen concentration level than the mild one. Downstream the fourth traverse, for both cases, the oxygen concentration is uniform. The furnace is practically filled by

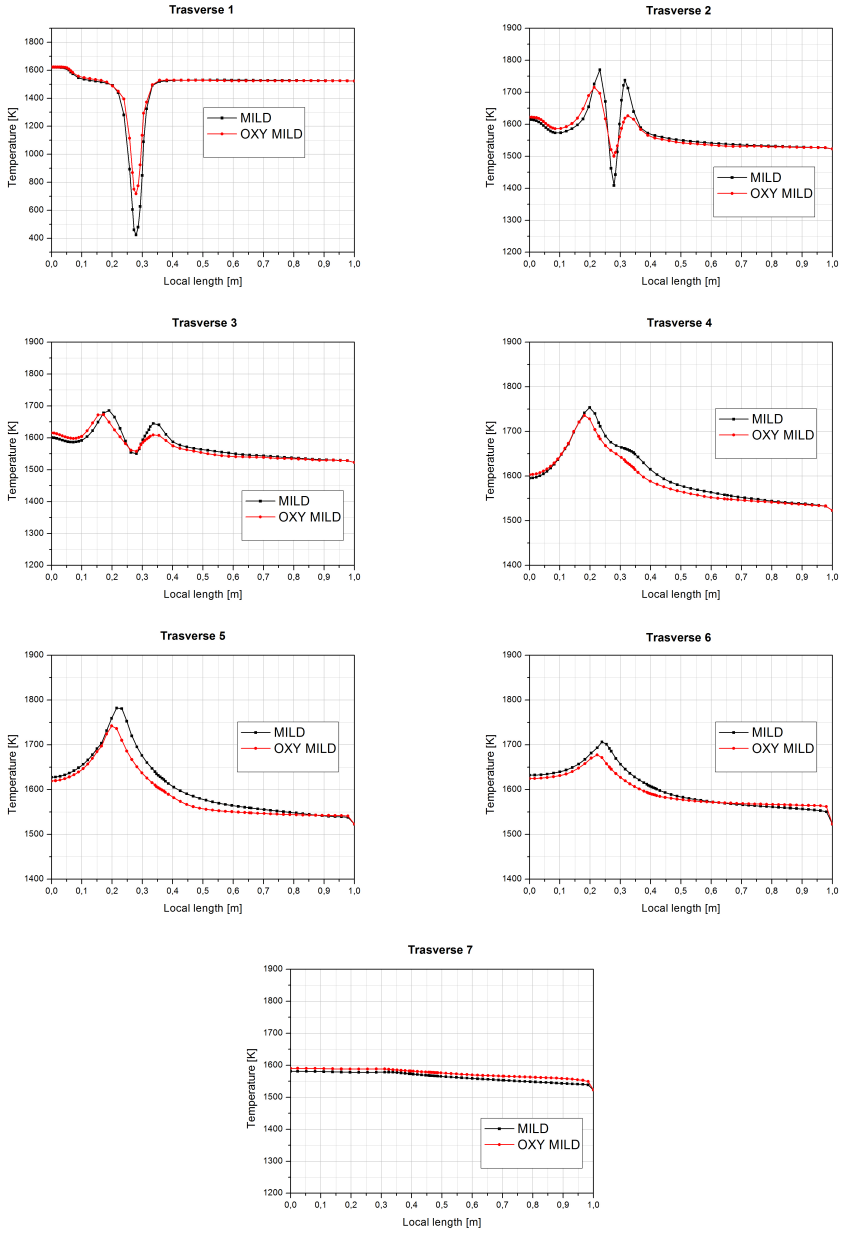

FIGURE 4.19: Temperature profiles for different traverses in oxy-mild combustion]

oxygen at 3% for the first case and around 2.7% for the second one. This different concentration and distribution around the flame zone affect the Fuel NO_x.

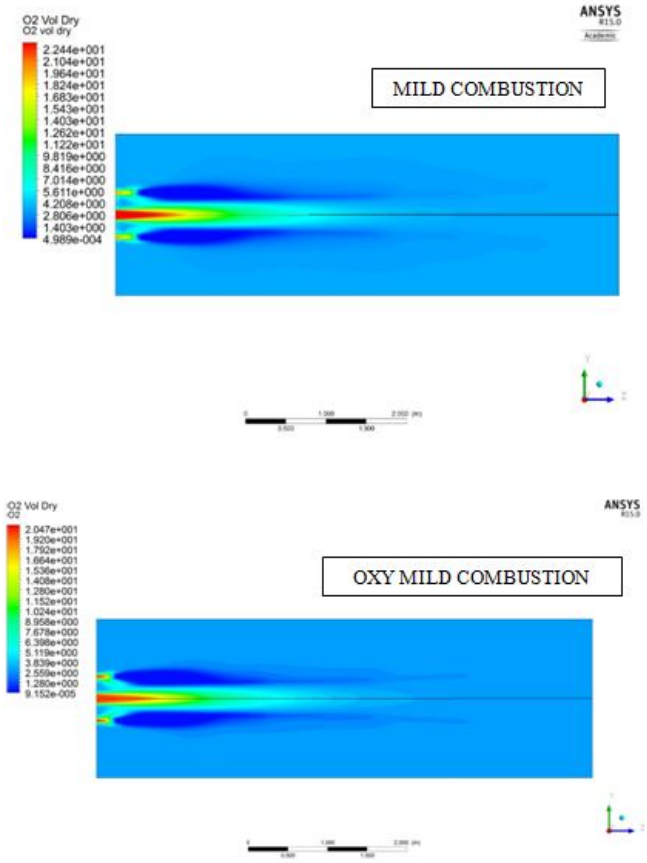

FIGURE 4.20: Contour plot of oxygen concentration for MILD and Oxy combustion

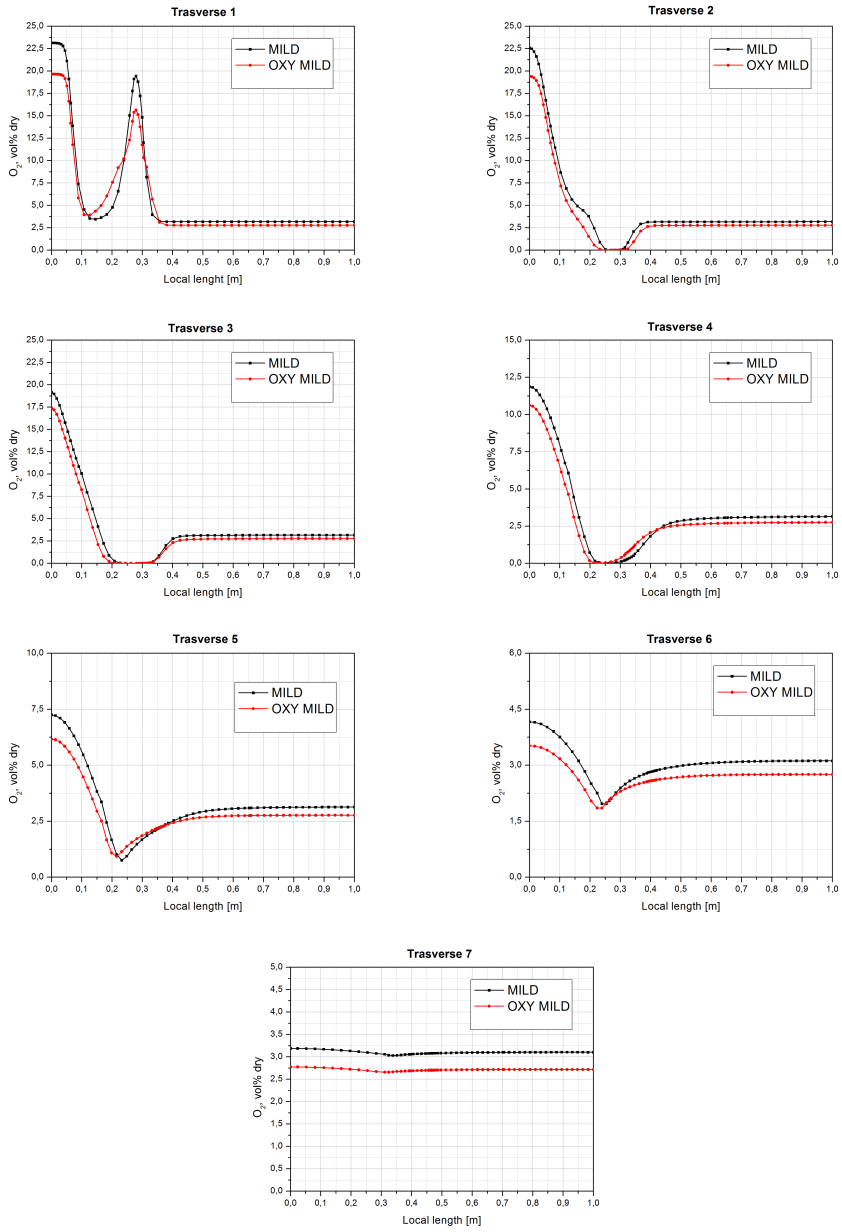

FIGURE 4.21: Oxygen concentration profiles for different traverses in oxy-mild combustion

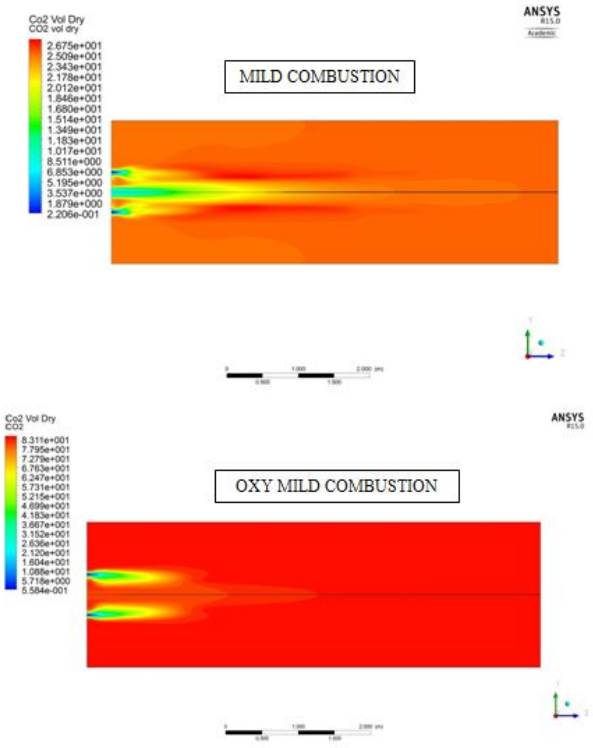

FIGURE 4.22: Contour plot of carbon dioxide concentration for MILD and Oxy combustion

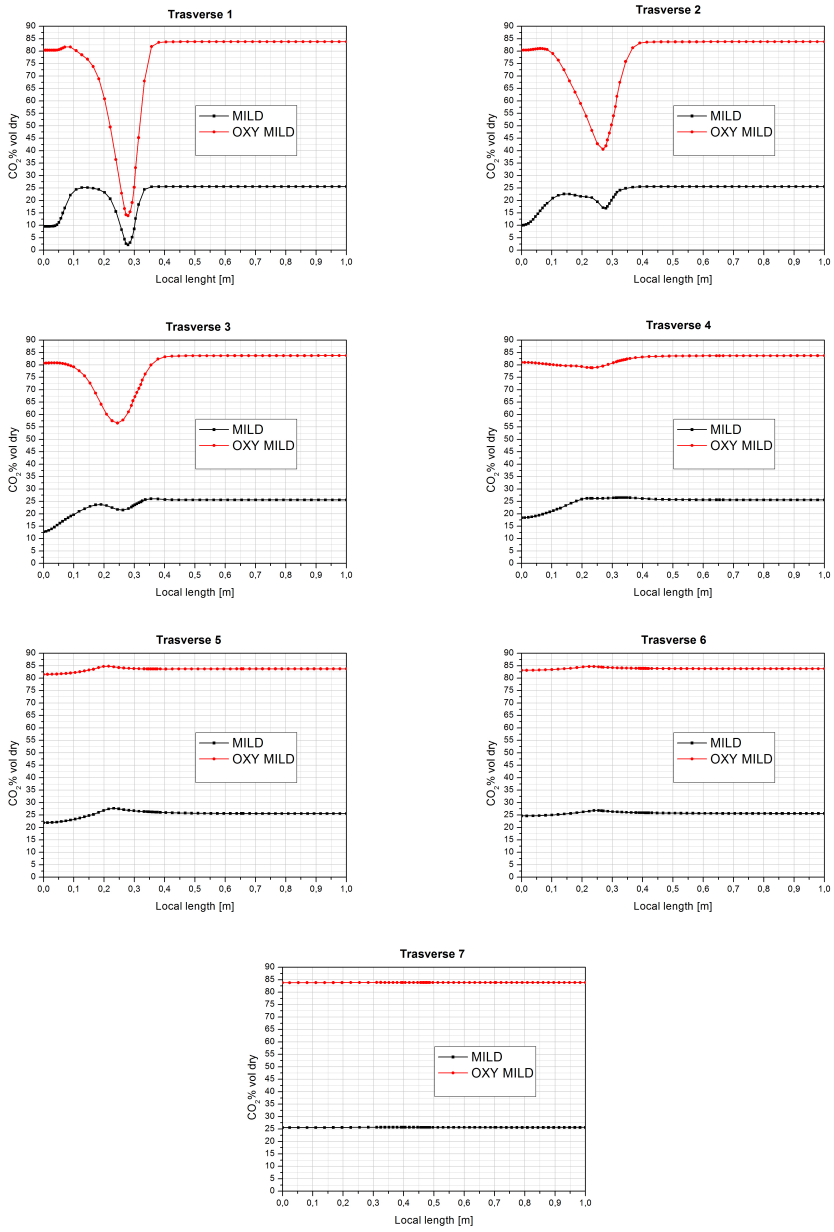

FIGURE 4.23: Carbon dioxide concentration profiles for different traverses in oxy-mild combustion

Carbon dioxide contour plot is shown in figure 4.22, while in figure 4.23 shows the carbon dioxide concentration profile along the seven traverses. In this case the difference is huge in term of values of concentration. Clearly, this is due to the oxy condition in the second case. The oxy mild combustion allow to fill the furnace with high level of carbon dioxide. This condition is very important because it allows to capture in easy way the carbon dioxide. The percentage of carbon dioxide concentration at the outlet of furnace is between the 80% and 85%. The higher the value of CO_2 concentrations the easier it is to capture. Good values are above the 90%. This could be done by substituting the transport air with carbon dioxide, in order to eliminate the nitrogen in the combustion process.

The formation of NO_x has been analyzed according to the model proposed in chapter 3. In the first case the NO_x emissions are due to all types of NO_x especially thermal and fuel. In the second one, they are mainly due to fuel NO_x. The second case shows lower values of NO_x compared to the first one, because the thermal NO_x are practically missing and the fuel-NO_x are lower than the first case because of lower values of oxygen concentration profile. Keep in mind that the fuel NO_x increase when the oxygen concentrations grows. In table 4.10 are given the numerical results of NO_x concentration at the furnace outlet.

TABLE 4.10: Computed values of NO_x concentration at the furnace outlet

Case	NO_x ppm dry	NO_x@6O_2%
1	323	272
2	270	222

In this section, a preliminary study has been performed on the potential gains of the oxy-mild combustion of pulverized coal in a pilot furnace. The idea of the author is to combine the advantages of the two technologies in order to investigate the temperature, species concentration profiles and the NO_x pollutant emissions in a pilot furnace. The influence of a CO_2 dilution in the oxidizer respect to the standard case has been examined . The results show the advantages of oxy-mild combustion in term of NO_x emissions. This condition allows to understand how future works about this new technology can improve the efficiency of combustion process in order to obtain environmentally-friendly technologies. Anyway, the external recirculation of carbon dioxide needs a high electrical power, thus, to avoid this lost efficiency in the system, the CO_2 can be used as a primary jet by transporting the coal. Probably, this condition could provide good results as well, with the advantage of reducing the electrical power for external recirculation.

In the next section this perspective will be analyzed with application in boiler.

4.3 Application in Boiler

In this section, the possibility to combine the two combustion technologies in a novel concept of boiler will be analyzed. In order to understand if it is possible to combine them, the author has performed several numerical simulations by considering two types of boilers: a small and a medium boiler. Different shapes, geometric parameters as well as different models for the char combustion have been analyzed to investigate the best configuration. The aim is to find the configuration that combines the advantages of Oxy and MILD combustion. With this purpose, the author has investigated the temperature and specie concentrations field, the wall heat flux and some statistical parameters, which allow to provide information about the uniformity of temperature and specie concentration in the whole volume of the boiler. A uniform distribution of wall heat flux allows to employ the boiler in super-critical power plant. Thus, the main goals of this section are:

- To combine the Oxy and MILD combustion.
- To investigate different shape and geometric parameters.
- To consider different model for the char combustion.

In term of results:

- To analyze the temperature and species concentration distribution.
- To provide information about the char burnout.
- To investigate the wall heat flux. Analyze the uniformity of temperature in the whole volume by means of statistical parameters.

These results will be compared with standard boiler and with several findings by other authors.

4.3.1 Small Boiler

The first researchers who have introduced a novel concept of boiler in ultra-supercritical plant were Schaffel et al. [42]. This work starts from this type of boiler, but differently from the Schaffel's boiler, the goal is to investigate the possibility of obtaining mildness condition in small boiler under oxy-combustion condition. This is a challenge because it is more difficult to obtain mild combustion in a small boiler. Indeed, there have to be a great combustion chamber in order to allow the internal recirculation of combustion products. By this mean, a first hypothetical small boiler has been presented.

4.3.1.1 Properties of Janina Coal

The coal used to perform the numerical simulations is the Janina Coal, which originated from a large coal mine in Poland. This kind of coal is classified as sub-bituminous coal. Table 4.11 and table 4.12 show the proximate and ultimate analysis of this coal, respectively.

Table 4.11: Janina Coal Proximate Analysis

Composition	wt%
Moisture	10.70
Volatile Matter	44.64
Fixed Carbon	35.66
Ash	9.0
LHV	31.74 (MJ/kg)

Table 4.12: Janina Coal Ultimate Analysis (dry-ash-free basis)

Composition (wt% daf)	
C	67.42
H	5.01
N	0.71
O	26.66
S	0.2

Because the goal is to burn the coal directly in the boiler, it is necessary to calculate the ultimate analysis as received (table 4.13)

Table 4.13: Janina Coal Ultimate Analysis (as received)

Composition (wt% as received)	
C	56.32
H	41.85
N	0.59
O	22.27
S	0.17

4.3.1.2 Geometry, Mesh Description and Numerical Setting

The burner is located at the top wall of the boiler, while the outlets of combustion products are set on the side of it. The burner presents the FLOX configuration. A detailed description of this type of burner can be found in section 2.3.1. This burner is made up of a central jet of coal and four oxygen jets, instead of air. It is important to underline that that the combustive agent is composed by pure oxygen and not by a mixture of oxygen and carbon dioxide. The goal is to recirculate, externally, a little part of carbon dioxide in order to reduce the electrical power required to the fans. For

this reason, the carbon dioxide is used as a primary jet by transporting the coal.

The shape and size of boiler are shown in figure 4.24, while figure 4.25 shows the top wall, in which the burner is located. The boiler has 3.6X2.56 m cross section and a height of about 7 m.

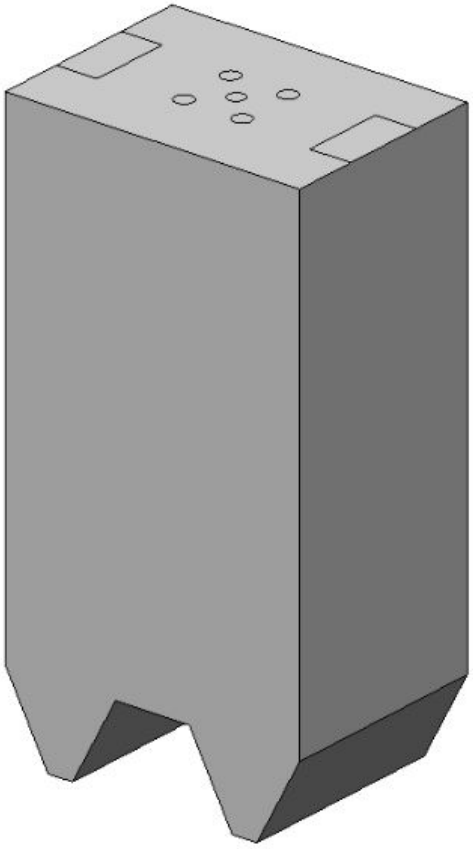

FIGURE 4.24: 3D view of small boiler

In order to discretize the computational domain, a structured mesh has been used. The number of rectangular cells is about 900000. The grid size is finer near the burner, where the combustion of coal takes place. Figure 4.26 shows the computational domain of the top wall.

The mass, momentum, energy and species conservation equations are solved using the finite volume technique. Because the flow developed in the combustion chamber is at a low speed and incompressible ($M < 0.3$), the pressure-based approach is used to solve the governing equations. The velocity field is obtained from the momentum equations, while the pressure field is determined by solving the pressure correction equation, which allow to obtain the pressure field in all points of the computational domain. The SIMPLE (Semi-Implicit Method for Pressure-Linked Equations) is the algorithm for the calculation on staggered grid of pressure. The option chosen for the interpolation of pressure values at the faces is the PRESTO! (PREssure STaggering Option) [92].

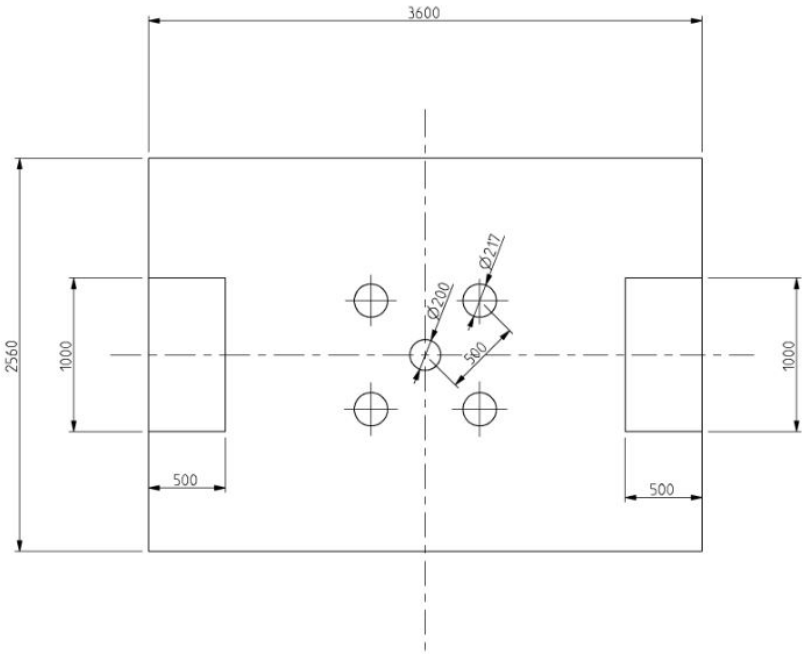

FIGURE 4.25: Top wall of small boiler

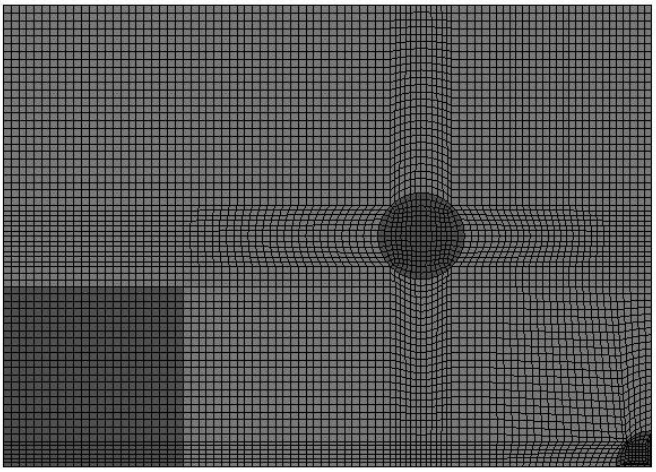

FIGURE 4.26: MSpatial discretization of top wall of a quarter of small boiler

4.3.1.3 Boundary Conditions

In table 4.14 are summarized the boundary conditions used in this first kind of boiler.

The burner works with a relative air-fuel ratio of $\lambda = 1.1$ (10% of oxygen in excess). The velocity and temperature of oxygen is very high in order to both obtain an internal recirculation and to allow the reactions to take place at temperatures above the self-ignition temperature, in a distributed large volume instead rather than a highly convoluted one, thin and stretched flame front.

Table 4.15 summarizes the sub-model used.

TABLE 4.14: Boundary Conditions

Name	type	number	settings
O_2 Inlet	Velocity Inlet	4	wt% O_2 = 100 %; $\dot{m} = 6.56kg/s$; v = 137 m/s; T= 1200 K
Transport CO_2 Inlet	Velocity Inlet	1	wt% CO_2 = 100%; $\dot{m} = 1.26kg/s$; v = 22.5 m/s; T = 300 K
Coal Inlet	Injection	1	$\dot{m}$ = 3.68 kg/s; v = 22.5 m/s; T = 300 K
Outlet	Pressure Outlet	1	p = 101325 Pa
Walls	Wall	-	$\epsilon = 0.6; T = 800K$

TABLE 4.15: Mathematical Model for MILD combustion in furnace

Physical Process	Sub-Models
Turbulence	k-ϵ Model
Chemistry-Turbulence Interaction	Eddy Dissipation Model
Lagrangian Particle Tracking	Discrete Phase Model
Devolatilization	Two Compenting Rates
Char Combustion	Diffusion-Limited Surface Reaction
Radiation Model	P1 Model

4.3.1.4 Results and Discussion

In this section, the first numerical results will be presented. In figure 4.27 and in figure 4.28 the temperature field are shown. The slice planes cut the boiler both along the symmetry and the centerline oxygen inlets.

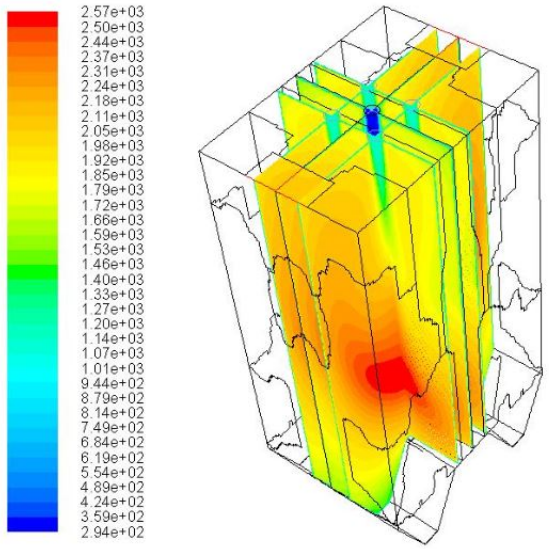

FIGURE 4.27: Temperature field in the boiler

The temperature range is 1600-2600 K, as shown in figure 4.28. The peak temperature is high enough for HTAC combustion. Likely, it is due to a poor recirculation of combustion products. For this reason the coal does not entrain a large

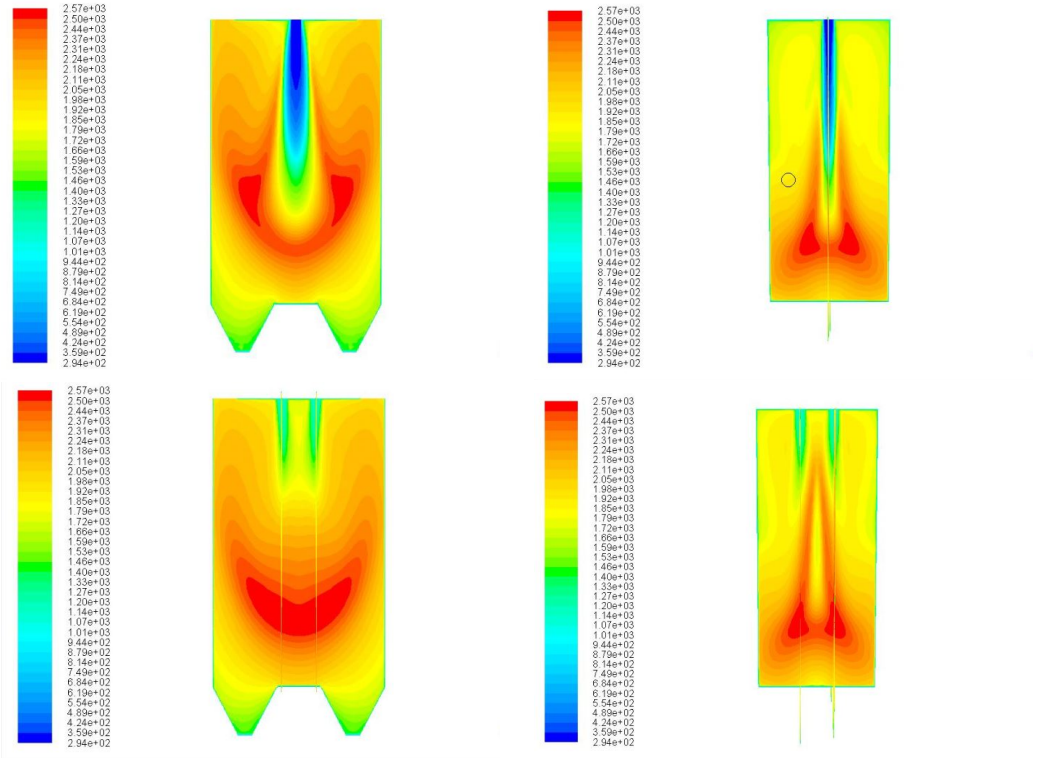

FIGURE 4.28: Temperature distribution in different slice planes

amount of combustion products, but there are zones in which the coal locally burns. The temperature at the outlet of boiler is around 1997 K.

The oxygen field is shown in figure 4.29. The average concentration of oxygen is around 27%, and the distribution is not very uniform. On the left, the figure shows a more uniform distribution because the exits of furnace are located along the higher dimension of boiler. Thus, the recirculation is naturally higher on these planes. In the coal devolatilization region, the oxygen concentration drops to almost zero. The oxygen concentration in flue gas is 20%. This means that the burn out of char is not optimal, indeed the value is 83%. Figure 4.30 shows the carbon dioxide concentration on dry basis.

In oxy-coal combustion, the carbon dioxide distribution and the value at the exit of boiler are important results for the capture of CO_2. Indeed, the higher the flue gas CO_2 concentration is, the easier to separate. In case of high concentration (greater than 90%), it would be enough only to condense the water vapor. The carbon dioxide concentration on dry basis is 79% and it is not a desired value. These results strongly depend on the char model used. In these first findings, the only contribution to the char combustion is given by the heterogeneous reactions of char with the oxygen, according to the diffusion-limited model.

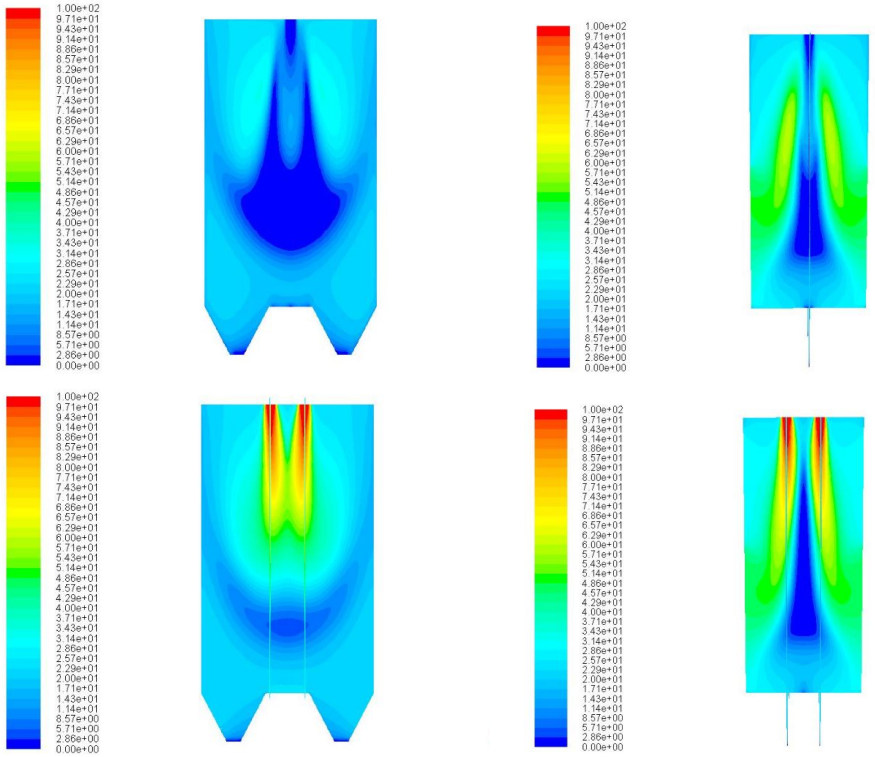

FIGURE 4.29: Oxygen concentration distribution in different slice planes

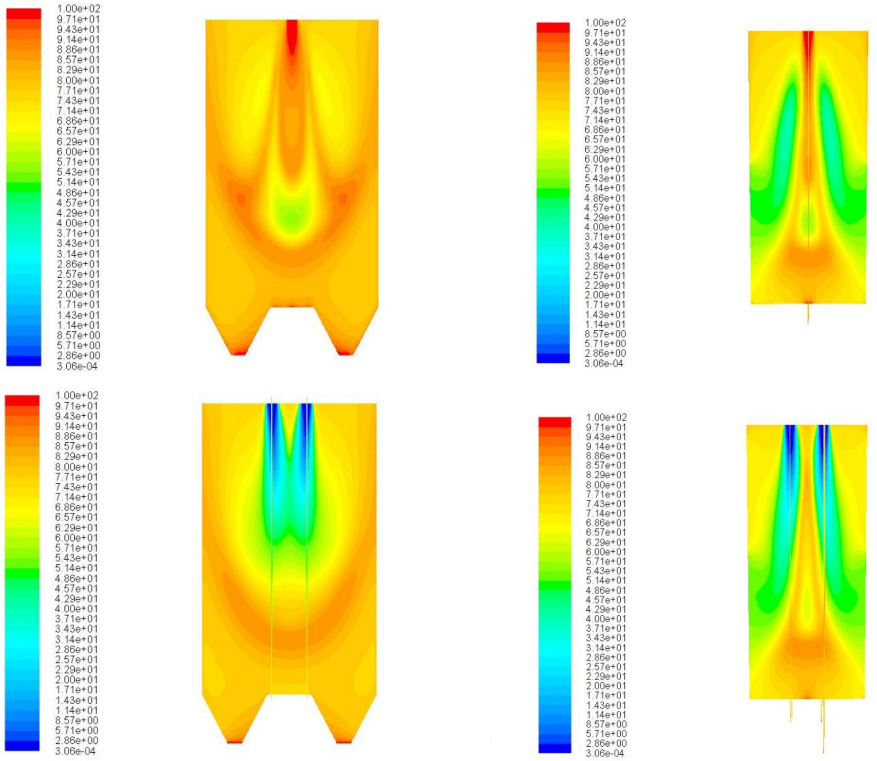

FIGURE 4.30: Carbon dioxide concentration distribution in different slice planes

4.3.1.5 Different Shape of Boiler

In order to improve the internal recirculation and thus have a more uniform distribution of temperature and species concentrations, another type of boiler is presented. This new boiler has a different square cross section (4X4 m), but keeps the other sizes equal to the previous one. The shape is shown in figure 4.31.

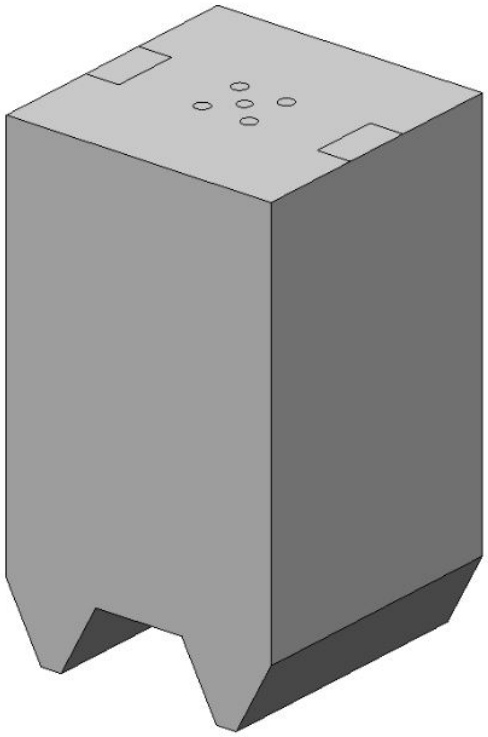

FIGURE 4.31: 3D view of square small boiler

The following figures show the comparison between the square and the rectangular boiler, respectively. The boundary conditions and the models used are the same for both boilers.

Figure 4.32 shows the temperature distribution of square boiler (on the left) and rectangular one.

First of all, the square boiler shows a more uniform distribution of temperature and the combustion takes place mainly in the bottom region of boiler. This is due to the larger volume. A smaller volume obstructs the flue gases to recirculate completely from the bottom to the top of the boiler. Thus, in this new configuration the combustion products have more volume in which they can recirculate. This is also highlighted in figure 4.33, which shows the oxygen concentration field.

The square boiler is filled by an oxygen concentration of 20% and the value in flue gases at the outlet is 17%, while the carbon dioxide is 85.6%. The burnout is improved and the value is 91%. This demonstrates that a larger volume and a square shape improve the burnout and the distribution of temperature and species.

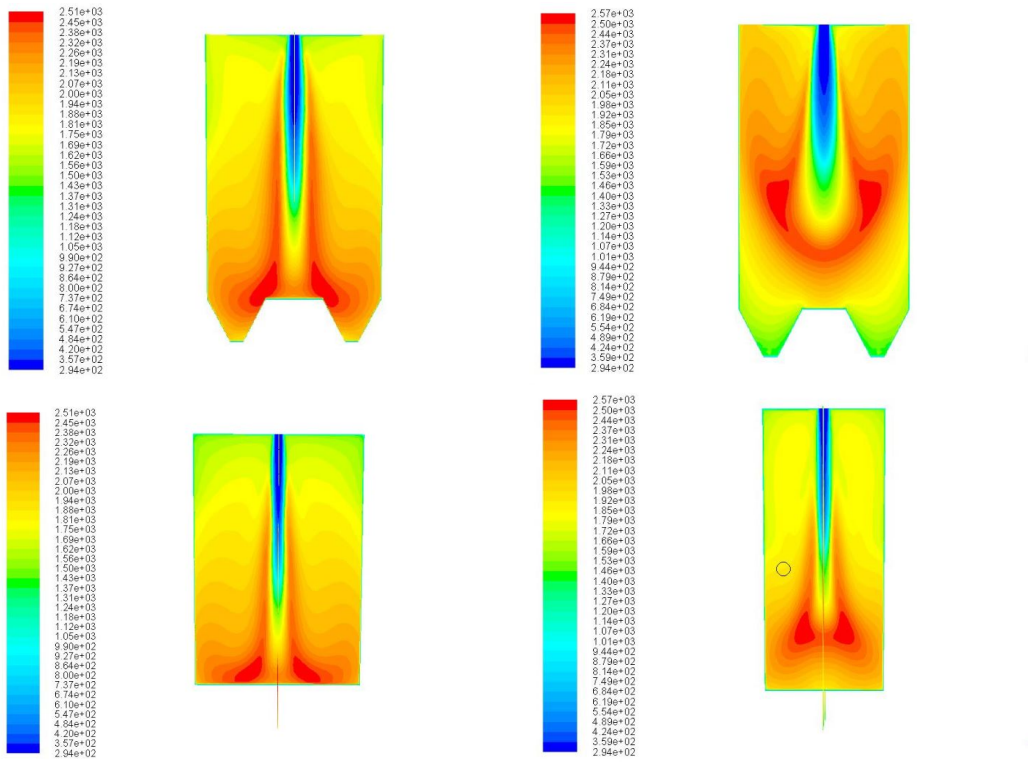

FIGURE 4.32: Temperature distribution in symmetry planes for different shape of boiler (left: square; right: rectangular)

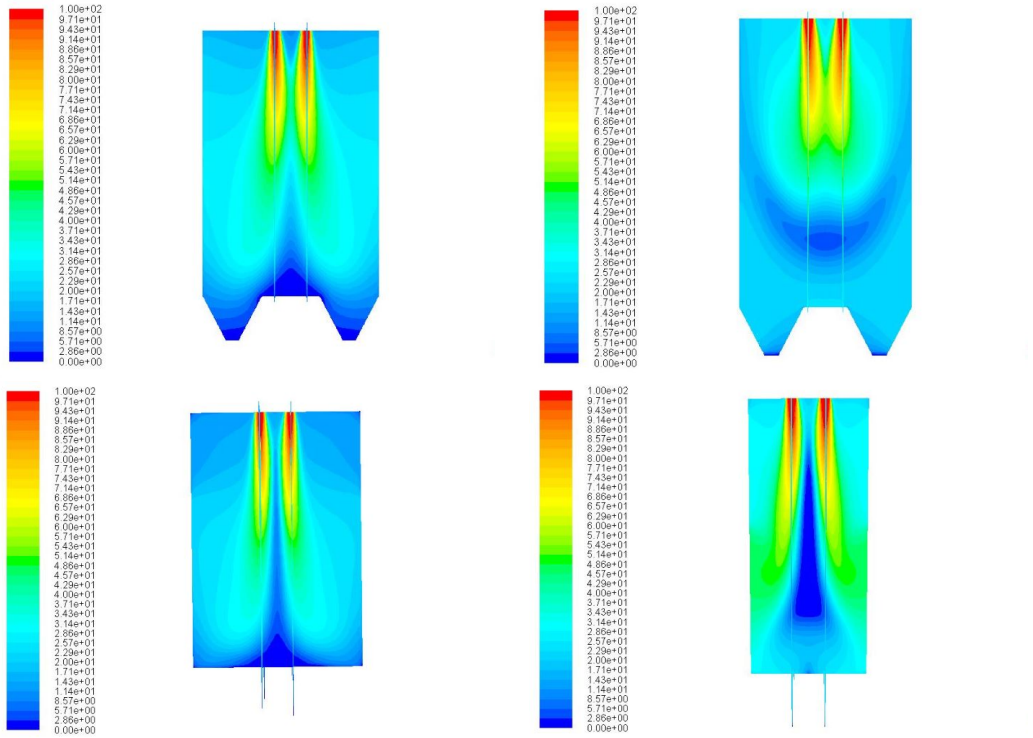

FIGURE 4.33: Oxygen distribution in symmetry planes for different shape of boiler (left: square; right: rectangular)

In order to obtain a burnout of 100% and improve the oxy-mild combustion, another kind of char model is used: the multiple surface reaction. This type of model includes the effect of heterogeneous reactions of CO_2 on the surface of char (char gasification).

4.3.1.6 Model Char Combustion Comparison

Figure 4.34, figure 4.35 and figure 4.36 show the temperature, the oxygen and the carbon dioxide concentration field for two different char model of the square boiler.

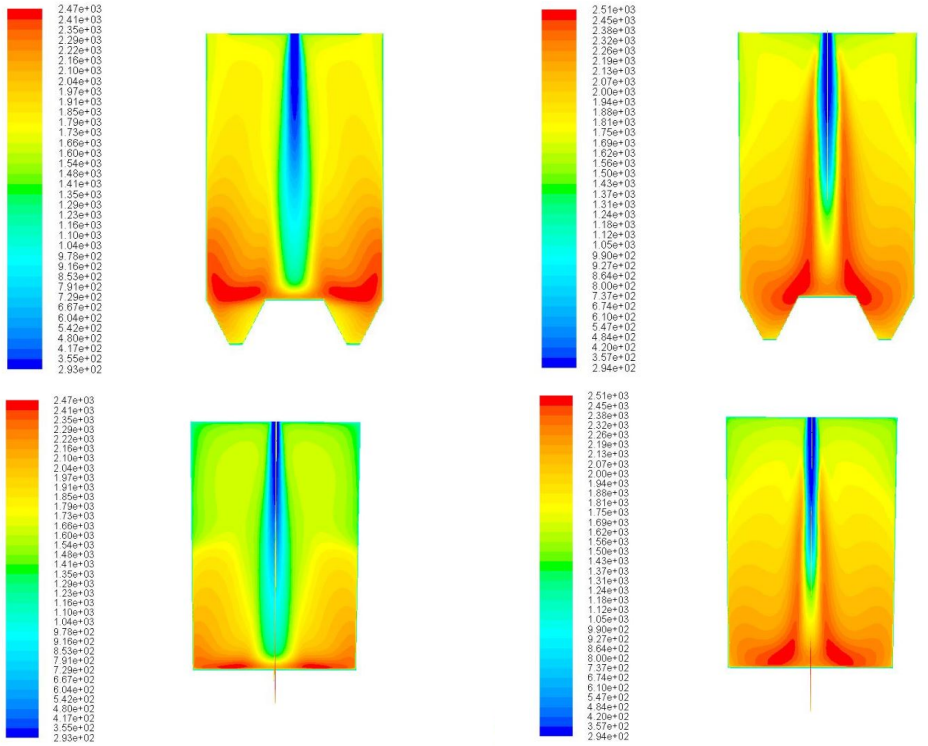

FIGURE 4.34: Temperature distribution in symmetry planes for different char combustion model: multiple surface reactions (left); diffusion-limited (right)

In table 4.16 is listed the comparison between the two char combustion models.

TABLE 4.16: Char model comparison: results at the outlet of boiler

Char Model	T [K]	O_2 [%]	CO_2 [%]	burnout [%]
Diffusion-limited	1683	17.0	85.6	91.0
Multiple surface reactions	1682	12.5	87.0	100

Despite the fact that the temperature at the outlet is equal in both cases, the multiple surface reactions model allows to obtain the 100% of burnout and a better consumption of oxygen. The high concentration of CO_2 in the bulk case influences the pulverized char combustion.

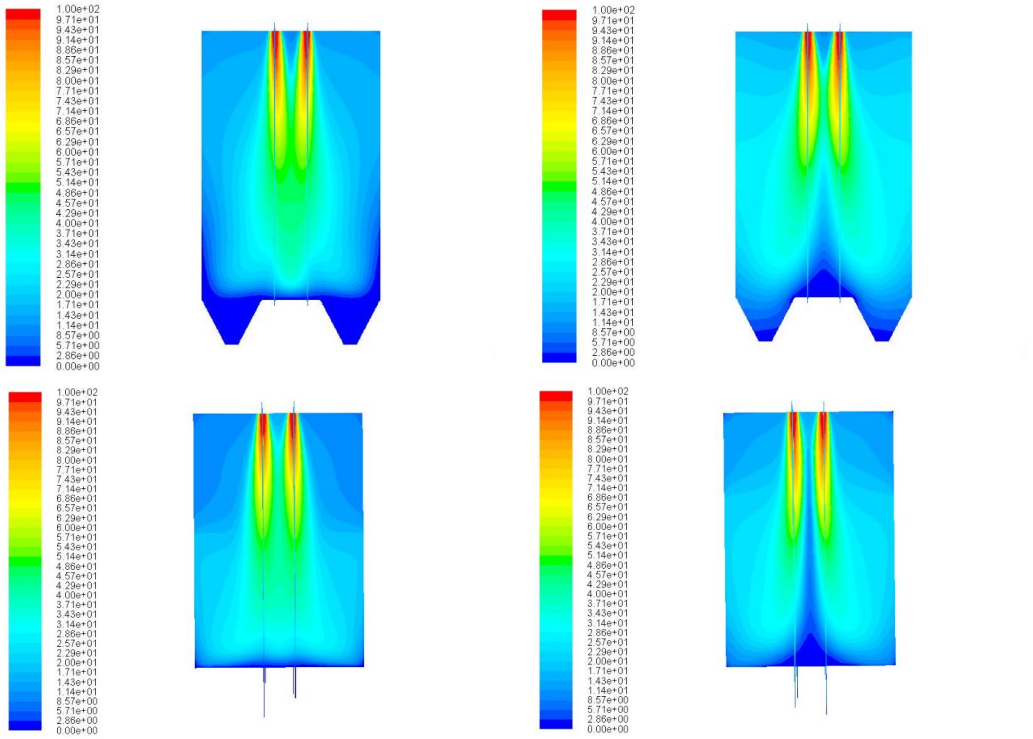

FIGURE 4.35: Oxygen concentration distribution in symmetry planes for different char combustion model: multiple surface reactions (left); diffusion-limited (right)

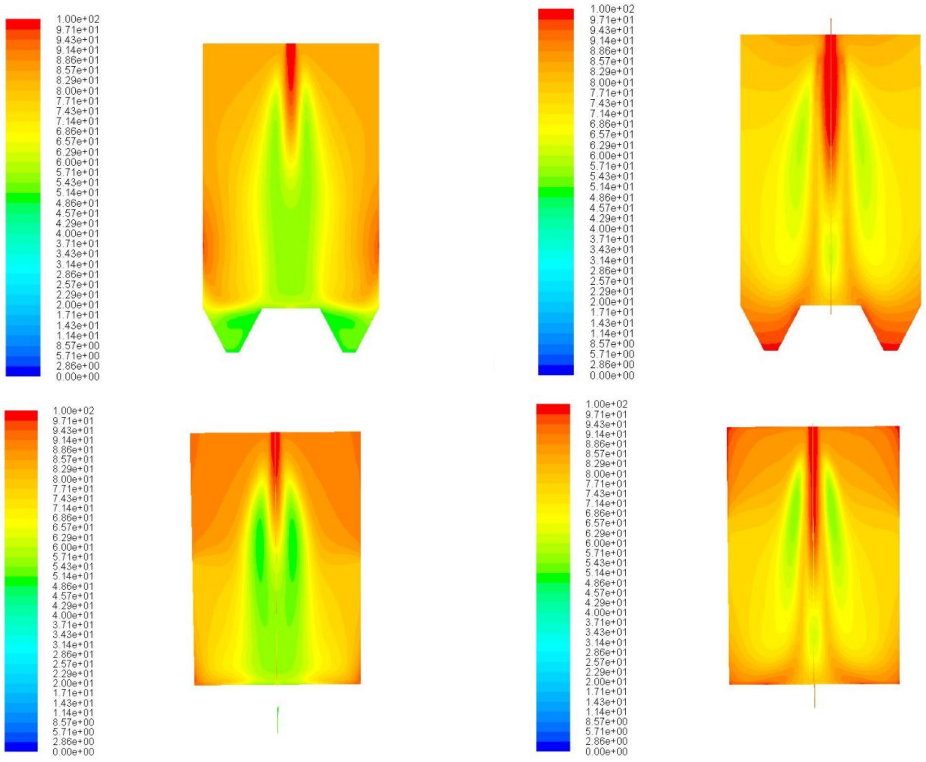

FIGURE 4.36: Carbon dioxide concentration distribution in symmetry planes for different char combustion model: multiple surface reactions (left); diffusion-limited (right)

4.3.1.7 Density Firing Comparison

Another important feature of mild combustion is the uniformity of wall heat flux due to the strong recirculation inside the combustion chamber and thus the uniformity of temperature and species concentration fields. In this section, the wall heat flux for three different density firings will be analyzed. Table 4.17 lists the boundary conditions used for this comparison. The values are referred to a quarter of boiler. The idea is to maintain the same combustion condition ($\lambda = 1.1$) by modifying the oxygen mass flow and the coal mass flow.

TABLE 4.17: Boundary conditions for wall heat flux comparison

Firing Density	Oxygen Mass Flow [kg/s]	Coal Mass Flow [kg/s]
187 kW/m^3	1.64	0.92
240 kW/m^3	2.10	1.17
375 kW/m^3	3.23	1.84

In order to calculate the average wall heat flux, an UDF has been written (User Defined Function), and the heat flux at various elevations of the domain have been calculated . Figure 4.37 shows the wall heat flux profiles along the height of boiler for three different density firings: 187 kW/m^3, 240 kW/m^3, 375 kW/m^3.

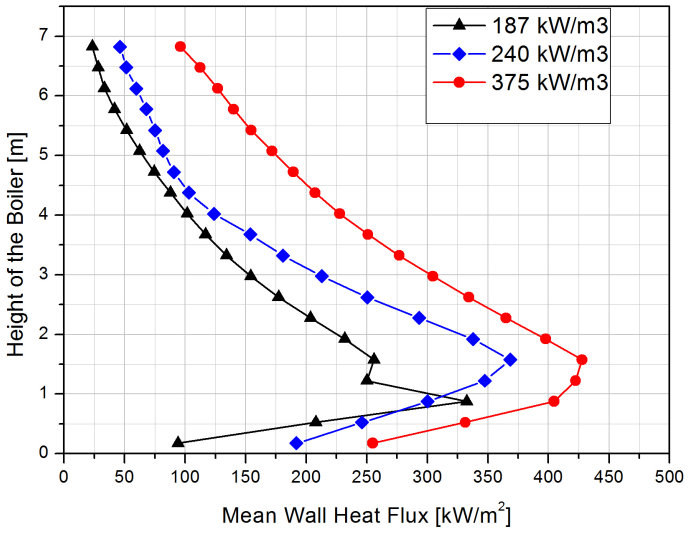

FIGURE 4.37: Wall heat flux for different firing density

The heat should be transferred to the water/steam mixture at wall. For this reason, a uniform distribution is necessary. Actually, neither of the three density firings presents a uniform distribution, but the boiler with 240 kW/m^3 density firing shows the typical trend of a conventional boiler, in which the typical local values for the heat flux are in the range of 50 - 300 kW/m^2. This irregular distribution is due to either poor recirculation

or local combustion of coal. Probably, the main cause is the combustion in pure oxygen, which provides high values of temperature localized in the bottom of the boiler. It has been necessary to calculate statistical parameters by means of UDF in order to analyze the deviation of temperature from the average value in the domain. These statistical parameters are:

- Standard deviation,
- Skewness,
- Kurtosis,

Table 4.18 presents these parameter for the three density firings.

TABLE 4.18: Statistical parameters for different firing density of boilers

Firing Density	T_{max}	T_{ave}	Standard Deviation	Skewness	Kurtosis
187 kW/m^3	2253	1429	223.35	0.40	$1.19e^{-9}$
240 kW/m^3	2187	1480	205.60	0.20	$1.76e^{-9}$
375 kW/m^3	2318	1614	237.6	0.09	$1.15e^{-9}$

All three cases present a symmetric and a Mesokurtic distribution of temperature. This is due to the values fixed by skewness and kurtosis. Kurtosis provides the height and sharpness of the central peak, relative to that of a standard bell curve. Because all three configurations present the same values of skewness and kurtosis, the density firing with a more uniform distribution is $240kW/m^3$, which provides the lowest value of standard deviation.

In figure 4.38, figure 4.39 and figure 4.40 the temperature field used to highlight the high local temperature at the bottom of boiler is shown.

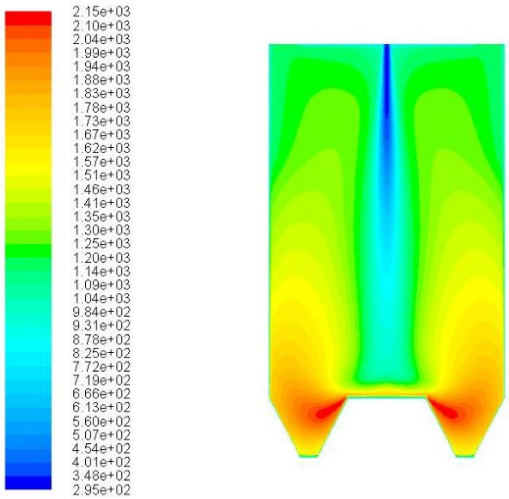

FIGURE 4.38: Temperature field for 187 kW/m^3 firing density

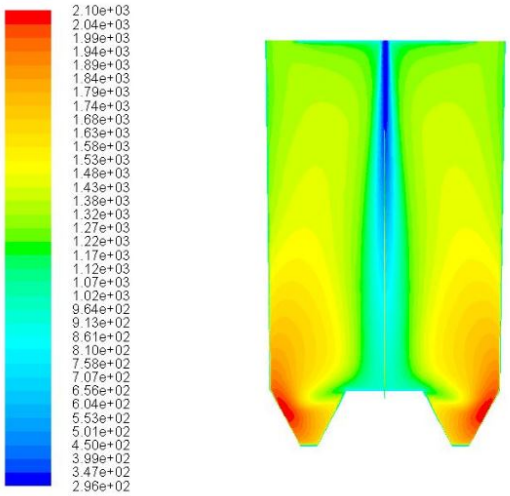

FIGURE 4.39: Temperature field for 240 kW/m^3 firing density

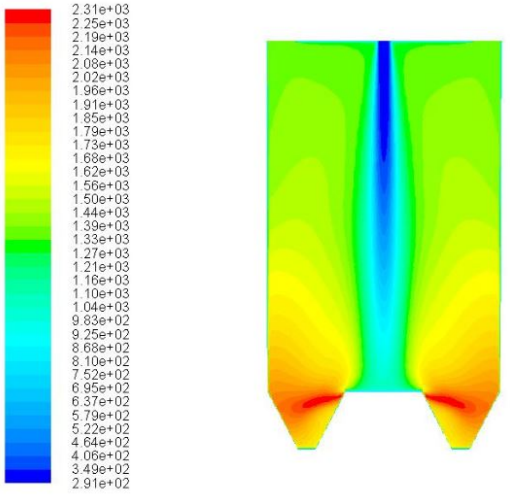

FIGURE 4.40: Temperature field for 375 kW/m^3 firing density

It is important to underline that a small boiler does not give proper results in term of uniform distribution of temperature and species concentration as well as the wall heat flux. Consequently, it is necessary to consider a higher boiler. In the next section, a medium boiler made up of 5 burners will be presented.

4.3.2 Medium Boiler

In this section, the numerical results in term of temperature and species concentrations field for a boiler with sizes higher than the previous one will be presented. This new type of boiler is composed by five FLOX burners. Every burner is composed of six oxygen inlets localized along a circumference of radius of 0.5 m. The coal and the carbon dioxide transport are at the center of this circumference. A detailed description of the geometry will be given in the next section.

The main objective is to obtain a more uniform distribution of temperature, specie concentrations and wall heat flux in respect to the previous boiler. For this reason, it has been necessary to consider a boiler with higher sizes.

4.3.2.1 Geometry and Mesh Description

Figure 4.41 illustrates the geometry of medium boiler, while figure 4.42 shows a detail of the top boiler, in which the burners and the outlets of flue gas are located.

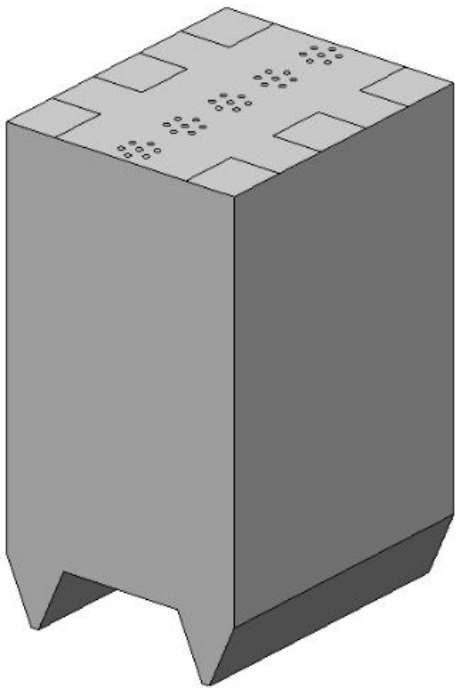

FIGURE 4.41: 3D View of medium boiler

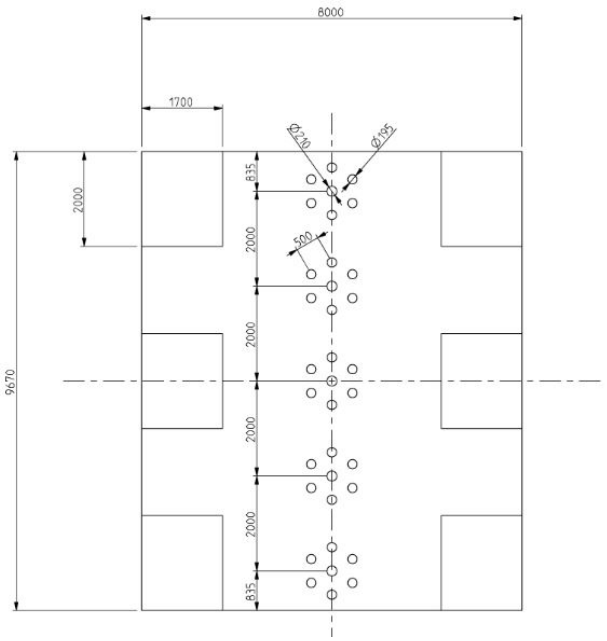

FIGURE 4.42: Detail of top medium boiler

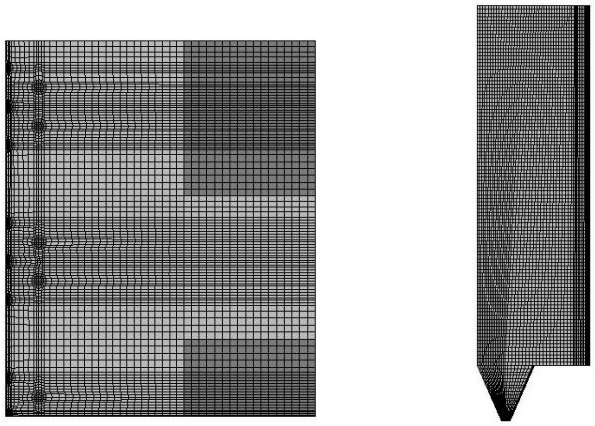

FIGURE 4.43: Spatial discretization of top boiler (left), symmetry plane (right)

4.3.2.2 Boundary Conditions

In table 4.19 are listed the boundary conditions.

Table 4.19: Boundary conditions for medium boiler

Name	type	number	settings
O_2 Inlet	Velocity Inlet	30	wt% O_2 = 100 %; $\dot{m} = 18.6kg/s$; v = 120 m/s; T= 1200 K
Transport CO_2 Inlet	Velocity Inlet	5	wt% CO_2 = 100%; $\dot{m} = 0.8kg/s$; v = 22.5 m/s; T = 300 K
Coal Inlet	Injection	5	$\dot{m}$ = 10.56 kg/s; v = 22.5 m/s; T = 300 K
Outlet	Pressure Outlet	6	p = 101325 Pa
Walls	Wall	-	$\epsilon = 0.6; T = 800K$

The burners work with a relative air fuel ratio of $\lambda = 1.1$.

Table 4.20: Thermal Balance

T_i [K]	$\dot{H}_i$ [MW]	T_o [K]	$\dot{H}_o$ [MW]	$\dot{Q}$ [MW]
1200	260	1635	208	52

The total thermal enthalpy supplied to the boiler is equal to 260 MW and the enthalpy of the exhaust gas is equal to 208 MW. The difference is the sum of thermal energy transferred to the walls and the heat of reaction. The volume of boiler is around 1080 m^3, thus the firing density is around 240 kW/m^3.

4.3.2.3 Results and Discussion

In Figure 4.44 and in Figure 4.45 the temperature, oxygen concentration and carbon dioxide field in the whole boiler and in the symmetry plane are respectively shown.

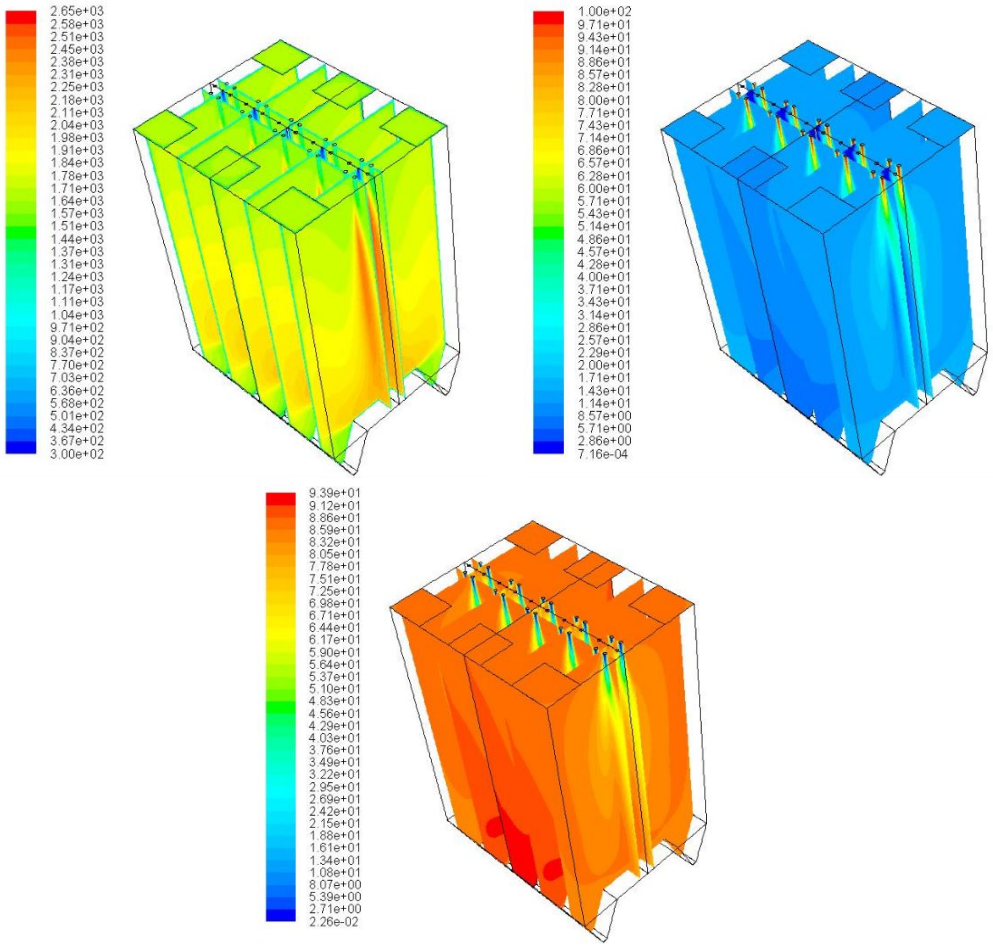

FIGURE 4.44: Temperature field (top-left), oxygen concentration (top-right), carbon dioxide concentration (bottom-center) for the medium boiler

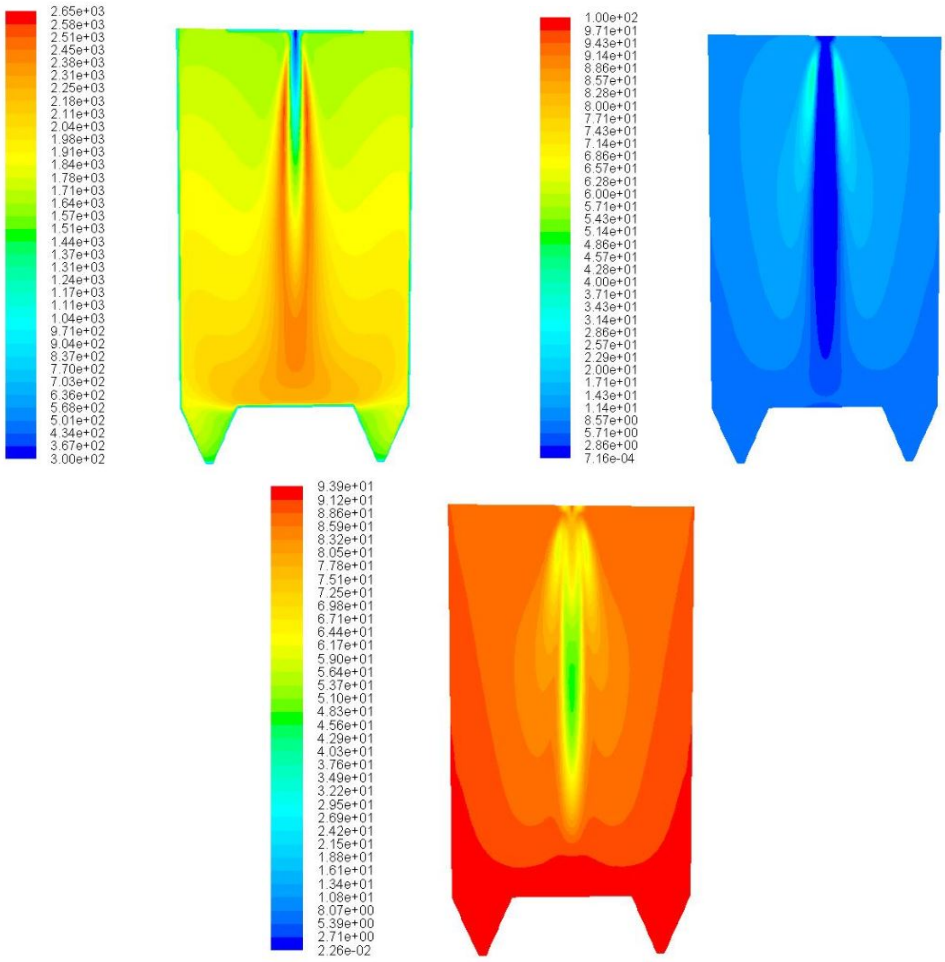

FIGURE 4.45: Temperature field (top-left), oxygen concentration (top-right), carbon dioxide concentration (bottom-center) in symmetry plane

The previous figures show a more uniform distribution of temperature, oxygen and carbon dioxide concentration. This is due to the large volume of boiler. It is necessary to notice that this kind of boiler provides a better recirculation of combustion products. The pulverized coal meets and entrains a large amounts of flue gases and thus can burn in diluted environment. Above all, this condition is very useful because it allows to get a better distribution of temperature, with an average value of 1895 K, but also to capture the carbon dioxide at the outlet of the boiler. Table 4.21 presents the values of temperature, species concentrations at the outlet as well as the burnout of char. In figure 4.46 the volatiles mass fraction field is shown.

Because the coal meets the hot combustion products, the devolatilization happens very fast. The ignition is very close to the burner. Table 4.21 presents the values of temperature, specie concentrations at the outlet as well as the burnout of char.

These values diverge from the theoretical values by 22%. The burnout of coal is around 100%, and the hot combustion products allows to eliminate the problem of

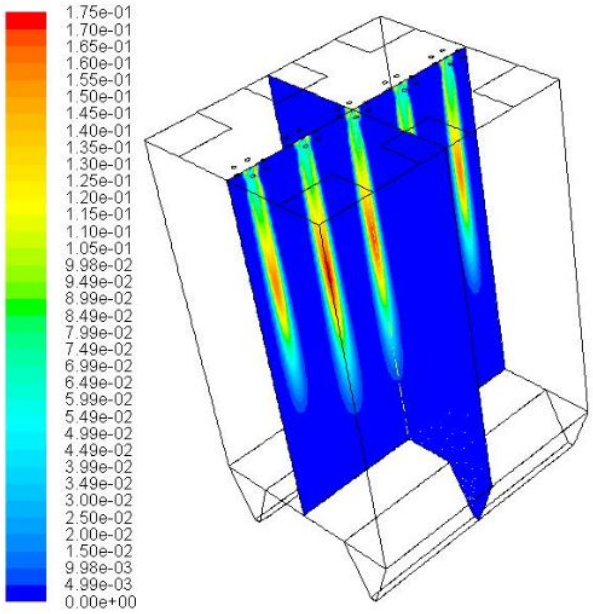

FIGURE 4.46: Volatile mass fraction field

TABLE 4.21: Medium Boiler: results at the outlet of boiler

T [K]	O_2 [%]	CO_2 [%]	burnout [%]
1623	12.7	87.0	100

ignition. Table 4.22 presents the statistical parameter for temperature in a medium boiler.

TABLE 4.22: Statistical parameters for different firing density of boiler

T_{max}	T_{ave}	Standard Deviation	Skewness	Kurtosis
2662	1895	207	0.54	$2.0e^{-9}$

The values of skewness and kurtosis are 0.5 and 0, respectively. This means that the temperature distribution in the boiler is approximately symmetric (skewness=0.5) and it assumes a Mesokurtic distribution (kurtosis =0) [105].

It is worthwhile to highlight the relevance of the recirculation. For this reason, in figure 4.47 the axial velocity field is shown.

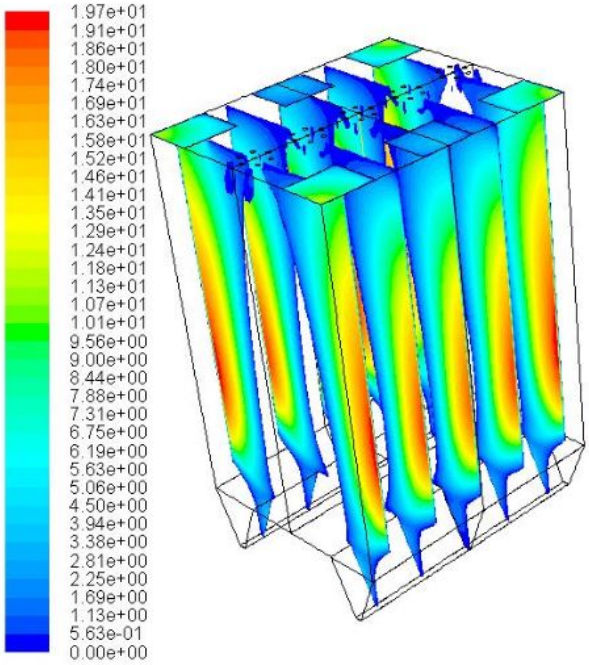

FIGURE 4.47: Axial velocity

Almost the whole volume of the boiler is characterized by a strong recirculation. The combustion products rise toward the top of the boiler and the recirculation intensity is greater in the external part of it.

A strong recirculation with a uniform distribution of temperature provides a uniform distribution and profile of heat flux at the wall.

Figure 4.48 shows the wall heat flux (average).

The heat transfer in the boiler is improved by high and uniform heat fluxes. High values of radiative heat lead results to an increase of firing density, thus it is possible to reduce the size of the boilers. The high values and distribution of heat transfer is very relevant for analyzing the heat transferred from the combustion products inside the chamber to the water/steam mixture inside the boiler tubes of an ultra-super critical power plant. Figure 4.49 shows the wall heat flux profiles for two values of firing density: an high value 430 kW/m^3 and a medium value 240 kW/m^3.

This comparison was necessary in order to analyze which kind of firing density value is the best in term of uniform profile and absolute value. This result has been obtained by means of an UDF (User Defined Function), which allows to calculate the average value of heat flux at the wall.

Moreover, in order to make a better comparison, it important to consider the heat flux profile of standard boilers. figure 4.50 shows the comparison between the heat flux profiles provided by Schaffel et al. [40] and the one provided in this work.

The oxy-mild combustion allows to maintain the uniformity of heat flux found in the Schaffel work but, at the same time, presents higher values than Schaffel results. This

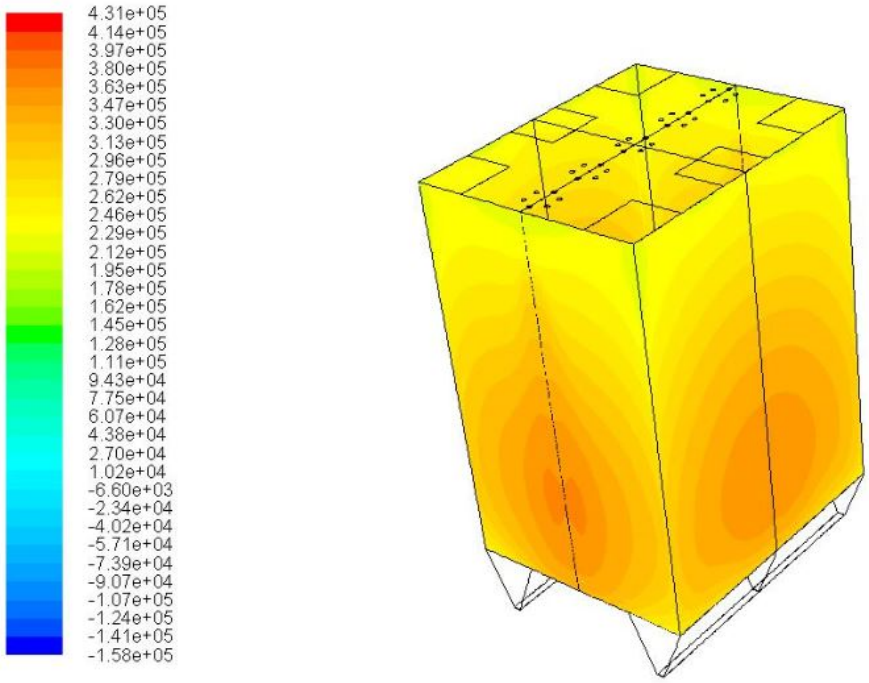

FIGURE 4.48: Contour plot of wall heat flux

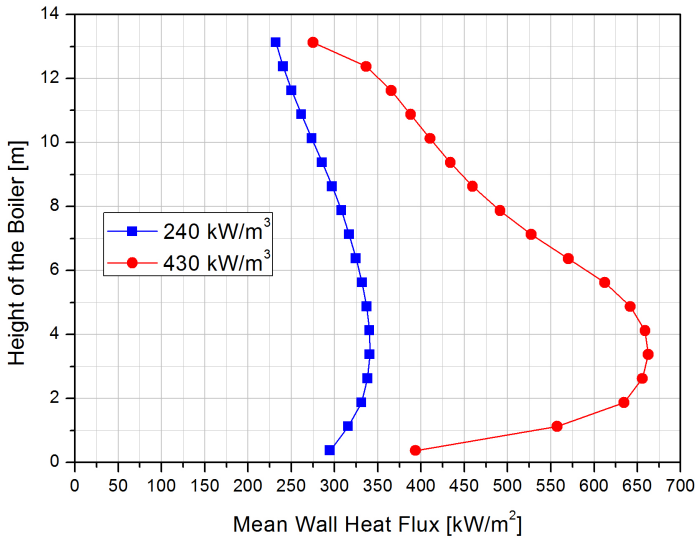

FIGURE 4.49: Wall heat flux comparison for different density firing

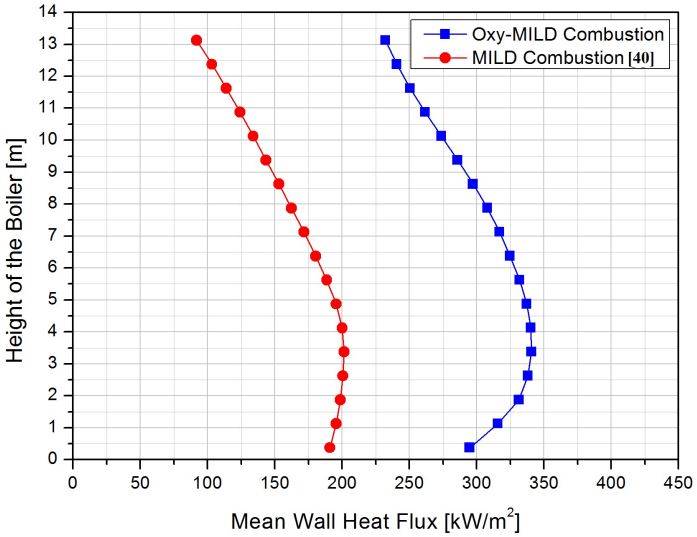

FIGURE 4.50: Wall heat flux comparison between Schaffel et al. result and this work one

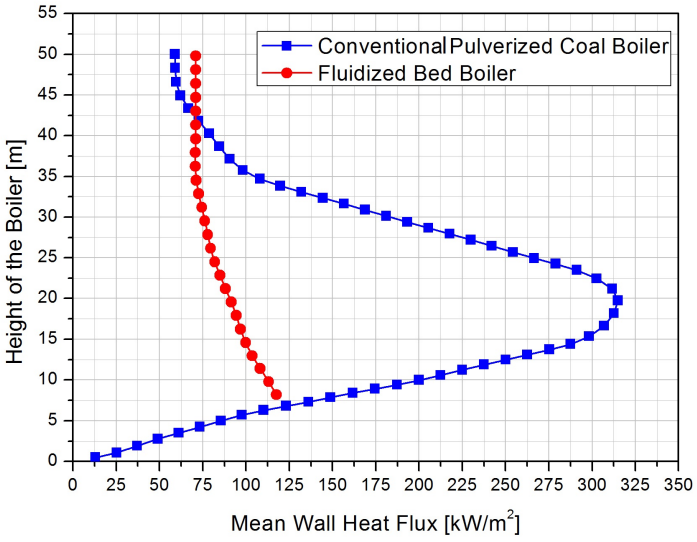

FIGURE 4.51: Wall heat flux comparison between conventional pulverized coal boiler and fluidized bed boiler

is due to the radiative properties of CO_2, which in oxy-combustion became prevalent because of the high concentration values. The heat flux profile provided in this work combines the advantages of a fluidized bed boiler (uniformity) [106] and of conventional pulverized coal boiler (high values) [107], as shown in figure 4.51.

Thus, the oxy-mild combustion, in term of heat flux allow to obtain:

- Uniformity of wall heat flux

- Values comparable with the conventional boiler

The application of oxy-mild combustion in a medium boiler has highlighted remarkable results in respect to the current boiler and to the work of several researchers.

Chapter 5

Conclusions and outlooks

In this work, the Oxy-MILD combustion of pulverized coal has been analyzed and a three dimensional, steady state model has been used with the ANSYS FLUENT numerical code.

Afterward, several models and sub-models were implemented for the combustion of pulverized coal in different applications, in order to compare it with the state of the art of furnace and boilers. In particular, MILD combustion with different positions of jet coal in furnace and Oxy-MILD combustion boilers with several shapes and char models have been investigated.

The results obtained through simulation analysis showed that Oxy-MILD combustion represents a promising technology to reduce the nitric oxide emissions and capture carbon dioxide. This is an interesting result if considered that it is extremely difficult to combine these two goals. A reduction of nitric oxide has been obtained in the application in furnace in configuration 3, in which the distance between the coal and the oxidizer jet are furthest. In configuration 3, the nitric oxide is about 220 ppm @ 6% of O_2 respect to 320 ppm @ 6% of O_2 provided by configuration 1. This result is mainly a consequence of the reduction of oxygen concentration and thus the one of fuel nitric oxide. The results obtained in these simulations are in good agreement with the experimental results provided by [41]. In order to investigate the potentials of Oxy-MILD combustion, a preliminary application at the same furnace with configuration 2 has been investigated. These simulations start from the same boundary conditions of previous applications to finally understand the only effect of a strong external recirculation of carbon dioxide on temperature and nitric oxide. A 20% reduction of nitric oxides in oxy-mild combustion has been obtained, mainly because of the absence of nitrogen in the oxidant and thus of thermal NO_x. But, at the same time, oxy-mild combustion has been providing high values of carbon dioxide concentration. In order to identify the effectively potential of oxy-mild combustion and possible applications on an industrial scale, an application in boiler has been realized.

A preliminary application in a small rectangular boiler has not showed a good distribution of temperature and specie concentrations, instead provided by a square and a higher volume. A smaller volume, indeed, prevents the flue gases to recirculate completely from the bottom to the top of the boiler. A better result has been obtained when a multiple surface reaction on char particle has been considered and applied to the square shape boiler. The multiple surface reaction model has provided the same average temperature, but better depletion of char. Consequently, the oxygen concentration at the outlet boiler is lower than the one at the rectangular boiler and thus the burnout is 100%. This result might seem in contrast with Shaddix and Molina et al. [57], who stated that the presence of CO2 could reduce the burning rate because it can hinder the diffusion. This is true in standard oxy-mild combustion, but not in oxy-mild in which the high pre-heated oxygen jet encourages the diffusion. The wall heat flux has also been analyzed with different firing densities, but as a consequence of a non-optimal uniform distribution, the profiles presents local peaks. Consequently, it has been necessary to consider a higher boiler. Numerical simulations have been performed and the main results can be summarized in the following points:

- The temperature and species concentration distributions have reached an acceptable uniformity.
- The wall heat flux profile is uniform and assumes values comparable with a conventional pulverized coal boiler.

The first point is a consequence of the strong recirculation reached in the whole volume of the boiler, while the second one is a consequence of a combination of the first one and radiative properties of carbon dioxide. These findings play a crucial role in the production of steam in ultra-super critical power plant. To summarize, this solution allows to:

- Reduce the nitric oxide
- Capture the carbon dioxide
- Produce steam in ultra-super critical power plant in optimal manner

Another aspect to consider is the elimination of external recirculation. The simulations in the boiler have been performed by considering a little external recirculation of carbon dioxide. The carbon dioxide is needed only for the transport of pulverized coal.

The results presented show the great potential of the Oxy-MILD combustion of pulverized coal in boilers with application in ultra-super-critical power plant, but also the need of further studies by considering different sub-models for the devolatilization,

char combustion and the use of detailed kinetic mechanism. The key element of the commercial success of the Oxy-MILD combustion is in the possibility to substitute the old generation of boiler with an innovative boiler obtained by combining the two technologies. The process described in this study could be further improved, too. In particular:

- Application in small boiler by optimizing the geometry and the velocity of oxygen jet.
- Allow a fuel flexibility by considering different low rank coals.

The coals were the Guasare and the Janina, which have similar properties. Consequently, an analysis of the effect of coal properties is needed in order to establish the range of coals for this kind of boiler.

References

[1] BP p.l.c., Statistical Review of World Energy 2010, London, United Kingdom, June 2010.

[2] International Energy Agency, World Energy Outlook 2011, IEA, 696 p, ISBN: 978 92 64 12413 4, November 2011.

[3] EIA, U.S. Energy Information Administration, International Energy Outlook 2011, DOE/EIA0484, 2011.

[4] BP p.l.c., BPs Energy Outlook 2030, January 2013.

[5] Opaprakasit, Interaction and the structures of coal. The Pennsylvania State University, ProQuest Dissertations and Theses, 199 p, 2003.

[6] ASTM D388, Standard Classification of Coal by Rank, CFR Section: 40, CFR 60.251(b), American Society for Testing and Materials, 1998.

[7] L.D. Smoot, D.T. Pratt, Pulverized Coal Combustion and Gasification: Theory and Applications for Continuous Flow Process, Springer, New York, 1979.

[8] Miller, B.G., Tillman, D., Combustion Engineering Issues for Solid Fuel, Systems. Elsevier Academic Press, San Diego, California, ISBN: 0123736110, 528, 2008.

[9] E. Yantovsky, J. Gorski, M. Shokotov, Zero Emissions Power Cycles, first ed., Taylor Francis, 2009.

[10] Kosowska, M., The Thermal Fragmentation of Coal during Combustion Process. PhD Thesis., Czestochowa University of Technology, 2005.

[11] Basu, P., Combustion and Gasification in Fluidized Beds, CRC Press, 2006.

[12] Higuera, F.J., Numerical Simulation of the Devolatilization of a Moving Coal Particle, Combustion and Flame, 156, 10231034, 2009.

[13] Basu, P., Combustion of coal in circulating fluidized-bed boilers: a review. Chemical Engineering Science, 54, 55475557, 1999.

[14] Hambly, E.M., The Chemical Structure of Coal Tar and Char during Devolatilization, MSc Thesis, Brigham Young University, 1998.

[15] Fletcher, T.H., Kerstein, A.R., Pugmire, R.J., Solum, M.S., and Grant, D.M., A chemical percolation model for devolatilization: 3. Chemical structure as a function of coal type. Energy and Fuels, 6, 414431, 1992.

[16] M. Lackner, F. Winter, A. Agarwal, Handbook of Combustion, Wiley-Vch, 2010.

[17] Feng,J.K.,Shen,Y.T.,andYang,R.C., Boiler Principles and Calculation, 3rd edn, Science Press, Beijing, 2003.

[18] Xu, X.C. and Zhou, L.X., Stock and Pulverized Coal Fire Boilers, Ch 12 in Combustion Technology Handbook, Chemical Industry Press, Beijing, 2008.

[19] Field, M.A., Pulverized Coal Combustion, Plenum Press, New York, 1987.

[20] Feng,J.K.,Shen,Y.T.,andYang,R.C., Boiler Principles and Calculation, 3rd edn, Science Press, Beijing, 2003.

[21] Mao, J.X., Mao, J.M., and Zhao, S.M., Clean Coal Combustion, Science Press, Beijing, China, 1998.

[22] Glassman I.: Combustion (3rd ed.). Academic Press, INC., San Diego, London, Boston, New Yorok, Sydney, Tokyo, Toronto, 1996.

[23] Zeldovich J.B., Rajzer I.P., Fizyka udarnych woln I wysokotemperaturnych girodynamiczeskich jewlenij, Nauka, Moskwa, 1963.

[24] R.K. Wilk, Low Emission Combustion, Wysawnictwo Politechniki Slaskiej, Gliwice, 2002.

[25] Katsuki, M. and Hasegawa, T., The science and technology of combustion in highly preheated air, Proc. Combust. Inst. 27, 31353146, 1998.

[26] de Joannon, M., Saponaro, A., and Cavaliere, A., Zero-Dimensional Analysis of Methane Diluted Oxidation in Rich Conditions. Proc. Combust. Inst. 28, 16391646, 2000.

[27] HiTAC, Symposium of High Temperature Air Combustion and Applications, Hsinchu, 2000.

[28] HiTAC, Proceedings of the 5th International Symposium on High Temperature Air Combustion and Gasification, Yokohama, 2002.

[29] Cavaliere, A. and de Joannon, M., Mild Combustion, Prog. Energy Combust. Sci., 30(4), 329366, 2004.

[30] de Joannon, M., Cavaliere, A., Faravelli, T., Ranzi, E., Sabia, P., and Tregrossi, Analysis of process parameters for steady operations in methane Mild combustion technology. Proc. Combust. Inst. 31. 2007.

[31] Peters, N., Principles and Potential of HiCOT Combustion. Proceedings of the Forum on High Temperature Air Combustion Technology, 2001.

[32] Flamme M., Low NO_x Combustion Technologies for High Temperature Application, Proceeding of 2nd International Symposium on Advanced Energy Conversion System and Related Technologies, December 1-3, Nagoya, Japan, 152-159, 1998.

[33] Milani A., Wunning J.G. Technical and Economical Assessment of Highly Preheated Air in Furnace Technology. Proceedings of 2nd International Symposium on Advanced Energy Conversion System and Related Technologies, December 1-3, Nagoya, Japan, 150-151, 1998.

[34] Wunning J.A. Wunning J.G. Ten Years of Flamless Oxidation: Technical Applications and Potentials Proceedings of 4th Symposium High Temperature Air

Combustion and Gasification (2), 20-30.11., Rome, 2001.

[35] M. Morita, T. Hasegawa, M. Katsuki, K. Kishimoto, AA K. Gupta, High Temperature Air Combustion: From Energy Conservation to Pollution Reduction, CRC Press, 2002.

[36] Medwell, P., Kalt, P., and Dally, B., Simultaneous imaging of OH, formaldehyde, and temperature of turbulent non premixed jet flames in a heated and diluted coflow. Combustion and Flame, 148, 4861, 2007.

[37] Galletti, C., Parente, A., and Tognotti, L., Numerical and Experimental Investigation of a MILD Combustion Burner. Combustion and Flame, 2007.

[38] Orsino, S., Weber, R., and Bollettini, U., Numerical Simulation of Combustion of Natural Gas With High Temperature Air. Combustion Science and Technology, 170, 134, 2001.

[39] M. Katsuki and T. Hasegawa. The Science and Technology of in Highly Preheated Air. Proc. Combust. Inst., 27:31353146, 1998.

[40] N. Schaffel Mancini, Ecological Evaluation of the Pulverized Coal Combustion in HTAC Technology, PhD Thesis, Clausthal-Zellerfed, Gliwice, 2009.

[41] N. Schaffel, M. Mancini, A. Szlek, R. Weber, Mathematical modeling of MILD combustion of pulverized coal, Combustion and Flame, 156: 1771-1784, 2009.

[42] N. Schaffel, M. Mancini, A. Szlek, R. Weber, Novel Conceptual Design of a Supercritical Pulverized Coal Boiler Utilizing High Temperature Air Combustion (HTAC) Technology, Energy, 35, 2752-2760, 2010.

[43] Camporeale, S.M., Casalini, F., and Saponaro, A., Proceedings of the 7th Biennial Conference on Engineering Systems Design and Analysis, ESDA200458472, 2004.

[44] Milani, A. and Saponaro, A., Diluted combustion technologies. IFRF Combust. J., Article 200101, February, ISSN 1562479X, 2001.

[45] Martinez-Frias, J., Aceves, S.M., and Smith, J.R., Thermodynamic Analysis of Zero Atmospheric Emission Power Plant. Proceedings of the AES-IMECE 2003,

ASME, International Mechanical Engineering Congress Exposition, Washington, DC, 2003.

[46] D. Toporov, Combustion of Pulverised Coal in a Mixture of Oxygen and Recycled Flue Gas, Elsevier, 2015.

[47] J. Katzer (Hrsg.), The Future of Coal, Options for a Carbon-Constrained World, Massachusetts Institute of Technology, 2007.

[48] D. Adams, J. Davison, Capturing CO_2/Report, International Energy Agency Greenhouse Gas RD Programme, Forschungsbericht, 2007.

[49] J. Davison, Performance and costs of power plants with capture and storage of CO_2, Energy 32, 11631176, 2007.

[50] Ph. Armstrong, T. Foster, D. Bennett, V. Stein, ITM Oxygen: Scaling up a Low-Cost oxygen Supply Technology, in: Gasification Technologies Conference, Washington, DC, pp. 14, 2006.

[51] R. Hassa, Carbon capture and storage a technology for the coal fired power plant of the future, International Journal for Electricity and Heat Generation, VGB Power Tech 12, 3941, 2008.

[52] L. Zheng, Oxy-fuel combustion for power generation and carbon dioxide (CO_2) capture, Woodhead Publishing Limited, Oxford, Cambridge, Philadelphia, New Delhi, 2001.

[53] A. Yamamoto, T. Suda, K. Okazaki, Mechanism of ignition delay in O_2/CO_2 pulverized coal combustion, in: 21th Annual Pittsburgh Coal Conference, Osaka, Japan, 2004.

[54] Suda T, Masuko K, Sato J, Yamamoto A and Okazaki K (2007), Effect of carbon dioxide on flame propagation of pulverized coal clouds in CO_2/O_2 combustion, Fuel, 86, 20082015.

[55] Shaddix C. R. and Molina A., Particle imaging of ignition and devolatilization of pulverized coal during oxy-fuel combustion, Proc. Combust. Inst., 32, 19051912, 2009.

[56] Molina A, Hecht E S and Shaddix C R, Ignition of a group of coal particles in oxyfuel combustion with CO_2 recirculation, Proc. AIChE Conf., 31, 19051912, 2009.

[57] Shaddix C. R. and Molina A., Effect of O_2 and High CO_2 Concentrations on PC Char Burning Rates during Oxy-Fuel Combustion, Proceedings of the 34th International Technical Conference on Coal Utilization and Fuel Systems, Clearwater, FL, 15 June 2008.

[58] S. Schiebahn, Numerische Untersuchung des Einflusses der Kohlendioxidvergasung auf den OXYCOAL-Prozess, Institute of Heat andMass Transfer, RWTH Aachen Univesity, Diplomarbeit, Germany, 2008.

[59] M. Geier, E. Hecht, C. Shaddix, Evaluation of effect of particle size on oxy-fuel combustion of pulverised coal, in: 26th Annual International Pittsburgh Coal Conference, Pittsburgh, PA, September, pp. 2023, 2009.

[60] D. Toporov, M. Frster, R. Kneer, Combustion of pulverized fuel under oxycoal conditions at low oxygen concentrations, in: Third International Conference on Clean Coal Technologies for our Future, Cagliari, Sardinia, Italy, May 1517, 2007.

[61] K. Andersson, F. Johnsson, Flame and radiation characteristics of gas-fired O_2/CO_2 combustion, Fuel 86, 656668, 2007.

[62] F. Liu, H. Guo, G. Smallwood, The chemical effect of CO2 replacement of N2 in air on the burning velocity of CH4 and H2 premixed flames, Combustion and Flame, 133, 495497, 2003.

[63] E. Croiset, K.V. Thambimuthu, NOx and SO2 emissions from O_2/CO_2 recycle coal combustion, Fuel 80, 21172121, 2001.

[64] D. Toporov, P. Bocian, P. Heil, A. Kellermann, H. Stadler, S. Tschunko, M. Frster, R. Kneer, Detailed investigation of a pulverized fuel swirl flame in CO_2/O_2 atmosphere, Combustion and Flame, 155, 605618, 2008.

[65] F. Normann, K. Andersson, B. Leckner, F. Johnsson, Emission control of nitrogen oxides in the oxy-fuel process, Progress in Energy and Combustion Science, 35, 385397, 2009.

[66] K. Okazaki, T. Ando, NO_x-reduction mechanism in coal combustion with recycled CO_2, Energy, 22, 207215, 1997.

[67] Y.Q. Hu, N. Kobayashi, M. Hasatani, Effects of coal properties on recycle-NO_x reduction in coal combustion with $O_2/recycled flue gas, Energy Conversion and Management$, 44(2003)23312340.

[68] H. Liu, K. Okazaki, Simultaneous easy CO_2recovery and drastic reduction of SO_x and NO_x in O_2/CO_2 coal combustion with heat recirculation, Fuel, 82, 4271436, 2003.

[69] H. Liu, R. Zailani, B.M. Gibbs, Comparisons of pulverized coal combustion in air and in mixtures of O_2/CO_2, Fuel, 84, 833840, 2005.

[70] C. Shaddix, A. Molina, NO_x formation in laboratory investigations of oxy-coal combustion, in: 2007 Fall Meeting of the Western States Section of the Combustion Institute, Sandia National Laboratories, Livermore, CA, October 1617, 2007.

[71] A. Blokh, Heat Transfer in Steam Boilers, Hemisphere, Washington, DC, 1988.

[72] H. Hottel, A. Sarofim, Radiative Transfer, McGraw-Hill, New York, 1967.

[73] Dong-Chan Park, Stuart J. Day, Peter F. Nelson, Nitrogen release during reaction of coal char with O_2, CO_2 and H_2O, Proceedings of the Combustion Institute, 30, 21692175, 2005.

[74] H. Liu, K. Okazaki, Simultaneous easy CO_2 recovery and drastic reduction of SO_x and NO_x in O_2/CO_2 coal combustion with heat recirculation, Fuel, 82, 14271436, 2003.

[75] R. Goulard (Hrsg.), R. Thompson (Hrsg.), Handbook of Infrared Radiation from Combustion Gases, Scientific and Technical Information Office NASA,Washington, DC, 1973.

[76] P. Canning, A. Jones, P. Balmbridge, NO_x control for large coal-fired utility boilers: selection of the most appropriate technology, Australian Coal Review, 3542, 1999.

[77] Y. Tan, M.A. Douglas, K.V. Thambimuthu, CO_2 capture using oxygen enhanced combustion strategies for natural gas power plants, Fuel, 81, 10071016, 2002.

[78] K. Andersson, F. Johnsson, Flame and radiation characteristics of gas-fired O_2/CO_2 combustion, Fuel, 86, 656668, 2007.

[79] N. Laurendeau, Heterogeneous kinetics of coal char gasification and combustion, Progress in Energy and Combustion Science, 4, 221270, 1978.

[80] R. Hurt, Structure, properties, and reactivity of solid fuels, in: 27th Symposium (International) on Combustion, The Combustion Institute, 28872904, 1998.

[81] R.H. Essenhigh, Rate equations for the carbon-oxygen reaction: an evaluation of the Langmuir adsorption isotherm at atmospheric pressure, Energy and Fuel, 5, 4146, 1991.

[82] L. Duan, C. Zhao, W. Zhou, C. Qu, X. Chen, Investigation on coal pyrolysis in CO_2 atmosphere, Energy and Fuel, 23, 38263830, 2009.

[83] Hurt, R., Sun, J., and Lunden, M., A kinetic model of carbon burnout in pulverized coal combustion, Combustion and Flame, 113, 181197, 1998.

[84] Walsh, P.M., Analysis of carbon loss from a pulverized coal-fired boiler, Energy and Fuels, 11, 965, 1997.

[85] Chen, J.-Y., Mann, A.P., and Kent, J.H. (1992). Computational modeling of pulverized fuel burnout in tangentially fired furnaces. In Proc. 24th International Symp. On Combustion, July 5-10, 1992, pp. 13811389.

[86] G.H. Yeoh, K.K. Yuen, Computational Fluid Dynamics in Fire Engineering: Theory, Modelling and Practice, Elsevier, USA, 2009.

[87] Favre, A. Equation des gaz Turbulents Compressibles, J. Mechanique, 4, 361-392, 1965.

[88] Favre, A. Statistical Equations of Turbulent Gases, Problems of Hydrodynamics Continuum Mechanics, SIAM, Philadelphia, p. 231, 1969.

[89] Launder, B. E. and Spalding, D. B., The Numerical Computation of Turbulent Flows, Comp. Meth. Appl. Mech. Eng., Vol. 3, pp. 269-289, 1974.

[90] Boussinesq, J., Theorie de lEcoulement Tourbillant, Mem. Presentes par Divers Savants Acad. Sci. Inst. Fr., Vol. 23, pp. 46-50, 1877.

[91] Magnussen, B. F. and Hjertager, B. H., On Mathematical Modeling of Turbulent Combustion with Special Emphasis on Soot Formation and Combustion, Sixteenth Symposium (International) on Combustion, The Combustion Institute, Pittsburgh, PA, pp. 719-729, 1976.

[92] Fluent Inc. of ANSYS Inc, Fluent 14.5 Documentation. Theorys Guide, 2012.

[93] H. Kobayashi, J. B. Howard, and A. F. Sarofim."Coal Devolatilization at High Temperatures". In 16th Symp. (Intl.) on Combustion. The Combustion Institute. 1976.

[94] T. H. Fletcher and A. R. Kerstein."Chemical percolation model for devolatilization: 3. Direct use of C NMR data to predict effects of coal type". Energy and Fuels. 6. 414. 1992.

[95] T. H. Fletcher, A. R. Kerstein, R. J. Pugmire, and D. M. Grant.."Chemical percolation model for devolatilization: 2. Temperature and heating rate effects on product yields". Energy and Fuels. 4, 54, 1990.

[96] D. M. Grant, R. J. Pugmire, T. H. Fletcher, and A. R. Kerstein.."Chemical percolation model of coal devolatilization using percolation lattice statistics". Energy and Fuels, 3, 175, 1989.

[97] M. M. Baum and P. J. Street."Predicting the Combustion Behavior of Coal Particles". Combust. Sci. Tech.. 3(5). 231243. 1971.

[98] I.W. Smith, The Combustion Rates of Coal Chars: A Review, In 19th Symp. (Intl.) on Combustion. The Combustion Institute, 10451065, 1982.

[99] M. Baum and P. Street., Predicting the Combustion Behavior of Coal Particles. Combustion Science and Technology, 3(5),231243, 1971.

[100] G. G. DeSoete., Overall Reaction Rates of NO and Formation from Fuel Nitrogen, In 15th Symp. (Intl.) on Combustion. The Combustion Institute, 10931102, 1975

[101] J. M. Levy, L. K. Chen, A. F. Sarofim, and J. M. Beer., NO/Char Reactions at Pulverized Coal Flame Conditions, In 18th Symp. (Intl.) on Combustion, The Combustion Institute, 1981.

[102] R. Weber, J. Smart, and W. Vd Kamp. On the MILD Combustion of Gaseous, Liquid, and Solid Fuels in High Temperature Preheated Air. Proc. Combust. Inst., 30,26232629, 2005.

[103] D. Genetti, T.H. Fletcher, R. Pugmire, Development and application of a correlation of C-13 NMR chemical structural analyses of coal based on elemental composition and volatile matter content, Energy and Fuels, 13(1), 60-8. 1999.

[104] M. Vascellari, G. Cau, Influence of turbulence-chemical interaction on CFD pulverized coal MILD combustion modeling, Fuel 101 , 90-101, 2011.

[105] Westfall PH, Kurtosis as Peakedness, 1905 - 2014. R.I.P. The American Statistician 68,191-195, 2014.

[106] R. Lundquist, A. Schrief, P. Kinnunen, K. Myohanen, and M. Seshamani. A Major Forward-The Supercritical CFB Boiler. In Power-Gen International 2003, Las Vegas, USA, 2003.

[107] A. Saario and A. Oksanen. Effect of Computational Grid in Industrial-Scale Boiler Modeling. Int. J. of Numerical Methods for Heat Fluid Flow, 19, 93117, 2009.

[108] Y. Hino, C. Zhang, and T. Ishii. Comparison of measurements and predictions of flame structure and NO_x emissions in a gas-fired furnace. In AIAA/ASME Joint Thermophysics and Heat Transfer Conference, Albuquerque, New Mexico, USA, 1998.

[109] T. Ishii, C. Zhang, and S. Sugiyama. Numerical analysis of NO_x formation rate in a regenerative furnace. In Joint Power Generation Conference, Denver, Colorado, USA, 1997.

[110] C. Zhang, T. Ishii, and S. Sugijama. Numerical modeling of the thermal performance of regenerative slab reheating furnaces. Num. Heat Transf., 32, 613631, 1997.

[111] H. Guo, Y. Ju, and K. Mauta. Numerical investigations for NO_x emissions in high temperature air combustion. In First Asia-Pacific Conference on Combustion, Nagoya, Japan, 1997.

[112] J.G. Wunning. Flammlose Oxidation von Brennstoff, PhD thesis, Aachen University of Technology, 1996. (in German).

[113] R. Weber, A. Verlaan, S. Orsino, and N. Lallemant. On emerging furnace design methodology that provides substantial energy savings and drastic reductions in CO_2, CO and NO_x emissions. J. Inst. Energy, 72, 7783, 1999.

[114] R. Weber, A. Verlaan, S. Orsino, and N. Lallemant. Combustion of natural gas with high temperature air and large quantities of flue gas. Proc. Combust. Inst., 28, 13151321, 2000.

[115] S. Orsino, R. Weber, and U. Bollettini, Numerical simulation of natural gas combustion with high-temperature air. Combust. Sci. Tech., 168, 134, 2002.

[116] M. Mancini and R. Weber. Formation and destruction of nitrogen oxides in combustion of natural gas with high temperature air, In 5th HiTACG Symposium, Yokohama, Japan, 2002.

[117] M. Mancini, P. Schwoppe, R. Weber, and S. Orsino. On mathematical modeling of flameless combustion. Combust. Flame, 150, 5459, 2007.

[118] P. Coehlo and N. Peters. Laseroptical investigation of highly preheated combustion with strong exhaust gas recirculation. Proc. Combust. Inst., 27, 31973204, 1998.

[119] S. Yang andW. Blasiak. Numerical study of fuel temperature influence on single gas jet combustion in highly preheated and oxygen deficient air, Energy, 30, 385398, 2005.

[120] S. Yang and W. Blasiak. Numerical simulation of properties of a LPG flame with high-temperature air, International Journal of Thermal Sci., 44, 973985, 2005.

[121] S. Yang and W. Blasiak. Mathematical modelling of NO emissions from high-temperature air combustion with nitrous oxide mechanism. Fuel Proc. Tech.,86, 943957, 2005.

[122] W. Dong and W. Blasiak. Numerical modeling of highly preheated air combustion in a 580kW testing furnace at IFRF. In 3rd CRST International Symposium, Yokohama, Japan, 2000.

[123] B. Pasenti, P. Evrard, and P. Lybaert. NO_x production and radiative heat transfer from an autoregenerative flameless oxidation burner, In 4th HiTACG Symposium, Rome, Italy, 2001.

[124] D. Tobacco, C. Innarella, and C. Bruno. Theoretical and numerical investigation on flameless combustion. Combust. Sci. Tech., 174, 135, 2002.

[125] A. Cavaliere and M.D. de Joannon. Zero-dimensional analysis of diluted oxidation of methane in rich conditions. Proc. Combust. Inst., 28, 16391646, 2000.

[126] L. Porcheron, L. Ferrand, E. Masson, F. Aguile, A. Quinqueneau, D. Honore, and M. Boukhalfa. High Temperature Air Combustion burner: semi-industrial scale experiment and CFD simulation, In 6th HiTACG Symposium, Essen, Germany, 2005.

[127] B.T. Burggraaf, B. Lewis, P.D.J. Hoppesteyn, N. Fricker, S. Santos, and B.K. Slim. Towards industrial application of High Efficiency Combustion. In 15th IFRF Members Conference, Pisa, Italy, 2007.

[128] D. Lupant, B. Pesenti, P. Evrard, and P. Lybaert. Numerical and experimental characterization of a self-regenerative flameless oxidation burner operation in pilot- scale furnace. In 6th HiTACG Symposium, Essen, Germany, 2005.

[129] T. Misztal. Badanie emisji NO podczas spalania oleju w warunkach wysokotemperaturowego podgrzewu powietrza spalania. PhD thesis, Silesian University of Technology, Faculty of Environmental Protection Technology and Energy, 2005. (in Polish).

[130] P. Heil, U. Renz, and R. Kneer. Experimentelle Untersuchung eines FLOX-Brenners bei Druckkohlenstaubfeuerungsbetrieb. In 4. Druckflamm Seminar, Dortmund, Germany, 2004. (in German).

[131] D. Szewczyk, J. Sudoh, A. Widerski, and B. Forsberg. Over decade of the industrial experience in high temperature air combustion applied with HRS regenerative burners. In 6th HiTACG Symposium, Essen, Germany, 2005.

[132] M. Mortberg, W. Blasiak, and A.K. Gupta. Flameless Combustion of Methane Fuel Jet injected into Transverse High Temperature Air Flow. In 6th HiTACG Symposium, Essen, Germany, 2005.

[133] J. Massingham. Evaluation of low NO_x burners for steel industry applications. in 2nd International Seminar on High Temperature Air Combustion, Stockholm, Sweden, 2000.

[134] J. Wunning. Regenerative Burner Using Flameless Oxidation. In IGRC, Cannes, France, 1995.

[135] R. Weber, A.L. Verlaan, S. Orsino, and N. Lallemant. On emerging furnace design methodology that provides substantial energy savings and drastic reductions in CO_2, CO and NO_x emissions. In 2nd International Seminar on High Temperature Air Combustion, Stockholm, Sweden, 2000.

[136] B.T. Burggraaf, B. Lewis, P.D.J. Hoppesteyn, N. Fricker, S. Santos, and B.K. Slim. Towards industrial application of High Efficiency Combustion. In 15th IFRF Members Conference, Pisa, Italy, 2007.

Activities

Education

Teoria e sviluppo dei processi chimici held by Prof. F. Di Maio and A. Di Renzo at University of Calabria

Centrali termoelettiche held by Prof. O. Mainieri at University of Calabria

Apparecchiature per il trattamento dei solidi held by Prof. B. Formisani at University of Calabria

Academic English Skills held by Centro Linguistico di Ateneo (CLA) at University of Calabria

Workshop Mathematica held by Prof. L. Bruno at University of Calabria

Lezioni su Scienza, Ingegneria Cultura del Cibo Mediterraneo held by Prof. P. Volpentesta and Prof. N. A. Uccella at University of Calabria

Workshop for Transferrable Skills Training: IPR Valorisation Fundraising held by Prof. Mundo at University of Calabria

Opportunità di finanziamento per progetti di ricerca individuali: Azioni Marie Sklodowska-Curie – Programma di borse di studio per la ricerca e Starting Grants dello European Research Council e progetti SIR del MIUR held by Prof. Ing. F. Furgiuele, Prof. D. Mundo at University of Calabria

Protezione e valorizzazione della proprietà intellettuale e Creazione di spin-off accademici e di start up innovative held by Prof. G. Danieli, Prof. G. Iazzolino, Prof. F. Longo at University of Calabria.

Percorso Formativo in materia di Innovazione, Ricerca e Trasferimento Tecnologico organized by Liaison Office at University of Calabria

Conference

69^{th} Conference of the ATI Engineering Association

Preliminary Study of Hydrodynamics and Heat Transfer in a Bubbling

Fluidized Bed Containing Sand Particle using CFD D. Perrone

70^{th} Conference of the ATI Engineering Association
Study of Oxy-Coal Combustion with wet recycle using CFD Modeling D. Perrone

71^{th} Conference of the ATI Engineering Association
Numerical Investigation of Oxy-Mild combustion of Pulverized Coal in a Pilot Furnace D. Perrone

1^{th} AIGE-IIETA International Conference
Numerical Simulation of MILD (Moderate or Intensive Low-oxygen Dilution) Combustion of Coal in a Furnace with Different Coal Gun Positions D. Perrone

Publications

Numerical Simulation of MILD (Moderate or Intensive Low-oxygen Dilution) Combustion of Coal in a Furnace with Different Coal Gun Positions D.Perrone, M. Amelio, International Journal of Heat and Technology, Volume 34, Special Issue 2, Pages 242-248, (2016)

Numerical Investigation of Oxy-Mild combustion of Pulverized Coal in a Pilot Furnace D.Perrone, M. Amelio, Energy Procedia, Volume 101, Pages 1191-1198, (2016)

Study of Oxy-Coal Combustion with wet recycle using CFD Modeling D.Perrone, M. Amelio, Energy Procedia, Volume 82, Pages 900-907, (2015)

Preliminary Study of Hydrodynamics and Heat Transfer in a Bubbling Fluidized Bed Containing Sand Particle using CFD D.Perrone, M. Amelio, Energy Procedia, Volume 81, Pages 1041-1054, (2015)

Mobility

21^{th} Semptember 2015 - 21^{st} March 2016 Institute of Thermal Technology, Poland (Gliwice)